

**STUDIES OF BEAM LIFETIME IN SYNCHROTRON RADIATION  
SOURCE INDUS-2**

*By*

**PRADEEP KUMAR**

Enrolment No.: PHYS03200804009

Raja Ramanna Centre for Advanced Technology, Indore

*A thesis submitted to  
Board of Studies in Physical Sciences  
in partial fulfilment of requirements  
for the degree of*

**DOCTOR OF PHILOSOPHY**

*of*

**HOMI BHABHA NATIONAL INSTITUTE**



**August, 2014**

## Homi Bhabha National Institute

### Recommendations of the Viva Voce Committee

As members of the Viva Voce Committee, we certify that we have read the dissertation prepared by **Pradeep Kumar** entitled "**Studies of beam lifetime in Synchrotron Radiation Source Indus-2**" and recommend that it may be accepted as fulfilling the thesis requirement for the award of Degree of Doctor of Philosophy.

Chairman - Prof. S. B. Roy



Date: 29.5.15

Guide/ Convener - Prof. Pitamber Singh



Date: 29.5.2015

The Technology Adviser - Shri Gurnam Singh



Date: 29.5.2015

Member 1 - Prof. G. S. Lodha



Date: 29.5.15

Member 2 - Prof. V. S. Pandit



Date: 29/5/2015

External Examiner – Prof. R.G. Pillay



Date: 29/5/15

Final approval and acceptance of this thesis is contingent upon the candidate's submission of the final copies of the thesis to HBNI.

I hereby certify that I have read this thesis prepared under my direction and I recommend that it may be accepted as fulfilling the thesis requirement.

Date: May 29, 2015

Place: RRCAT, Indore.



29.5.2015  
Pitamber Singh  
Guide

## STATEMENT BY AUTHOR

This dissertation has been submitted in partial fulfilment of requirements for an advanced degree at Homi Bhabha National Institute (HBNI) and is deposited in the Library to be made available to borrowers under rules of the HBNI.

Brief quotations from this dissertation are allowable without special permission, provided that accurate acknowledgement of source is made. Requests for permission for extended quotation from or reproduction of this manuscript in whole or in part may be granted by the Competent Authority of HBNI when in his or her judgment the proposed use of the material is in the interests of scholarship. In all other instances, however, permission must be obtained from the author.

  
Pradeep Kumar

## DECLARATION

I, hereby declare that the investigation presented in thesis is carried out by me. The work is original and has not been submitted earlier as a whole or in a part for degree / diploma at this or any other Institution / university.

  
Pradeep Kumar

## LIST OF PUBLICATIONS ARISING FROM THE THESIS

### Journal:

1. “Measurement of parameters in Indus-2 synchrotron radiation source”, A.D. Ghodke, Riyasat Husain, **Pradeep Kumar**, Surendra Yadav and T.A. Puntambekar, Review of Scientific Instruments 83, 103303 (2012).
2. “Beam lifetime measurement and analysis in Indus-2 electron storage ring”, **Pradeep Kumar**, A.D. Ghodke and Gurnam Singh, PRAMANA: Journal of physics, 80(5), 855 (2013).
3. “Measurements of aperture and beam lifetime using movable beam scrapers in Indus-2 electron storage ring”, **Pradeep Kumar**, A. D. Ghodke, Akhilesh Karnewar, A. C. Holikatti, Surendra Yadav, T. A. Puntambekar, Gurnam Singh and Pitamber Singh, Review of Scientific Instruments 84, 123301 (2013).
4. “Dependence of loss rate of electron due to elastic gas scattering on the shape of vacuum chamber”, **Pradeep Kumar**, Gurnam Singh, A.D.Ghodke, H. Vaishnav and Pitamber Singh, Accepted for publication in Journal “VACUUM”.

### Conferences:

1. “Beam lifetime studies in Indus-2 electron storage ring”, **Pradeep Kumar**, Riyasat Husain, A.D. Ghodke and Gurnam Singh, in proceedings of InPAC-2006 held at BARC/TIFR. (Selected for poster presentation prize)
2. “Studies of beam lifetime in Indus-2 electron storage ring”, **Pradeep Kumar**, A.D. Ghodke and Gurnam Singh, in proceedings of InPAC-2011 held at IUAC New Delhi.

3. “Effect of RF phase modulation on longitudinal parameters in Indus-2 electron storage ring”, **Pradeep Kumar**, A.D. Ghodke, Gurnam Singh and Pitamber Singh, in proceedings of InPAC-2013 held at VECC Kolkata.

  
Pradeep Kumar

## **DEDICATIONS**

*I dedicate this dissertation to my beloved grandparents and parents*

## **ACKNOWLEDGEMENT**

*It is my pleasure to acknowledge here the efforts of many colleagues who have made it possible for me to complete the research work described in this dissertation. Foremost among them is my technical adviser Sh. Gurnam Singh, presently Raja Ramanna Fellow at RRCAT. He encouraged and guided me to pursue this research work when he was Head, Indus Operation and Accelerator Physics Design Division (IOAPDD) and later. Two important things which I have learnt from him during the course of this work are the patience and the perfection in research work. I am extremely grateful to my Guide Professor Pitamber Singh, Head, Ion Accelerator Development Division, BARC, Mumbai, who encouraged, guided and supported me at every moment to pursue the research work. I am grateful to the members of my Doctoral committee Professor S.B. Roy, Professor G.S. Lodha, Professor V.S. Pandit and invited members Sh. A.D. Ghodke, Dr. K.K. Pant and Dr. Vinit Kumar for their valuable and constructive criticism, guidance and support.*

*It is also my pleasure to thank Professor P.D. Gupta, Director, RRCAT, who granted me the permission and also encouraged and extended full support to pursue the Ph.D. work. I am thankful to Sh. P.R. Hannurkar, Head, IOAPDD, for encouragement, support and for providing the beam time necessary to conduct beam lifetime experiments in Indus-2, whenever required.*

*I thank Dr. Amalendu Sharma for fruitful discussions on my research work and help in using ELEGANT code and Sh. P.K. Thander and Sh. Rajesh Verma of Computer Division for help in running this computer code on our scientific server. I also thank colleagues Sh. A.A. Fakhri, Sh. R.S. Saini, Sh. R. Husain, Sh. A. Rahim, Sh. S.K. Jena, Sh. P. Kant, Sh. P.K. Goyal, Sh. V.K. Meena, Sh. Deepak Tyagi, Sh. Debasis, Ms Urmila, Sh. H. Vaishnav, Sh. S.K.*

*Prajapati, Sh. R. Pramod, Sh. R. Malik, Sh. P.K. Jana and all shift crew members of Indus operation for help and support and discussions during beam lifetime experimental studies.*

*I am also thankful to Dr. M. Borland (APS, USA), Dr. L. Nadolski, Dr. J. Zhang (Soleil, France), Dr. X. Huang (SLAC, USA), Dr. T. Kaneyasu (SAGA, Japan), Sh. G.K. Sahoo (DESY, Germany), Ms D. A. Kalinin (STFC, Daresbury, U.K) and Sh. Beni Singh (DLS, UK) for useful discussions on beam lifetime in synchrotron radiation sources.*

*I also thank Dr. K.S. Bartwal, Dr. Atul Kumar, Dr. Arvind Kumar, Dr. M.P. Singh, Sh. V.K. Saini, Sh. D.P. Yadav, Sh. Nitesh Tiwari, Dr. G. Haridas and Sh. V. Bhatnagar for boosting my efforts to complete my Ph.D. work. It is a pleasure to remember and thank Professor N.D. Kaushika, IIT Delhi and Professor Ashok Kumar Sharma, R.K. Post-graduate College, Shamli (U.P.) for encouragement at the start of my research career.*

*I am grateful to my beloved mother late Smt. Rajkali Devi, who always inspired me and taught how to face difficulties in life. Last, but not least, I want to thank my wife Vandana and my sons Prakhar and Tejasav for healthy and enjoyable environment, which helped me in pursuing the research work.*

  
Pradeep Kumar

# CONTENTS

	<b>Page No.</b>
<b>SYNOPSIS</b>	<b>1</b>
<b>LIST OF FIGURES</b>	<b>11</b>
<b>LIST OF TABLES</b>	<b>18</b>
<b>CHAPTER 1 THE BEAM LIFETIME AND ACCEPTANCES IN INDUS-2 ELECTRON STORAGE RING</b>	<b>19</b>
1.1 Introduction	19
1.2 Indus-2 electron storage ring	20
1.3 Beam dynamics relations for studies of beam motion in storage ring	24
1.3.1 <i>Coordinate system</i>	24
1.3.2 <i>Motion of electrons in storage ring</i>	25
1.3.3 <i>Motion of electrons in transverse plane</i>	25
1.3.4 <i>Twiss parameters propagation in ring</i>	30
1.3.5 <i>Equilibrium emittance in an electron storage ring</i>	31
1.4 Longitudinal motion of electron	35
1.4.1 <i>Longitudinal equation of motion</i>	38
1.4.2 <i>Damping of synchrotron oscillation</i>	39
1.5 Electron beam sizes in longitudinal and transverse plane	41
1.6 Beam loss mechanism in Indus-2	42
1.6.1 <i>Acceptance of electron beam in Indus-2</i>	44
1.6.1.1 <i>Physical aperture</i>	44
1.6.1.2 <i>Dynamic aperture</i>	47
1.6.1.3 <i>Momentum aperture</i>	49

1.7	Closed orbit distortion and its correction	52
1.7.1	<i>MICADO method</i>	54
1.7.2	<i>Harmonic correction method</i>	55
1.7.3	<i>Local orbit bump method</i>	55
1.7.4	<i>Singular value decomposition (SVD) method</i>	55
1.8	Estimation of beam lifetime in Indus-2 storage ring	56
1.8.1	<i>Estimation of Quantum lifetime</i>	56
1.8.2	<i>Estimation of vacuum lifetime due to beam-gas interaction</i>	59
1.8.3	<i>Estimation of Touschek lifetime due to electron-electron interaction within a bunch</i>	62
<b>CHAPTER 2 DEPENDENCE OF ELECTRON LOSS ON THE SHAPE OF VACUUM CHAMBER</b>		<b>65</b>
2.1	Introduction	65
2.2	Beam lifetime due to elastic coulomb scattering	67
2.3	Expressions for shape factor $F$	69
2.3.1	<i>Shape factor for rectangular vacuum chamber</i>	70
2.3.2	<i>Shape factor for elliptical vacuum chamber</i>	75
2.4	Estimation of shape factor	80
2.4.1	<i>Estimation of average shape factor</i>	84
<b>CHAPTER 3 STUDIES OF ELECTRON-ELECTRON INTERACTION WITHIN A BUNCH</b>		<b>86</b>
3.1	Introduction	86
3.2	Expression of Touschek lifetime	87
3.3	Methods for the enhancement of Touschek lifetime	88
3.3.1	<i>Vertical beam size in Indus-2</i>	88
3.3.1.1	<i>Measurement of betatron coupling in Indus-2</i>	89

3.3.1.2	<i>Measurement of vertical dispersion in Indus-2</i>	90
3.3.1.3	<i>Beam size measurement at beamline-16</i>	91
3.3.2	RF phase modulation	92
3.3.2.1	<i>Longitudinal beam dynamics under RF Phase modulation</i>	92
3.3.2.2	<i>Criterion for RF phase modulation</i>	93
3.3.2.3	<i>Effect of RF phase modulation on distribution of electrons in a bunch</i>	94
3.3.2.4	<i>Effect of RF phase modulation on longitudinal beam parameters</i>	96
3.3.2.5	<i>Implementation of RF phase modulation in Indus-2</i>	97
<b>CHAPTER 4 EXPERIMENTAL STUDIES OF BEAM LIFETIME IN INDUS-2 STORAGE RING</b>		<b>99</b>
4.1	Introduction	99
4.2	Effect on beam lifetime due to the emission of synchrotron radiation	100
4.3	Effect of aperture on beam lifetime	102
4.4	Equation of beam current decay with time	104
4.5	Beam current decay and lifetime with 900 kV RF cavity voltage	105
4.5.1	<i>Beam current decay and lifetime with 750 kV RF cavity voltage</i>	107
4.6	Beam current decay and lifetime in different bunch filling pattern	108
4.7	Analysis of measured beam lifetime	110
4.8	Estimation of Vacuum lifetime	114
4.8.1	<i>Vacuum lifetime due to elastic scattering</i>	114
4.8.2	<i>Vacuum lifetime due to inelastic scattering</i>	114
4.8.3	<i>Estimation of average pressure <math>\bar{P}</math> and average of <math>\beta_x \cdot P</math> and <math>\beta_z \cdot P</math></i>	115
4.8.4	<i>Estimation of available aperture for beam motion</i>	117
4.9	Estimation of Touschek Lifetime $\tau_{\text{tous}}$	118
4.10	Estimation of vacuum and Touschek lifetime from measured beam lifetime	120

<b>CHAPTER 5 MEASUREMENTS OF APERTURE AND BEAM LIFETIME USING BEAM SCRAPERS IN INDUS-2</b>	<b>122</b>
5.1 Introduction	122
5.2 Experimental set-up for aperture measurement	125
5.3 Measurement of beam lifetime with scraper movement	126
5.3.1 <i>Beam lifetime with vertical scraper movement</i>	126
5.3.2 <i>Beam lifetime with horizontal scraper movement</i>	128
5.4 Analysis of measured beam lifetime with movement of vertical and horizontal scrapers	129
5.4.1 Beam lifetime due to elastic coulomb scattering $\tau_{el}$	129
5.4.1.1 $\tau_{el}$ with movement of vertical scraper	131
5.4.1.2 $\tau_{el}$ with movement of horizontal scraper	132
5.4.2 Beam lifetime due to inelastic scattering $\tau_{br}$	133
5.4.2.1 $\tau_{br}$ with movement of vertical scraper	133
5.4.2.2 $\tau_{br}$ with movement of horizontal scraper	133
5.4.3 Beam lifetime due to Touschek scattering $\tau_{tous}$	134
5.4.3.1 $\tau_{tous}$ with the movement of vertical scraper	134
5.4.3.2 $\tau_{tous}$ with the movement of horizontal scraper	134
5.4.4 Quantum lifetime $\tau_q$	134
5.4.4.1 $\tau_q$ with movement of vertical scraper	135
5.4.4.2 $\tau_q$ with movement of horizontal scraper	135
5.5 Verification of theoretical calculated results	136

5.6	Further experiments for beam lifetime improvement	140
5.7	Beam experiments using single bunch mode	142
5.7.1	<i>Effect of RF voltage on beam lifetime</i>	144
	<b>SUMMARY AND CONCLUSIONS</b>	<b>146</b>
	<b>APPENDIX</b>	<b>149</b>
	<b>REFERENCES</b>	<b>150</b>

## SYNOPSIS

Electrons travelling at a relativistic speed and forced to change the direction of their motion under the influence of magnetic field emit electromagnetic radiation with peculiar characteristics known as synchrotron radiation. These electromagnetic radiations cover a wide range of photon energies from the infrared to hard X-ray regions of electromagnetic spectrum. The sources of these radiations are high energy electron or positron circular synchrotrons or storage rings. The storage rings designed specifically for the production of synchrotron radiation across the world such as Diamond light source (U.K.), Soleil (France), Australian light source (Australia) and Indus-2 (India) are known as synchrotron radiation sources. The motion of electrons in a synchrotron or storage ring is guided by an external magnetic field created by periodic arrangement of dipoles, quadrupoles and sextupoles magnets whereas it gets acceleration or the compensation of energy lost due to the emission of synchrotron radiation from an external electric field created by radio frequency (RF) cavities.

In an electron storage ring like Indus-2, the electrons are confined within bunches inside a vacuum chamber. The number of stored bunches in a storage ring may be equal or less than the available RF buckets. The number of maximum RF buckets in the ring is equal to the ratio of the resonant frequency of RF cavity to the revolution frequency of electrons. The electrons which are confined within a bunch execute betatron oscillations about the closed orbit in transverse planes and also execute synchrotron oscillations with respect to synchronous electrons in longitudinal plane. The electrons within a bunch are scattered due to coulomb repulsion with each other and also get scattered due to the interaction with residual gas atoms present in the vacuum chamber. Due to the scattering of electrons within a bunch and with residual gas atoms, electrons are deflected and also undergo changes in energy

which cause an increase in amplitude of betatron oscillations and are lost from the bunch either due to the aperture limitations in transverse plane or due to momentum aperture limitations either in transverse or in longitudinal plane. So the study of the aperture in a storage ring is essential for the estimation of beam lifetime. The experimental studies and theoretical analysis of beam lifetime of stored electrons in Indus-2 storage ring are the objective and scope of the thesis.

The stored electrons orbiting in an electron storage ring may be lost due to various causes. For a well designed storage ring, there are two main classes for electron losses, first is the loss due to scattering and another is the loss due to beam instabilities. While the electron losses due to scattering with other particles is a single particle effect leading to a gradual loss of electrons from the electron beam whereas electron losses due to beam instabilities is a multi particle effect and later can lead to a partial or complete loss of electron beam. This work is mainly focused on the gradual loss of electrons which are mainly due to beam-gas scattering and electron-electron scattering within a bunch known as Touschek scattering. The lifetime  $\tau_t$  of stored electron beam during beam current decay is estimated as  $-I/(dI/dt)$  where  $dI/dt$  is the instantaneous decay rate at particular current  $I$  at time  $t$ . The experimental studies and theoretical analysis of beam lifetime of stored electron beam in multi-bunch mode at beam energy 2.0 and 2.5 GeV with stored current 100 mA in Indus-2 was carried out.

The electrons within a bunch are scattered by the residual gas atoms present in the vacuum chamber. The scattering may be elastic or inelastic. In the initial stage of Indus-2 operation, the vacuum pressure in the storage ring increased due to the photo induced desorption of gases from the surface of vacuum chamber caused by the incident synchrotron radiation emitted by the circulating electron beam. The pressure in the ring gradually reduced with

time due to the cleaning of the surface of vacuum chamber by synchrotron radiation. The beam current decay data with the reduction in pressure with time was studied and the beam lifetime was found to increase with the reduction in vacuum pressure.

When the electrons are scattered elastically with the nuclei of residual gas atoms, they are deflected and the amplitude of betatron oscillation about the closed orbit is increased and are lost at a location where the available aperture for electron motion is less than the betatron oscillation amplitude. The effect of aperture was studied by conducting beam lifetime experiments without and with closed orbit correction in both vertical and horizontal plane. By minimizing closed orbit distortion in vertical and horizontal plane, there is an increase in available aperture for beam motion and also reduction in vacuum pressure was observed, which resulted into an increase in beam lifetime.

The beam lifetime due to elastic scattering between electrons and nuclei of residual gas atoms depends on the shape of the vacuum chamber. The effect of rectangular and elliptical shape of vacuum chamber on beam lifetime due to elastic coulomb scattering was studied using linear beam dynamics. As the vacuum pressure along the circumference in a storage ring is not uniform so analytical formulations for the shape factor for rectangular and elliptical shape of the vacuum chamber as a function of position along the circumference were developed. The analytical expression of the shape factor for elliptical shape of vacuum chamber as a function of longitudinal position was found to be different than the existing expression. The existing expression for shape factor is obtained by considering electron loss at only one location whereas expression was derived by considering the loss at maximum  $\beta_x$  and  $\beta_z$  locations which are applicable in modern storage ring. These studies show that the effect of shape on shape factor is much smaller as compared to the values obtained using existing analytical expressions.

The contribution of vacuum lifetime and Touschek lifetime to total beam lifetime was separated experimentally by storing same amount of average beam current uniformly in all 291 RF buckets in first experiment and by filling two-third RF buckets and the rest of the RF buckets kept empty in second experiment. The experimental studies show that the vacuum pressure at the same stored beam current is the same at all Bayard Alpert Gauges (BAGs) installed for vacuum pressure measurement in case of uniformly filled all RF buckets and filling two-third RF buckets and the rest of the RF buckets kept empty. By conducting these experiments, we are able to know whether the beam lifetime is limited due to vacuum or Touschek lifetime.

During electro-electron scattering within a bunch and inelastic scattering between stored electrons and nuclei of residual gas atoms, the energy of scattered electrons changes, if this change in energy is more than the momentum aperture, the scattered electrons are lost from the beam. The limitation of momentum aperture which may be either in transverse or in longitudinal plane was studied by conducting experiments with different RF cavity voltages.

The studies of beam lifetime in single bunch mode in Indus-2 were carried out. The objective of these studies was to study the effect on beam lifetime in electron-electron interaction due to increase in electron density within a single bunch.

The Touschek lifetime varies proportionally with vertical beam size which depends on linear betatron coupling in the storage ring. The measurement of betatron coupling in Indus-2 was carried out using minimum tune separation technique and found to be less than 1%. The vertical beam size obtained using betatron coupling was found to be closely same as the vertical beam size obtained using XRF microprobe beamline in Indus-2.

Long beam lifetimes are desirable for the users of synchrotron radiation sources since it gives higher integrated photon flux, reduce the number of refills necessary and improve the

stability by reducing thermal loading effects due to the varying current. In a low emittance electron storage ring, the beam lifetime is dominated by Touschek scattering within a bunch. Simulation studies were carried out to find the effect of RF phase modulation on bunch length. These studies show that by applying phase modulation in main RF, there is an increase in bunch length that leads to the reduction in Touschek scattering within a bunch. The simulation studies were carried out using particle tracking code ELEGANT.

To know the aperture available for stable motion of electrons in a storage ring, movable beam scrapers are used. The measurements of aperture were carried out using movable vertical and horizontal beam scrapers installed in one of the long straight sections in Indus-2. The objective of these measurements was to find out the minimum aperture requirement for undulators which are planned to be installed in long straight sections and also to find the contributors of beam loss. Using the measured aperture and residual gas pressure, the contribution of beam lifetime due to vacuum lifetime, Touschek lifetime and quantum lifetime was obtained. The values of vacuum and Touschek lifetime were compared with the values obtained using partial bunch fill experiments and found to be closely same. The results of vertical and horizontal beam sizes obtained by moving scrapers towards the beam centre in quantum lifetime limit were compared with the beam sizes obtained using X-ray diagnostic beamline and were found to be nearly same.

The thesis is organized into five chapters. The chapter wise summary is as follows:

Chapter 1: The beam lifetime and acceptances in an electron storage ring

In this chapter, an introduction of Indus-2 storage ring and the dependence of beam loss due to quantum excitation, beam-gas scattering and Touschek scattering will be presented. The acceptance available in the ring i.e. physical acceptance, dynamic acceptance and RF

acceptance will also be summarized. The theoretical estimation of quantum lifetime, vacuum lifetime and Touschek lifetime will also be discussed.

## Chapter 2: Dependence of electron loss on the shape of vacuum chamber

As the vacuum pressure in a storage ring is not uniform along the circumference and it varies from place to place. In order to calculate beam lifetime due to elastic scattering between electrons and nuclei of residual gas atoms, the vacuum pressure and shape factor information at all locations in the ring is required. Due to non uniform pressure in storage ring, it is important to know the shape factor as a function of longitudinal position in the ring. Analytical expressions for the shape factor as a function of position along the circumference for rectangular and elliptical shape of the vacuum chamber was derived considering the aperture to be uniform along the circumference and the loss of electrons at the quadrupole locations. The expression given in the literature is for the average shape factors which are not applicable to the practical situations in which the pressure is not uniform at all places along the circumference of ring.

In this chapter, analytical formulations of shape factor due to elastic coulomb scattering between electron and nuclei of residual gas atoms will be presented considering rectangular and elliptical shape of vacuum chamber for Indus-2 storage ring. A comparison in the value of shape factor using existing expressions will also be presented.

## Chapter 3: Studies of electron-electron interaction within a bunch

The electrons in a storage ring are confined within bunches. As the density of electrons in a bunch increases, the scattering of electrons within the bunch increases which is known as Touschek scattering. Beam lifetime due to Touschek scattering depends on how strongly electrons are packed within a bunch. It thus depends not only on the beam current but also

upon the beam sizes in horizontal and vertical plane and the bunch length. The vertical beam size which depends on the coupling between the horizontal and vertical motion has been used for the calculation of Touschek lifetime. Linear betatron coupling in Indus-2 was measured using minimum tune separation technique and found to be less than 1%. The vertical beam size obtained using betatron coupling was found to closely agree with the vertical beam size obtained using XRF microprobe beamline in Indus-2. Linear betatron coupling and its measurement using minimum tune separation technique in Indus-2 will be presented.

In a low emittance electron storage ring, the beam lifetime is limited due to Touschek scattering. The Touschek scattering can be decreased by applying phase modulation in main RF system. Simulation studies on the effect of phase modulation of frequency nearly two-times of synchrotron frequency in main RF signal were carried out using particle tracking code ELEGANT. The tracking results of longitudinal phase space and the effect of phase modulation on beam parameters in longitudinal plane i.e. bunch length and energy spread in Indus-2 at beam energy 2.5 GeV will be presented.

#### Chapter 4: Experimental studies of beam lifetime in Indus-2

##### a) Experiments using multi-bunch mode

Beam lifetime experiments were conducted to study the effect of aperture on lifetime of stored electron beam. For the experiment, beam current decay was monitored without and with closed orbit correction in vertical and horizontal plane. The results of the effect of closed orbit correction on beam lifetime will be discussed. The increase in beam lifetime with reduction in pressure with time will also be discussed. An equation of beam current decay generated using a least square minimization method that closely follows the beam current decay of stored electron beam will also be discussed.

Beam lifetime experiments were also conducted by storing electrons uniformly in all 291 available RF buckets and also by storing electrons in two third RF buckets keeping rest of the RF buckets empty. The analysis of measured beam lifetime using vacuum pressure and RF cavity voltage was carried out. These results will be presented in this chapter. The results of the effect of bunch fill pattern and RF cavity voltage on beam lifetime will also be discussed. The separation of vacuum lifetime, Touschek lifetime from the measured beam lifetime will also be covered in this chapter.

a) Experiments using single bunch mode

To study the effect of beam energy on Touschek scattering, the beam current decay of equal amount of average current stored in single bunch in one RF bucket out of 291 RF buckets was observed at low beam energy i.e. 550 MeV and higher energy 2.5 GeV. A comparison of beam current decay in single bunch storage mode at these beam energy will be presented.

Chapter 5: Measurement of aperture and beam lifetime using movable beam scrapers

The vertical and horizontal apertures available for the stable beam motion at beam scraper locations were measured using vertical and horizontal movable beam scrapers which are installed in one of the long straight sections in Indus-2. With the movement of vertical and horizontal scrapers, the beam lifetime was measured at different positions of scrapers from the beam centre. By using the measured beam lifetime data with scraper position, the contribution of beam lifetime due to elastic scattering between electrons and residual gas atoms, bremsstrahlung, Touschek and quantum excitation was estimated. The measured value of vertical and horizontal aperture at scraper location was found to be  $\pm 4.1$  mm and  $\pm 12.45$  mm respectively at beam energy 2.5 GeV. The measurement and analysis of experimental data will be presented in this chapter.

## Summary:

The loss of electrons due to elastic scattering between electrons and the nuclei of the residual gas atoms for rectangular and elliptical shape of the vacuum chamber was studied using linear beam dynamics. Analytical expressions for the shape factors for rectangular and elliptical shape of vacuum chamber as a function of position along the circumference of storage ring were developed. The expressions were derived considering the loss of electrons at quadrupole locations i.e. at maximum  $\beta_x$  and maximum  $\beta_z$  locations. The expression for shape factor for elliptical shape of vacuum chamber is found to be different than the existing expression because in existing expression the loss of electrons was considered at one location only which is not applicable in modern electron storage ring. These expressions are very useful to estimate the beam lifetime due to elastic scattering of electrons with the nuclei of residual gas atoms in realistic conditions like non uniform vacuum pressure in storage ring. The contribution of vacuum lifetime and Touschek lifetime in measured beam lifetime was separated by storing electrons uniformly in all 291 RF buckets and also storing electrons in two-third RF buckets keeping rest of the RF buckets empty. These studies are very useful to know the limiting factor of beam lifetime i.e. either vacuum lifetime or Touschek lifetime.

The beam lifetime due to a high density of electrons in a bunch was studied by storing the electrons in a single RF bucket out of 291 RF buckets in Indus-2 ring.

The aperture available for stable beam motion in Indus-2 was measured by using movable beam scrapers. These studies are useful to choose an appropriate aperture for undulators which are planned to be installed in Indus-2. From the measured beam lifetime with scraper position from the beam centre, the contribution of beam lifetime due to elastic scattering of electron with the nuclei of residual gas atoms, bremsstrahlung, Touschek scattering and quantum excitation was estimated separately. The vacuum and Touschek lifetime obtained

using scrapers was closely same as obtained using partial bunch fill experiments. The vertical and horizontal aperture studies using movable beam scrapers show that the beam lifetime is limited due to elastic coulomb scattering and inelastic scattering between electrons and nuclei of residual gas atoms. The measured vertical aperture at scraper location was found to be less than from its theoretical estimated value. The vertical aperture was increased by minimizing the closed orbit distortion in vertical plane and resulted into ~40% increase in beam lifetime. The lifetime will further improve by reduction in vacuum pressure. The vertical aperture measurements carried out indicate that the beam lifetime will not be reduced after installation of insertion devices as the vertical aperture available will be  $\pm 8$  mm.

## LIST OF FIGURES

<b>Fig.</b>	<b>Caption of the figure</b>	<b>Page</b>
<b>No.</b>		<b>No.</b>
1.1	Schematic layout of Indus synchrotron radiation source facility	21
1.2	Indus-2 electron storage ring	21
1.3	One unit cell of Indus-2, BM: Dipole magnet; Q1D, Q3D, Q5D: Defocusing quadrupole magnets; Q2F, Q4F: Focussing quadrupole magnets; SF: Focussing sextupole, SD: Defocussing sextupole; CH: Horizontal steering magnet, CV: Vertical steering magnets, CHV: Combined horizontal and vertical steering magnet; BPI: Beam position indicator	22
1.4	Coordinates for describing the trajectories of electrons	24
1.5	Phase space ellipse at position $s$ in ring	28
1.6	Phase space ellipse at position $s$ in horizontal plane at dispersion location $\eta_x(s)$	29
1.7	Lattice functions in Indus-2, QD: defocusing quadrupole, QF: focusing quadrupole, BM: bending magnet, SF: focusing sextupole and SD: defocusing sextupole	31
1.8	Variation in horizontal beam emittance with beam energy	34
1.9	Variation in damping time in horizontal and vertical plane with beam energy	34
1.10	Path for on-momentum and off-momentum electrons	36

1.11	Phase stability of electrons	37
1.12	RF bucket in Indus-2	38
1.13	Longitudinal damping time and energy spread with beam energy	40
1.14	Physical acceptance in horizontal plane in Indus-2 for energy deviation $\delta=0, \pm 1\%$	45
1.15	Physical acceptance in vertical plane in Indus-2	46
1.16(a)	Dynamic aperture using MAD-8 code with systematic multi-pole field errors	48
1.16(b)	Dynamic aperture using ELEGENT code with systematic multi-pole field errors	48
1.16(c)	Dynamic aperture using RACETRACK code with systematic and random multi-pole field errors	48
1.17	Transverse momentum acceptance in one unit cell in Indus-2	50
1.18	Comparison of transverse and RF momentum acceptance in one unit cell in Indus-2	51
1.19	Momentum acceptance in Indus-2 using tracking code	52
1.20(a)	Quantum lifetime with ratio of vertical aperture to vertical beam size	58
1.20(b)	Quantum lifetime with ratio of horizontal aperture to horizontal beam size	58
1.20(c)	Quantum lifetime with ratio of RF acceptance to beam energy spread	58
1.21	RF Cavity voltage and acceptance with different beam energy	61

1.22	Vacuum lifetime due to beam-gas atoms interaction at different beam energy	61
1.23	Touschek lifetime at different beam energy	64
1.24	Beam lifetime at different beam energy in Indus-2	64
2.1	Scattering and beam loss locations in ring	69
2.2	Electron Positions (a) at maximum $\beta_x$ (dotted rectangle) with respect to their positions on the boundary of chamber at maximum $\beta_z$ and (b) at maximum $\beta_z$ (dotted rectangle) with respect to their positions on the boundary of chamber at maximum $\beta_x$	71
2.3	Electron positions (a) at maximum $\beta_x$ (dotted ellipse) with respect to their positions on the boundary of chamber at maximum $\beta_z$ and (b) at maximum $\beta_z$ (dotted ellipse) with respect to their positions on the boundary of chamber at maximum $\beta_x$	76
2.4	Shape factor variation for elliptical shape of chamber	79
2.5	Increase in shape factor along the circumference in ring	80
2.6	Comparison in shape factor in one unit cell for rectangular and elliptical shape of chamber in case Indus-2	81
2.7	Increase in shape factor from rectangular to elliptical shape	81
2.8	Comparison in shape factor in one unit cell for square and circular shape of chamber in case Indus-2	82
2.9	Increase in shape factor from square to circular shape	82

2.10	Comparison in shape factor in one unit cell for circular shape of chamber	83
2.11	Increase in shape factor for circular shape	83
3.1	Coulomb scattering of two electrons in centre of mass and laboratory system	86
3.2	The variation of $D(\xi)$ with $\xi$	87
3.3	Measured horizontal and vertical fractional betatron tunes with change of current in Q3D family of quadrupoles	90
3.4	Measured vertical dispersion at all BPI locations in Indus-2	91
3.5(a)	Electron distribution at the start of tracking with RF phase modulation $f_s$	95
3.5(b)	Electron distribution after 1000 turns with RF phase modulation $f_s$	95
3.5(c)	Electron distribution after 10,000 turns with RF phase modulation $f_s$	95
3.6(a)	Electron distribution at the start of tracking with RF phase modulation $2 * f_s$	95
3.6(b)	Electron distribution after 1000 turns with RF phase modulation $2 * f_s$	95
3.6(c)	Electron distribution after 10,000 turns with RF phase modulation $2 * f_s$	95
3.7(a)	Bunch length variation with RF phase modulation $f_s$	96
3.7(b)	Energy spread variation with RF phase modulation $f_s$	96
3.8(a)	Bunch length variation with RF phase modulation $2 * f_s$	96
3.8(b)	Energy spread variation with RF phase modulation $2 * f_s$	96
3.9	RF phase modulation in Indus-2, AFG is arbitrary frequency generator, $f_s$ is synchrotron frequency, LLRF is Low Level RF system, SSA is solid state	98

	amplifier	
3.10(a)	Beam spectrum without RF phase modulation	98
3.10(b)	Beam spectrum with RF phase modulation	98
4.1	Comparison in beam current decay with time	101
4.2	BAGs and vacuum pumps location in one unit cell of Indus-2	101
4.3	Average vacuum pressure and beam lifetime during beam current decay	102
4.4	Beam current decay without and with closed orbit correction	103
4.5(a)	Vertical orbit without and with closed orbit correction	103
4.5(b)	Horizontal orbit without and with closed orbit correction	103
4.6(a)	Vacuum pressure at stored current 100 mA	104
4.6(b)	Beam lifetime before and after closed orbit correction during beam current decay	104
4.7(a)	Measured beam current decay	106
4.7(b)	Beam lifetime at different stored beam current during beam current decay	106
4.8(a)	Beam current decay at different RF voltages	107
4.8(b)	Beam lifetime at different stored current at different RF voltages	107
4.9(a)	Wall current monitor signal at 100mA stored current when all 291 RF buckets are filled	108
4.9(b)	Wall current monitor signal at 100mA stored current when two-third RF	108

	buckets are filled	
4.10(a)	Beam current decay for two different RF buckets fill pattern	109
4.10(b)	Beam lifetime for two different RF buckets fill pattern	109
4.11	Measured vacuum pressure at all BAGs for two different filling pattern at stored current 100mA	110
4.11(a)	Measured beam current decay rate and fitted curve at different beam current	113
4.11(b)	Measured beam current decay and decay curve with coefficients <i>a</i> and <i>b</i>	113
4.12	Measured vacuum pressure during beam current decay	116
4.13	Variation of $\langle\beta_x.P\rangle$ , $\langle\beta_z.P\rangle$ during beam current decay	116
4.14	Vacuum lifetime during beam current decay	117
4.15	RF buckets for two different RF voltages	118
4.16	Touschek lifetime during beam current decay	119
4.17	Comparison of estimated and measured beam lifetime	119
5.1	Vertical and horizontal scrapers in the ring, mark (1) vertical scraper, (2) horizontal scraper, (3) stepper motors for vertical and horizontal movement of scraper blades	126
5.2	Beam lifetime with vertical scraper movement towards the beam centre	128
5.3	Beam lifetime with horizontal scraper movement towards the beam centre	129
5.4	Scattering angle and beam lifetime at different position of vertical scraper	132

5.5	Scattering angle and beam lifetime at different position of horizontal scraper	132
5.6	Momentum aperture with the horizontal scraper at $a=12.45-7.0$ mm	134
5.7	Calculated and measured beam lifetime with vertical scraper position	135
5.8	Calculated and measured beam lifetime with horizontal scraper position	136
5.9	Beam lifetime versus vertical scraper position with fitted curve	137
5.10	Comparison in beam current decay with 10% and 33% bunch gap	138
5.11	Vertical closed orbit before and after correction	141
5.12	Comparison in beam current decay before and after vertical orbit correction	141
5.13	Comparison in beam current decay before and after vertical orbit correction	142
5.14(a)	Wall current monitor signal (WCM) during beam accumulation in single bunch	143
5.14(b)	Wall current monitor signal showing the storage of single bunch at beam energy 2.5 GeV	143
5.15	Single bunch beam photograph taken using streak camera in visible diagnostic beamline	143
5.16	Beam current decay in single bunch mode at two different beam energy	143
5.17(a)	Measured bunch length during beam current decay at beam energy 550 MeV	144
5.17(b)	Measured bunch length during beam current decay at beam energy 2.5 GeV	144
5.18	Effect of RF voltage on beam lifetime at beam energy 2.5 GeV	145

## LIST OF TABLES

<b>Table</b>	<b>Title of the table</b>	<b>Page</b>
<b>No.</b>		<b>No.</b>
2.1	Comparison of estimated average shape factor using derived and existing expression for different shapes of vacuum chamber	84
5.1	Partial pressure of residual gases at stored beam current 100 mA	131
5.2	Value of Touschek lifetime from measured beam lifetime	139
5.3	Contribution of different lifetime in total beam lifetime at 100 mA stored beam current	140

# CHAPTER 1

## THE BEAM LIFETIME AND ACCEPTANCES IN INDUS-2 ELECTRON STORAGE RING

### 1.1 Introduction

When electrons travelling at a relativistic speed are forced to change the direction of their motion under the influence of magnetic field, they emit electromagnetic radiation with peculiar characteristics are known as synchrotron radiation. The synchrotron radiation covers a wide range of photon energies from infrared to hard X-ray regions of electromagnetic spectrum. Most useful properties of X-rays obtained from the synchrotron radiation sources are the flux (number of photons emitted per second per milli-radian in a given spectral band width) and the brightness (number of photons emitted per unit source area per unit solid angle in a given spectral band width) which are several order of magnitude higher than the conventional X-ray sources. The sources of the synchrotron radiations are high energy electron or positron circular synchrotrons or storage rings. Electron synchrotron is a circular accelerator in which magnetic field is used to guide the electrons to circulate in a closed orbit of fixed radius whereas storage ring is a synchrotron of constant electron energy in which motion of electrons is under constant magnetic field. There are many storage rings designed specifically for the production of synchrotron radiation across the world [1] such as Spring-8 (Japan), ESRF (France), Diamond light source (U.K.), Soleil (France), Australian light source (Australia), Pohang light source (Korea) and Indus-2 (India). There are various uses of synchrotron radiation in condensed matter physics, surface physics, chemistry, biochemistry, industry and medical research etc. Indus-2 storage ring is operational at beam energy 2.5 GeV and photon beam tapped through various beamlines is in use by synchrotron radiation users.

Beam lifetime of stored electrons is an important parameter for assessing the performance of any electron storage ring. The beam lifetime of stored electron beam in Indus-2 ring was studied by conducting beam experiments and analysis of the measured data. The experimental studies of lifetime of stored electrons in Indus-2 storage ring and its theoretical analysis are presented in this thesis. A brief introduction of Indus-2 is given in next section.

## **1.2 Indus-2 electron storage ring**

Two synchrotron radiation sources namely Indus-1 [2] and Indus-2 [3-9] have been developed and operational at RRCAT, Indore, India. These two sources form the Indus synchrotron radiation source facility as shown in Figure 1.1. A 20 MeV microtron serves as the pre-injector in which electrons are produced and accelerated to beam energy 20 MeV. A booster synchrotron serves as the injector for both Indus-1 and Indus-2 ring. Electrons are transferred from the microtron to the synchrotron through transfer line TL-1 and to Indus-1 through transfer line TL-2 and to Indus-2 through a part of TL-2 and transfer line TL-3. The magnetic lattice of Indus-2 is shown in Figure 1.2.

Electrons accelerated to beam energy 20 MeV in the microtron are injected in to the booster synchrotron through the injection septum, in which they are accelerated to 450 MeV if they are to be injected in to Indus-1 and to 550 MeV if they are required to be injected in to Indus-2. The repetition frequency of the microtron and the synchrotron is 1 Hz.

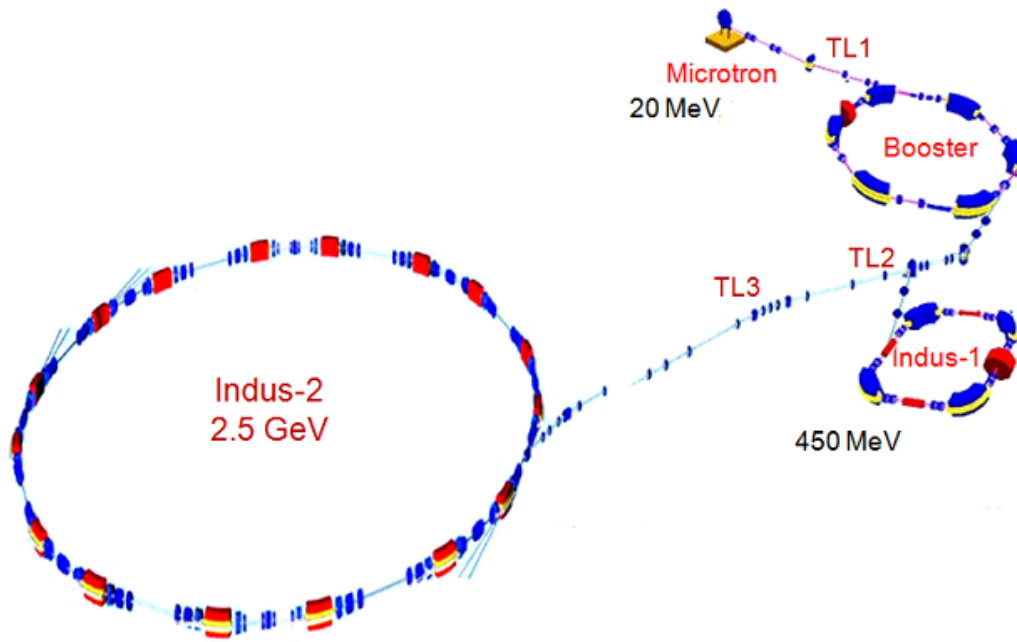


*Fig.1.1. Schematic layout of Indus synchrotron radiation source facility*

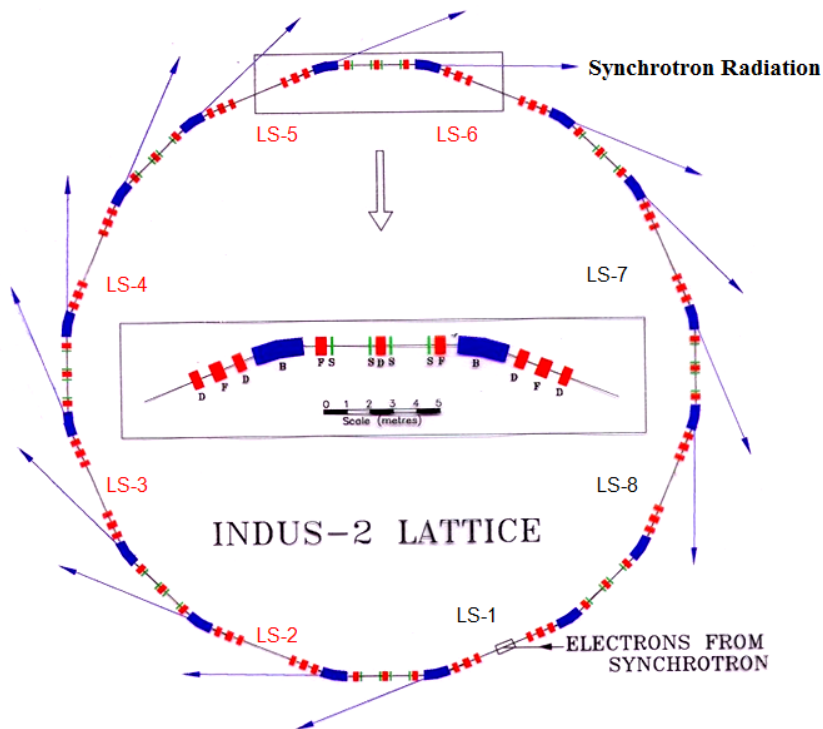


*Fig.1.2. Indus-2 electron storage ring (LS: Long straight section)*

As seen in Figure 1.2, Indus-2, a storage ring consists of eight periodic unit cells each of length 21.559 m. A unit cell with all magnets arrangement is shown in Figure 1.3.

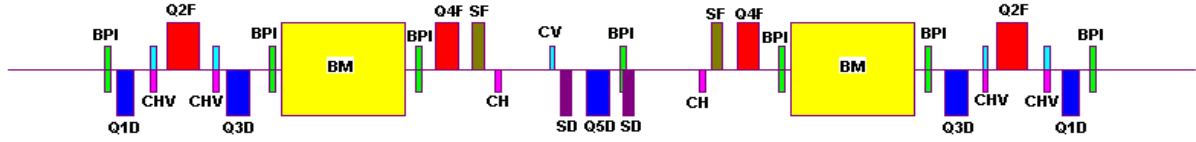


*Fig.1.3. One unit cell of Indus-2, BM: Dipole magnet; Q1D, Q3D, Q5D: Defocusing quadrupole magnets; Q2F, Q4F: Focussing quadrupole magnets; SF: Focussing sextupole magnets, SD: Defocussing sextupole magnets; CH: Horizontal steering magnets, CV: Vertical steering magnets, CHV: Combined horizontal and vertical steering magnets; BPI: Beam position indicator*

Each unit cell accommodate two dipoles, nine quadrupoles, four sextupoles, six horizontal and five vertical steering magnets, seven beam position indicators and a 4.5 m long straight section (LS). So the Indus-2 ring accommodates a total of sixteen dipoles, seventy two quadrupoles, thirty two sextupoles, forty eight horizontal steering and forty vertical steering magnets. All sixteen dipole magnets which are of rectangular magnets are connected in series and driven by a single power supply whereas seventy two quadrupoles are grouped in five families namely Q1D, Q2F, Q3D, Q4F and Q5D. The family of quadrupoles Q1D, Q2F, Q3D and Q4F consists of sixteen quadrupoles each whereas Q5D family consists of eight quadrupoles. A pair of quadrupoles in Q1D family are connected in series and driven by a single power supply, so sixteen quadrupoles of Q1D family are driven by eight power supplies. In a similar manner as for Q1D, the family of quadrupoles of Q2F and Q3D are driven by eight power supplies each. All sixteen quadrupoles of Q4F family are connected in series and driven by a single power supply and all eight quadrupoles of Q5D family are connected in series and driven by another single power supply. So, the forty eight quadrupoles of Q1D, Q2F and Q3D family are driven by twenty four power supplies and in

total 26 power supplies are used to energize all seventy two quadrupoles. Thirty two sextupoles are grouped in two families namely SF and SD and each family consists of sixteen sextupole magnets. All sixteen sextupoles of SF family are connected in series and driven by a single power supply similarly all sixteen sextupoles of SD family are driven by another single power supply. Forty eight horizontal and forty vertical steering magnets are driven by independent power supplies.

The dipole magnets are used to circulate the electron beam on a design closed orbit path, quadrupole magnets are used to confine the beam towards the closed orbit and sextupole magnets are used for the correction of chromatic aberration (variation in focussing strengths of quadrupole with electron energy) also known as chromaticity correcting sextupoles. Horizontal and vertical steering magnets are used to correct the closed orbit distortion in horizontal and vertical plane respectively. Beam position indicators are used to measure the beam position in horizontal and vertical planes in the ring. Long straight sections are used to accommodate injection septum, four injection kickers, four RF cavities and five proposed insertion devices. The energy loss of electrons due to the emission of synchrotron radiation from dipole magnets also known as bending magnets and insertion devices is compensated by applying an accelerating electric field created by four radio frequency (RF) cavities which are installed in the long straight section LS-8 in the ring.

To study the electron motion in storage ring, we need beam dynamics relations that will be used for the analysis of measured data are discussed in the next section.

### 1.3 Beam dynamics relations for studies of beam motion in storage ring

#### 1.3.1 Coordinate system

The motion of electrons is described using a coordinate system related to the ideal orbit of the beam. The coordinate  $s$  denotes the distance along this ideal orbit from an initial reference point. The origin of the coordinate system coincides with the position of right energy or the on-momentum electron also known as synchronous electron of energy  $E_0$  propagating along the ideal orbit. For small deviations from the ideal orbit the motion of the electrons are described by coordinates  $(x, z, s)$  as shown in Figure 1.4 and six phase space coordinates  $(x, x', z, z', s, \delta)$ . The horizontal or radial motion, perpendicular to the direction of motion of electron, is described by the horizontal displacement  $x$  and the horizontal angular deviation  $x' = dx/ds$  from the ideal orbit. Similarly vertical motion is described by the vertical displacement  $z$  and the vertical angular deviation  $z' = dz/ds$ . The longitudinal motion, tangential to the direction of synchronous electron, is described by the longitudinal displacement  $s$  (or in terms of time  $t$  or phase  $\phi$ ) and the relative momentum deviation  $\delta$ . The horizontal displacement  $x$  is positive in the outward direction and negative in the inward direction, the vertical displacement  $z$  is positive in upward direction and negative in downward direction and the longitudinal displacement  $s$  is positive in the forward direction of motion of electron.

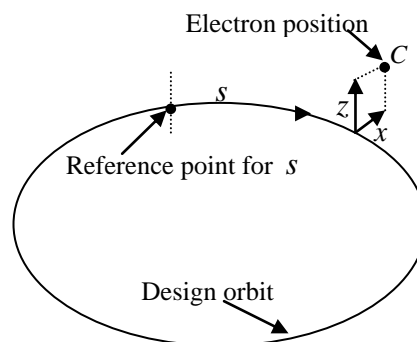


*Fig.1.4. Coordinates for describing the trajectories of electrons*

### 1.3.2 Motion of electrons in storage ring

In an electron storage ring, bunches of electrons are confined [10-11] inside the vacuum chamber of vacuum pressure of the order of  $1 \times 10^{-9}$  Torr. The number of bunches in a storage ring may be equal to or less than the number of available RF buckets. The maximum number of RF buckets in the ring is equal to the ratio of the resonant frequency of RF cavity  $f_{rf}$  to the revolution frequency of electrons  $f_{rev}$ . The electrons confined within a bunch execute oscillations about the closed orbit in horizontal and vertical plane (commonly known as transverse plane) as well as about the synchronous electrons in the longitudinal plane. The oscillations about the closed orbit in transverse plane are known as the betatron oscillations whereas the oscillations with respect to synchronous electrons in longitudinal plane are known as synchrotron oscillations. The number of betatron and synchrotron oscillations in one revolution is known as the betatron and synchrotron tune respectively.

### 1.3.3 Motion of electrons in transverse plane

We consider a magnetic field  $B(r)$  which has the property that there is a plane such that  $B$  at all points of the plane is perpendicular to the plane. This plane is known as median plane and is taken to be horizontal plane of motion.

The linear equations of motion for the horizontal  $x$  and vertical  $z$  motions of the electron are given by Hill's equation [10-14] as

$$\frac{d^2x(s)}{ds^2} + \left( \frac{1}{\rho_b^2(s)} - K(s) \right) x(s) = \frac{1}{\rho_b(s)} \delta \quad 1.1$$

$$\frac{d^2z(s)}{ds^2} + K(s) z(s) = 0 \quad 1.2$$

This is a second order linear differential equation with a coefficient  $K(s)$ , which describes the distribution of focussing strength around the ring. In case of storage ring,  $K(s)$  is

periodic  $K(s+C)=K(s)$ , where  $C$  is the circumference of the ring. The vertical motion  $z$  resembles the equations of motion for a simple harmonic oscillator. If  $K(s)$  would be constant then the solution would be a harmonic oscillation with a constant amplitude and a linear phase advance. The general solution of equation 1.2 describes a vertical betatron oscillation about the ideal orbit given by

$$z(s)=\sqrt{\varepsilon_z \beta_z(s)} \cos[\psi_z(s)+\psi_{z0}] \quad 1.3$$

where  $\varepsilon_z$  is the vertical emittance of the electron making this betatron oscillation,  $\beta_z(s)$  is the beta function at position  $s$  which is periodic with the same periodicity as  $K(s)$  in vertical plane  $\beta_z(s+C)=\beta_z(s)$  and  $\psi_z(s)$  is the vertical betatron phase given as

$$\psi_z(s)=\int_0^s \frac{1}{\beta_z(s)} ds, \psi_{z0} \text{ is an arbitrary constant phase.}$$

The equation of motion 1.1 for horizontal motion contains an additional geometrical focussing term  $(1/\rho_b^2)$  [ $\rho_b$ : bending radius] because of the curvature of the ideal orbit. Particles with different momenta experience different forces under the magnetic field of a bending magnet. A bending magnet which bends the electrons in horizontal plane generates different trajectories for electrons with different momenta. The magnet bends less to a higher momentum electron and bends more to an electron with a lower momentum. The change in closed orbit  $\Delta x$  with momentum change  $\Delta p/p$  is known as dispersion  $\eta_x [\Delta x/(\Delta p/p)]$ . There is no bending of electron in vertical plane so in an ideal storage ring i.e. no magnet alignment errors, vertical dispersion  $\eta_z$  is zero. So for an electron in horizontal plane with a momentum deviation the curvature of the orbit will differ from the ideal orbit, which gives rise to a term in the right hand side of the horizontal equation of motion that is non zero for electrons with a momentum deviation. The general solution of equation 1.1 is given as

$$x(s) = \sqrt{\varepsilon_x \beta_x(s)} \cos[\psi_x(s) + \psi_{x0}] + \eta_x(s) \delta \quad 1.4$$

First term describes the horizontal betatron oscillation about the closed orbit,  $\varepsilon_x$  is the horizontal emittance of the electron making this betatron oscillation,  $\beta_x(s)$  is the horizontal beta function at position  $s$ ,  $\psi_x(s)$  is the horizontal betatron phase  $\psi_x(s) = \int_0^s \frac{1}{\beta_x(s)} ds$ ,  $\psi_{x0}$  is an arbitrary constant phase and the second term describes the off-momentum closed orbit at position  $s$ , which is equal to dispersion function  $\eta_x(s)$  multiplied with the momentum deviation  $\delta$ .

The phase advance during a complete revolution around the storage ring is given by  $2\pi$  times the betatron tune. The betatron tunes in horizontal plane  $\nu_x$  and in vertical plane  $\nu_z$  are given as

$$\nu_x = \frac{\psi_x}{2\pi} = \frac{1}{2\pi} \oint \frac{1}{\beta_x(s)} ds \quad 1.5$$

$$\nu_z = \frac{\psi_z}{2\pi} = \frac{1}{2\pi} \oint \frac{1}{\beta_z(s)} ds \quad 1.6$$

where  $\oint$  is the integral around the whole ring. Differentiating equation 1.3 and 1.4 with respect to  $s$ , we get

$$z'(s) = -\sqrt{\frac{\varepsilon_z}{\beta_z(s)}} [\sin(\psi_z(s) + \psi_{z0}) + \alpha_z(s) \cos(\psi_z(s) + \psi_{z0})] \quad 1.7$$

$$x'(s) = -\sqrt{\frac{\varepsilon_x}{\beta_x(s)}} [\sin(\psi_x(s) + \psi_{x0}) + \alpha_x(s) \cos(\psi_x(s) + \psi_{x0})] + \eta'_x(s) \delta \quad 1.8$$

Using equations 1.3 and 1.7, we get

$$\varepsilon_z = \gamma_z(s) z^2(s) + 2\alpha_z(s) z(s) z'(s) + \beta_z(s) z'^2(s) \quad 1.9$$

Using equations 1.4 and 1.8, we get

$$\varepsilon_x = \gamma_x(s) [x(s) - \eta_x(s)\delta]^2 + 2\alpha_x(s) [x(s) - \eta_x(s)\delta][x'(s) - \eta'_x(s)\delta] + \beta_x(s) [x'(s) - \eta'_x(s)\delta]^2 \quad 1.10$$

Where  $\varepsilon_x$  and  $\varepsilon_z$  are the courant-snyder invariant and represent emittance in horizontal and

vertical plane respectively,  $\alpha_x(s) = -\frac{1}{2} \frac{d\beta_x(s)}{ds}$ ,  $\alpha_z(s) = -\frac{1}{2} \frac{d\beta_z(s)}{ds}$ ,  $\gamma_x(s) = \frac{1 + \alpha_x^2(s)}{\beta_x(s)}$ ,

$\gamma_z(s) = \frac{1 + \alpha_z^2(s)}{\beta_z(s)}$  and beta function  $\beta_x(s)$  and  $\beta_z(s)$  introduced in above equations are known

as twiss parameters. These twiss parameters  $\beta_x(s), \alpha_x(s), \gamma_x(s), \beta_z(s), \alpha_z(s), \gamma_z(s)$  with

dispersion function  $\eta_x(s)$  are known as the optical functions of the lattice. The optical

functions are all periodic functions of  $s$  with period  $C$ . In equation 1.8 and 1.10,

$\eta'_x(s) = \frac{d\eta_x(s)}{ds}$  is the derivative of dispersion function  $\eta_x(s)$  which is also periodic i.e.

$$\eta'_x(s+C) = \eta'_x(s).$$

Equations 1.9 and 1.10 are the equations of phase space ellipse in vertical and horizontal

plane respectively. The phase space ellipse at position  $s$  in vertical plane  $(z, z')$  is shown in

Figure 1.5 [15]. Similar equation of ellipse is obtained in horizontal plane  $(x, x')$  when  $\delta=0$

in equation 1.10.

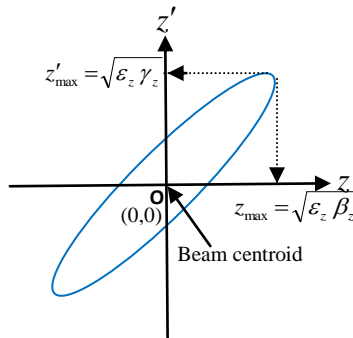


**Fig.1.5. Phase space ellipse at position  $s$  in the ring**

The shape and orientation of the two ellipses change as the  $s$  position vary and the electron moves along the ellipses in vertical and horizontal phase space. In the vertical phase space the ellipse at position  $s$  has its centre at  $z(s)=0$  and  $z'(s)=0$ , whereas in the horizontal phase space the ellipse centre at position  $s$  depends on the momentum deviation  $\delta$  of the electron and the ellipse has its centre at  $x(s)=\eta_x(s)\delta$  and  $x'(s)=\eta'_x(s)\delta$  as shown in Figure 1.6.

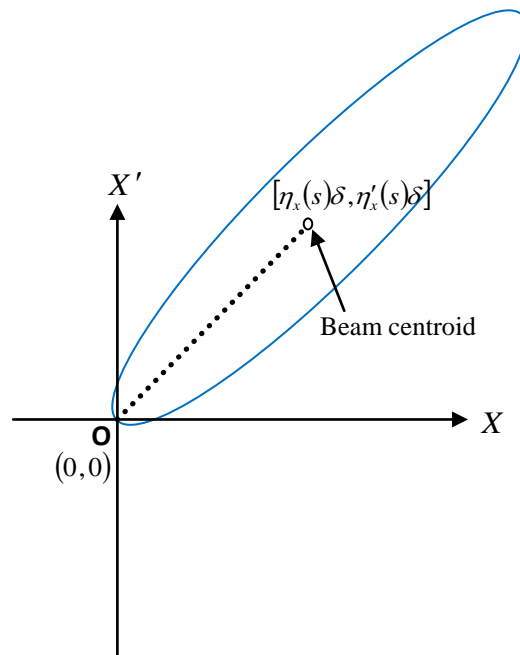


**Fig.1.6. Phase space ellipse at position  $s$  in horizontal plane at dispersion location  $\eta_x(s)$**

The phase space coordinate  $(y, y')$  where  $y=x, z$  represents for horizontal and vertical plane motion at a position  $s_0$  are related to the other position  $s_1$  through a transfer matrix  $M(s_1/s_0)$  as

$$\begin{pmatrix} y \\ y' \end{pmatrix}_{s_1} = M(s_1/s_0) \begin{pmatrix} y \\ y' \end{pmatrix}_{s_0} \quad 1.11$$

$$\text{where } M(s_1/s_0) = \begin{bmatrix} \frac{\sqrt{\beta_{s_1}}}{\sqrt{\beta_{s_0}}} (\cos \Delta\psi + \alpha_{s_0} \sin \Delta\psi) & \sqrt{\beta_{s_0} \beta_{s_1}} \sin \Delta\psi \\ \frac{(\alpha_{s_0} - \alpha_{s_1}) \cos \Delta\psi - (1 + \alpha_{s_0} \alpha_{s_1}) \sin \Delta\psi}{\sqrt{\beta_{s_0} \beta_{s_1}}} & \sqrt{\frac{\beta_{s_0}}{\beta_{s_1}}} (\cos \Delta\psi - \alpha_{s_1} \sin \Delta\psi) \end{bmatrix} \quad 1.12$$

where  $\beta_{s_0}, \beta_{s_1}$  and  $\alpha_{s_0}, \alpha_{s_1}$  are the twiss parameters as defined above at position  $s_0$  and  $s_1$  respectively and  $\Delta\psi$  is the phase difference between the position  $s_0$  and  $s_1$ .

For one turn transfer matrix, position  $s_0 = s_1$ , twiss parameters are periodic, we get from relation 1.12 as

$$M_y = \begin{bmatrix} \cos 2\pi\nu_y + \alpha_y \sin 2\pi\nu_y & \beta_y \sin 2\pi\nu_y \\ -\gamma_y \sin 2\pi\nu_y & \cos 2\pi\nu_y - \alpha_y \sin 2\pi\nu_y \end{bmatrix} \quad 1.13$$

The condition for stable motion,  $\cos 2\pi\nu_y \leq 1 \Rightarrow |\text{Trace } M_y| \leq 2$ .

### 1.3.4 Twiss parameters propagation in ring

Let the transfer matrix from position  $s_0$  to  $s_1$  is given as  $M(s_1/s_0) = \begin{bmatrix} m_{11} & m_{12} \\ m_{21} & m_{22} \end{bmatrix}$  then the

twiss parameter  $\beta, \alpha$  and  $\gamma$  propagation [14] from location  $s_0$  to  $s_1$  is given as

$$\begin{pmatrix} \beta(s_1) \\ \alpha(s_1) \\ \gamma(s_1) \end{pmatrix} = \begin{bmatrix} m_{11}^2 & -2m_{11}m_{12} & m_{12}^2 \\ -m_{11}m_{21} & m_{11}m_{22} + m_{12}m_{21} & -m_{12}m_{22} \\ m_{21}^2 & -2m_{21}m_{22} & m_{22}^2 \end{bmatrix} \begin{pmatrix} \beta(s_0) \\ \alpha(s_0) \\ \gamma(s_0) \end{pmatrix} \quad 1.14$$

The estimation of the periodic solution for the dispersion also proceeds in the same manner except for the use of  $3 \times 3$  order transfer matrix to describe one turn. The periodicity condition of dispersion is written as

$$\begin{bmatrix} \eta_x \\ \eta'_x \\ 1 \end{bmatrix} = \begin{bmatrix} m_{11} & m_{12} & m_{13} \\ m_{21} & m_{22} & m_{23} \\ 0 & 0 & 1 \end{bmatrix} \begin{bmatrix} \eta_x \\ \eta'_x \\ 1 \end{bmatrix} \quad 1.15$$

On solving relation 1.15, we get  $\eta'_x = \frac{m_{21}m_{13} + m_{23}(1 - m_{11})}{2 - m_{11} - m_{22}}$  and  $\eta_x = \frac{m_{12}\eta'_x + m_{13}}{1 - m_{11}}$ , using these

initial value of  $\eta_x$  and  $\eta'_x$  and using transfer matrix as in relation 1.15, we get the value of  $\eta_x$  and  $\eta'_x$  along the circumference of ring.

Using the above relation 1.14 and 1.15, we get the optical functions of the lattice along the circumference of the ring. The variation of beta function in horizontal plane  $\beta_x$ , in vertical plane  $\beta_z$  and dispersion  $\eta_x$  in one unit cell of Indus-2 is shown in Figure 1.7.

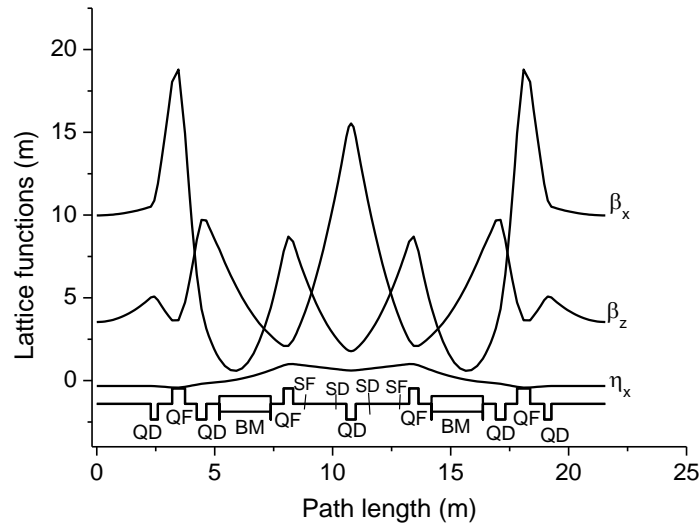


**Fig.1.7. Lattice functions in Indus-2, QD: defocusing quadrupole, QF: focusing quadrupole, BM: bending magnet, SF: focusing sextupole and SD: defocusing sextupole**

### 1.3.5 Equilibrium emittance in an electron storage ring

In an electron storage ring, beam sizes in horizontal, vertical and in longitudinal plane are important parameters for the analysis of beam lifetime data. The transverse beam sizes are obtained from the emittance of beam.

The energy loss per turn due to the emission of synchrotron radiation for synchronous electron is proportional to the fourth power of electron energy. The synchrotron radiation is

emitted along the instantaneous direction of motion of electron and the momentum of the electron is decreased along this direction. The RF cavity restores the momentum longitudinally without any change in transverse momentum. The net effect is a decrease in the transverse angular deviation and in the amplitude of betatron oscillation known as radiation damping. The discrete emission of the synchrotron radiation introduces quantum excitations on the horizontal betatron oscillations. If the photon is emitted at a location with dispersion, the electron will oscillate around a new off-momentum orbit which will on average increase the betatron oscillation amplitude. The equilibrium between the quantum excitation and the radiation damping gives a Gaussian distribution of the horizontal motion of the electrons. For the estimation of equilibrium emittance and other parameters like momentum compaction factor, damping time, natural energy spread etc. we require the evaluation of five synchrotron radiation integrals  $I_1$  to  $I_5$  [16-17] which are as follows:

$$\text{First synchrotron radiation integral } I_1 = \int_{\text{dipoles}} \frac{\eta_x(s)}{\rho_b(s)} ds \quad 1.16$$

$$\text{Second synchrotron radiation integral } I_2 = \int_{\text{dipoles}} \frac{1}{\rho_b^2(s)} ds \quad 1.17$$

$$\text{Third synchrotron radiation integral } I_3 = \int_{\text{dipoles}} \frac{1}{\rho_b^3(s)} ds \quad 1.18$$

$$\text{Fourth synchrotron radiation integral } I_4 = \int_{\text{dipoles}} \frac{\eta_x(s)}{\rho_b(s)} \left( \frac{1}{\rho_b^2(s)} + 2k(s) \right) ds, \quad k(s) \text{ is the}$$

$$\text{quadrupole strength } k(s) = -\frac{1}{B \rho_b} \frac{dB}{dx}, \text{ for separated function dipole } k(s) = 0. \quad 1.19$$

$$\text{Fifth synchrotron radiation integral } I_5 = \int_{\text{dipoles}} \frac{H(s)}{\rho_b^3(s)} ds, \quad H(s) \text{ is the } H \text{ function given as}$$

$$H(s) = \gamma_x(s) \eta_x^2(s) + 2\alpha_x(s) \eta_x(s) \eta_x'(s) + \beta_x(s) \eta_x'^2(s) \quad 1.20$$

For Indus-2 operating lattice, bending radius  $\rho_b=5.55m$ , the values of five synchrotron radiation integrals are as follows:

$$I_1=1.266m, I_2=1.132m^{-1}, I_3=0.204m^{-2}, I_4=0.0411m^{-1} \text{ and } I_5=0.0158m^{-1}.$$

Using the above integrals, the horizontal equilibrium emittance [11] in electron storage ring is given by

$$\varepsilon_x = c_q \gamma^2 \frac{I_5}{J_x I_2} \quad 1.21$$

where  $c_q \approx 3.83 \times 10^{-13}m$ ,  $\gamma$  is the relativistic factor,  $J_x$  is the horizontal damping partition

number given by  $J_x = 1 - \frac{I_4}{I_2}$ .

The emission of synchrotron radiation in an electron storage ring has a damping effect on transverse betatron oscillations, the horizontal damping time  $\tau_x$  is given by [11]

$$\tau_x = \frac{2}{J_x} \frac{E_0}{U_0} T_0 \quad 1.22$$

$E_0$  is the synchronous energy of electron,  $T_0$  is the revolution time and  $U_0$  is the energy loss per turn given as

$$U_0(KeV) = \frac{88.5 E_0^4 (GeV)}{\rho_b(m)} \quad 1.23$$

Similarly the vertical damping time is given by

$$\tau_z = \frac{2}{J_z} \frac{E_0}{U_0} T_0 \quad 1.24$$

$J_z$  is the vertical damping partition number and its value is 1 because the vertical dispersion is assumed to be zero, so  $I_4 = 0$ .

From relation 1.21, 1.22 and 1.23, we see that the horizontal emittance and damping time in horizontal and vertical plane depends on the beam energy. The variation in horizontal

emittance and the damping time in horizontal and vertical plane in Indus-2 with different beam energy are shown in Figure 1.8 and 1.9 respectively.

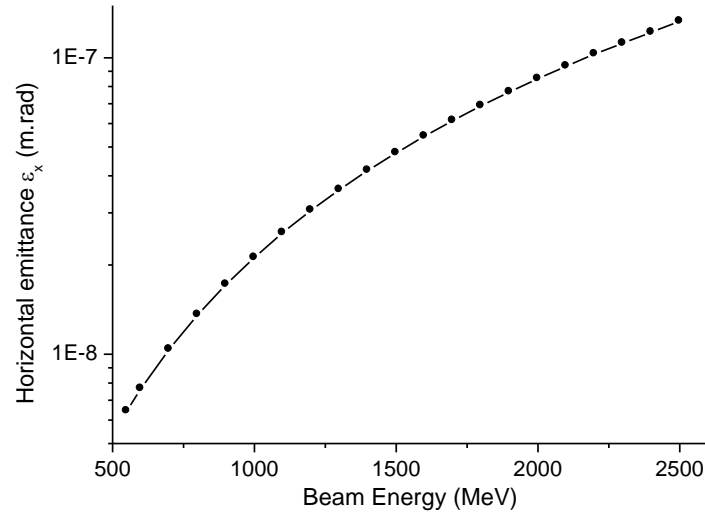


**Fig.1.8. Variation in horizontal beam emittance with beam energy in Indus-2**

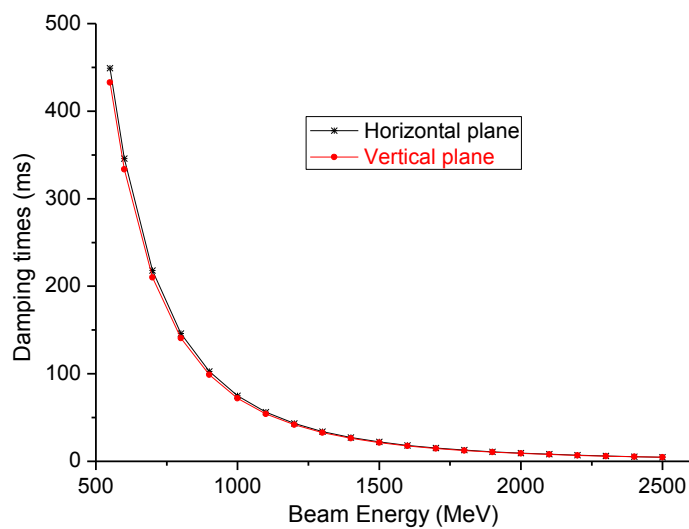


**Fig.1.9. Variation in damping time in transverse plane with beam energy in Indus-2**

The quantum excitation process that increases the horizontal betatron oscillation amplitude is not present for the vertical betatron oscillation amplitude. Due to finite opening angle of the

emitted synchrotron radiation there is small excitation in vertical betatron oscillations. The vertical emittance from the opening angle of the synchrotron radiation [18] is given by

$$\varepsilon_z = \frac{13}{55} \frac{c_q}{J_z I_2} \oint \frac{\beta_z(s)}{\rho_b^3(s)} ds \quad 1.25$$

The vertical emittance from the opening angle of the synchrotron radiation is a very small number. In practice, there are misalignments of the magnets like rotational error of quadrupoles about the beam direction, vertical misalignment of sextupoles, which give the coupling between horizontal and vertical betatron oscillations that determine the vertical emittance in an electron storage ring. The measurement of betatron coupling is thus important for the estimation of vertical beam emittance or the vertical beam size. The measurement of betatron coupling and vertical beam size in Indus-2 is presented in chapter 3.

#### 1.4 Longitudinal motion of electron

An electron with the nominal energy  $E_0$  travelling around the ring on the ideal orbit will emit a certain amount of energy  $U_0$  per turn. The energy loss due to the emission of synchrotron radiation is compensated by the accelerating radio frequency cavities in the ring. If the electron regains the energy  $U_0$  in each turn, it will continue to circulate on the ideal orbit. This electron is known as synchronous electron. In order for the synchronous electron to regain the same energy each turn the RF frequency  $f_{rf}$  must be an integer multiple of electron revolution frequency  $f_{rev}$ , so  $f_{rf} = h f_{rev}$  where  $h$  is the harmonic number. In Indus-2, harmonic number  $h$  is 291, so there are 291 points at a given time on the circumference of ring where an electron could be located and arrive synchronously. The segments of the circumference centred at these locations are called RF buckets. The group of electrons in these RF buckets are called bunches. Not all RF buckets need to be filled with electrons to minimize the ion trapping [19-22] problem in electron storage ring.

Due to the ultra-relativistic motion of electrons in storage ring, a small momentum deviation will not affect the velocity of the electron but will affect the electron orbit. An electron passing through RF cavity with a momentum deviation  $\delta$  will follow the dispersive orbit instead of the ideal orbit, which will give a different path length around the storage ring. The ratio of the relative change in path length to the momentum deviation is known as the momentum compaction factor  $\alpha_c$  and is given by  $\alpha_c = \frac{(\Delta C/C)}{\delta} = \frac{I_1}{C}$ , where  $\Delta C$  is the change in path length and  $C$  is the circumference of the ring,  $I_1$  is the first synchrotron integral defined above, The momentum compaction factor  $\alpha_c$  is positive, so an electron with normally positive momentum deviation will travel on a longer path around the ring as compared to path travel by synchronous electron as is shown in Figure 1.10 [13].

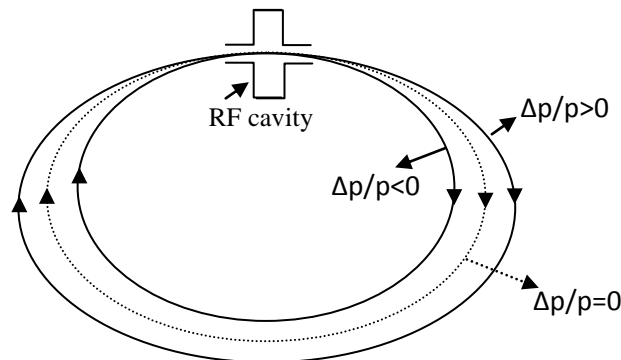


**Fig.1.10. Path for on-momentum and off-momentum electrons**

The phase stable region of RF for stable motion of electrons in an electron storage ring is

$\frac{\pi}{2} < \phi < \pi$ . An electron  $B_1$  that has the same momentum as the synchronous electron  $A_1$  but arrive at the RF cavity earlier than the synchronous electron as shown in Figure 1.11 will receive more energy gain than the synchronous electron. During the next turn it will travel on a longer path than the synchronous electron, so it will take a longer time than for the

synchronous electron. During the next pass of the RF cavity the electron will be closer in time to the synchronous electron. After a number of turns the electron will overtake the synchronous electron and receive a smaller energy gain than the synchronous electron. Similar explanation is for the electron  $C_1$  which gains less energy from RF cavity than for synchronous electron so it will move on a shorter path length and will take less time to reach RF cavity than synchronous electron in next turn. After a number of turns the electron  $C_1$  will overtake the synchronous electron and receive a larger energy gain than the synchronous electron. This process gives rise to an oscillation in the longitudinal phase space  $(\phi, \delta)$  around the synchronous electron. These oscillations are known as synchrotron oscillations. The electrons are stable i.e. they continue to make synchrotron oscillations inside the area of longitudinal phase space which is known as RF bucket. The RF bucket in Indus-2 for RF cavity voltage 1200 kV and beam energy 2.5 GeV is shown in Figure 1.12.

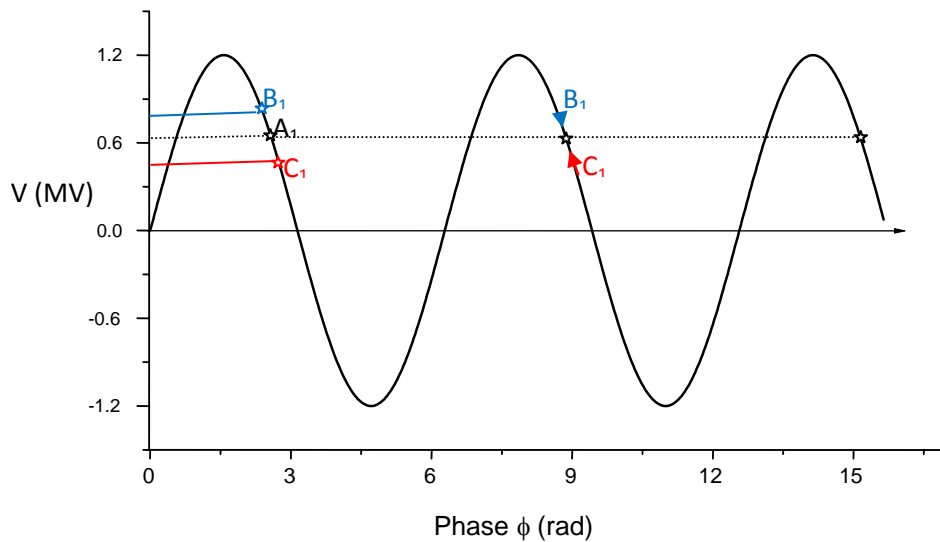


**Fig.1.11. Phase stability of electrons**

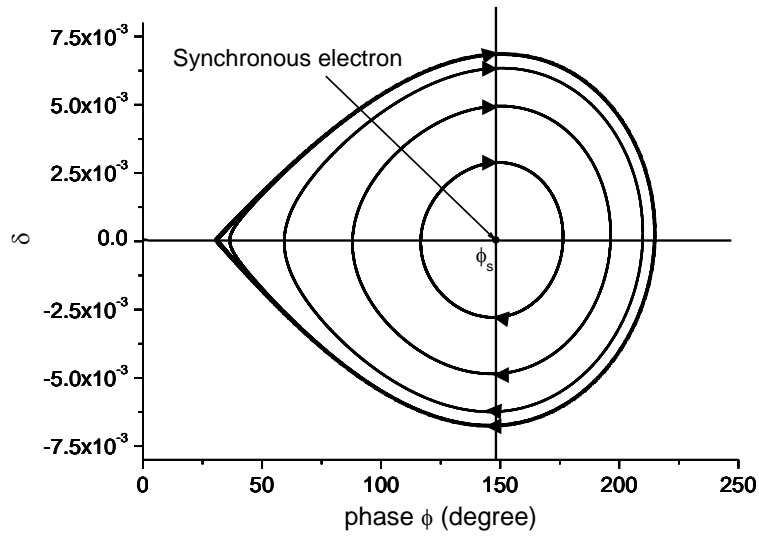


*Fig.1.12. RF bucket in Indus-2*

#### 1.4.1 Longitudinal equation of motion

The longitudinal equations of motion [14] are given as

$$\frac{d\phi}{dt} = -\alpha_c \omega_{rf} \delta \quad 1.26$$

$$\frac{d\delta}{dt} = \frac{eV_{rf}(\phi) - U(\delta)}{E_0 T_0} \quad 1.27$$

where  $\omega_{rf}$  is the angular RF frequency,  $V_{rf}(\phi)$  is the RF voltage,  $U(\delta)$  is the energy loss per turn,  $T_0$  is the revolution time of electron and  $E_0$  is the synchronous energy.

From the above equation we get

$$\frac{d^2\phi}{dt^2} + \omega_s^2 \phi = 0 \quad 1.28$$

where  $\omega_s$  is the angular synchrotron frequency given by

$$\omega_s = 2\pi \sqrt{-\frac{eV_{rf}}{E_0} \frac{\alpha_c h \cos \phi_s}{2\pi T_0^2}} \Rightarrow f_s = \frac{\omega_s}{2\pi} = \sqrt{-\frac{eV_{rf}}{E_0} \frac{\alpha_c h \cos \phi_s}{2\pi T_0^2}}$$

where  $\phi_s$  is synchronous phase. For small oscillation amplitude the electrons in longitudinal phase space  $(\phi, \delta)$  will perform synchrotron oscillation in elliptical orbit as shown in Figure 1.12 around the synchronous electron with synchrotron oscillation frequency given above. The number of synchrotron oscillation per turn is known as synchrotron tune  $\nu_s$  and is given as

$$\nu_s = \frac{f_s}{f_{rev}} = \sqrt{-\frac{eV_{rf}}{E_0} \frac{\alpha_c h \cos \phi_s}{2\pi}} \quad 1.29$$

Electrons with large amplitudes of synchrotron oscillation can escape from the RF bucket. This gives a maximum momentum deviation known as RF acceptance above which electron will be lost from the storage ring.

#### 1.4.2 Damping of synchrotron oscillation

The energy loss per turn  $U(\delta)$  depends on the momentum deviation. The electron of positive momentum deviation will lose more energy than synchronous electron and electron of negative momentum deviation will lose less energy than synchronous electron, it will give rise to a damping of synchrotron oscillation in longitudinal phase space. The longitudinal damping time is given by

$$\tau_\varepsilon = \frac{2}{J_\varepsilon} \frac{E_0 T_0}{U_0} \quad 1.30$$

where  $J_\varepsilon$  is the longitudinal damping partition number given by

$J_\varepsilon = 2 + \frac{I_4}{I_2}$ , where  $I_2$  and  $I_4$  are second and fourth synchrotron radiation integral defined as

above. So the emission of synchrotron radiation has a damping effect on the synchrotron oscillations. The discrete emission of synchrotron radiation induces noise on the beam and causes the amplitude of the synchrotron oscillations to increase. The equilibrium between the radiation damping and the quantum excitation gives the distribution of the momentum deviations of the electrons which is Gaussian and the standard deviation of the distribution is known as the equilibrium momentum spread or the natural momentum spread and is given by

$$(\sigma_\varepsilon/E_0)^2 = C_q \gamma^2 \frac{I_3}{J_\varepsilon I_2} \quad 1.31$$

where  $I_3$  is the third synchrotron radiation integral,  $J_\varepsilon$  is the damping partition number,  $I_2$  is second synchrotron radiation integral,  $C_q$  and  $\gamma$  are constant as defined above. The longitudinal damping time and equilibrium energy spread with beam energy in Indus-2 is shown in Figure 1.13.

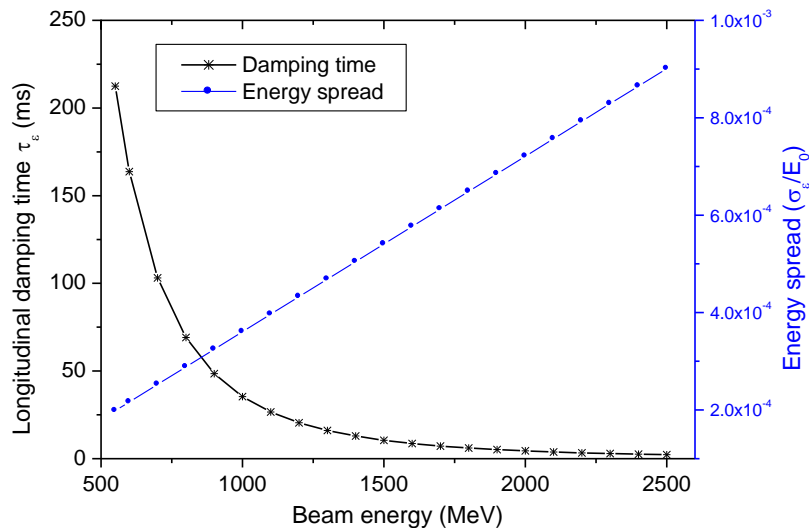


**Fig.1.13. Longitudinal damping time and energy spread with beam energy in Indus-2**

## 1.5 Electron beam sizes in longitudinal and transverse plane

For a sinusoidal RF system and assuming small synchrotron oscillation amplitudes, the longitudinal distribution [23-24] will also be Gaussian distribution if the momentum deviation distribution is a Gaussian distribution. The standard deviation of the distribution is called the bunch length and is given by

$$\sigma_s = \frac{\alpha_c c}{2\pi f_s} \frac{\sigma_\varepsilon}{E_0} = \sqrt{-\frac{E_0}{eV_{rf}} \frac{2\pi\alpha_c hc^2}{\omega_{rf}^2 \cos\phi_s} \frac{\sigma_\varepsilon}{E_0}} \quad 1.32$$

where  $c$  is the speed of light,  $f_s$  is the synchrotron frequency and  $(\sigma_\varepsilon/E_0)$  is the momentum spread as defined by relation 1.31 above.

The horizontal beam size and horizontal beam divergence of the electrons at location  $s$  in the storage ring is given by

$$\sigma_x(s) = \sqrt{\varepsilon_x \beta_x(s) + [\eta_x(s)(\sigma_\varepsilon/E_0)]^2} \quad 1.33$$

$$\sigma_{x'}(s) = \sqrt{\varepsilon_x \gamma_x(s) + [\eta'_x(s)(\sigma_\varepsilon/E_0)]^2} \quad 1.34$$

Similarly vertical beam size and vertical beam divergence of the electrons at location  $s$  in the storage ring is given by

$$\sigma_z(s) = \sqrt{\varepsilon_z \beta_z(s) + [\eta_z(s)(\sigma_\varepsilon/E_0)]^2} \quad 1.35$$

where  $\eta_z(s)$  is the vertical dispersion function at position  $s$

$$\sigma_{z'}(s) = \sqrt{\varepsilon_z \gamma_z(s) + [\eta'_z(s)(\sigma_\varepsilon/E_0)]^2} \quad 1.36$$

where  $\eta'_z(s)$  is the derivative of vertical dispersion function

where  $\beta_x(s), \beta_z(s)$  are the beta functions at position  $s$  in horizontal and vertical plane respectively.  $\gamma_x(s), \gamma_z(s)$  are the horizontal and vertical gamma functions (twiss parameter) at position  $s$  respectively.

The momentum spread and the bunch length at stored beam current  $I$  is constant around the ring whereas horizontal and vertical beam sizes and beam divergence depends on the position  $s$  in the ring.

## **1.6 Beam loss mechanism in Indus-2**

The stored electrons orbiting in an electron storage ring may be lost due to various causes [25-26]. For a well designed storage ring there are two main classes for electron losses, first is the loss due to scattering and another is the loss due to beam instabilities [27]. While the electron losses due to scattering with other particles is a single particle effect leading to a gradual loss of electrons from the electron beam whereas electron losses due to beam instabilities is a multi particle effect and later can lead to a partial or complete loss of electron beam. The multi particle effect arises due to electromagnetic interaction of the high intensity electron beam with its wake fields which are induced due to resistive wall of vacuum chamber, broad band impedance and narrow band impedance. The broad band impedance in the ring arises due to non uniform cross section of the components in the ring like bellows, kickers and beam position indicators etc. whereas narrow band impedance in the ring arises mainly due to RF cavities. The wake fields due to broad band impedance are short range whereas the wake field due to narrow band impedance are long range. The wake fields affect the electron beam transversely or longitudinally. Losses due to beam instabilities are generally very fast. Slow instabilities can be suppressed by natural damping i.e. radiation damping due to synchrotron radiation emission and Landau damping introduced by partial RF

buckets fill or efficiently cured by using transverse and longitudinal multi-bunch feedback systems [28].

The instantaneous lifetime  $\tau_t$  of stored electron beam during beam current decay is estimated as  $-I/(dI/dt)$  where  $dI/dt$  is the instantaneous decay rate at a particular current  $I$  at time  $t$ . Long beam lifetimes are desirable for the users of synchrotron radiation sources since it gives higher integrated photon flux, reduce the number of refills necessary and improve the stability by reducing thermal loading effects due to the varying current. There are several effects that limit the beam lifetime in an electron storage ring [25]. The beam lifetime is usually determined by the elastic and inelastic scattering of the electrons with the residual gas atoms known as vacuum lifetime  $\tau_v$ , the electron-electron scattering within the bunch known as Touschek lifetime  $\tau_{tous}$  and due to quantum excitation known as quantum lifetime  $\tau_q$ . The total beam lifetime  $\tau_t$  is defined as

$$\frac{1}{\tau_t} = \frac{1}{\tau_v} + \frac{1}{\tau_{tous}} + \frac{1}{\tau_q} \quad 1.37$$

The mechanism leading to electron loss varies for the different lifetime limitations. For the elastic scattering between electrons and residual gas atoms, the electrons are deflected and undergo large betatron oscillations. If the oscillation amplitude is larger than the acceptance of the ring, the electrons will be lost. For the electron-electron scattering within a bunch and inelastic scattering between electrons and residual gas atoms, there is a change in energy of electrons. If the change in energy is larger than the RF acceptance or transverse momentum acceptance, the electron will be lost. So the apertures are the main limitation in all accelerators and electron storage ring. The apertures of an accelerator are not only defined physically by the vacuum chamber but also by the electromagnetic fields which guide and accelerate the electron beam and confining it in six dimensional phase space. In designing

electron storage ring three apertures i.e. physical aperture, dynamic aperture and momentum aperture are defined which are explained as follows:

## 1.6.1 Acceptance of electron beam in Indus-2

### 1.6.1.1 Physical aperture

The physical aperture is defined from the particle transverse linear motion and the physical limit in horizontal and vertical plane  $a_x(s)$  and  $a_z(s)$  respectively. For horizontal motion, as from relation 1.4, the horizontal displacement of electron at location  $s$  is given as

$$x(s) = \sqrt{A_x \beta_x(s)} \cos \psi_x(s) + \eta_x(s) \delta$$

A particle will be lost if  $|x(s)| \geq a_x(s)$ , where  $a_x(s)$  is the half width of vacuum chamber. Since we consider many turns we drop the betatron phase and find the physical acceptance as the maximum possible betatron amplitude  $A_x$  known as admittance or maximum emittance by identifying  $x(s)$  with its limit  $a_x(s)$ .

The physical acceptance in horizontal plane  $A_{x,phys}$  is the minimum value of  $A_x$  which exists at least one location  $s_0$  around the ring for which  $x_{\max}(s_0) = a_x(s_0)$ . It gives the acceptance [29] that can be sustained by the ring, so

$$A_{x,phys}(\delta) = \min_{s_0 \in [0, C]} \left[ \frac{(a_x(s_0) - \eta_x(s_0) \delta)^2}{\beta_x(s_0)} \right] \quad 1.38$$

where  $\beta_x(s_0)$  and  $\eta_x(s_0)$  are the beta function and dispersion function at location  $s_0$ .

Physical acceptance  $x_{phys}(s, \delta)$  at location  $s$  with energy deviation  $\delta$ , using the above value of  $A_{x,phys}(\delta)$  is given as

$$x_{phys}(s, \delta) = \pm \left( \sqrt{A_{x,phys}(\delta) \beta_x(s)} \right) + \eta_x(s) \delta \quad 1.39$$

Using the Indus-2 lattice functions  $\beta_x, \eta_x$  and half width of vacuum chamber  $a_x=32$  mm at all locations along the circumference  $C$ , the physical acceptance in horizontal plane for energy deviation  $\delta=0$  and 0.01 was estimated using the above relations. A comparison in physical acceptance for  $\delta=0$  and 0.01 in one unit cell of Indus-2 is shown in Figure 1.14.

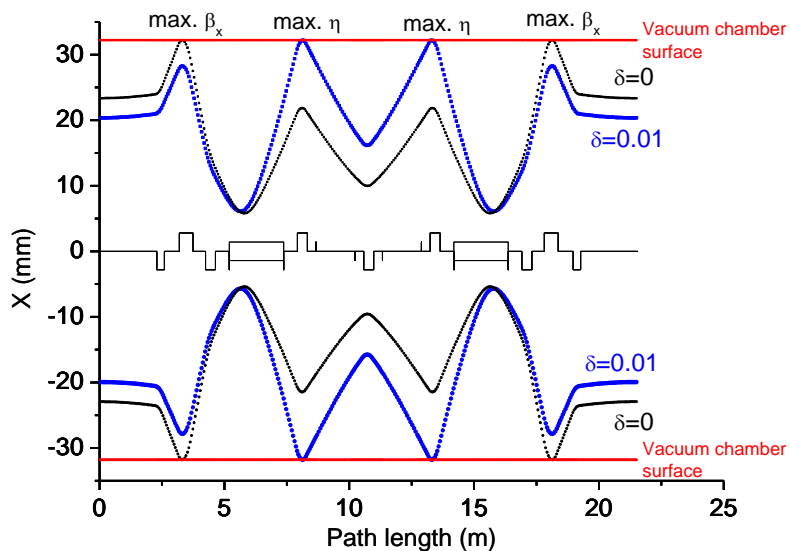


**Fig.1.14. Physical acceptance in horizontal plane in Indus-2 for energy deviation  $\delta=0, \pm 1\%$**

The above results show that the on-momentum electrons for which  $\delta=0$  are lost at maximum  $\beta_x$  locations whereas off-momentum electrons  $\delta \neq 0$  are lost at maximum dispersion  $\eta_x$  locations.

As there is no vertical dispersion (or negligible small), the physical acceptance  $A_{z,phys}$  is the minimum value of acceptance such that there exists at least one location  $s_0$  around the ring for which  $z_{\max}(s_0)=a_z(s_0)$ , where  $a_z(s_0)$  is the half width of vacuum chamber. It gives the minimum value of acceptance in vertical plane that can be sustained by the ring and is given as

$$A_{z,phys} = \min_{s_0 \in [0, C]} \left[ \frac{a_z^2(s_0)}{\beta_z(s_0)} \right] \quad 1.40$$

Physical acceptance in vertical plane  $z_{phys}$  at location  $s$ , using the above value of  $A_{z,phys}$  is given as

$$z_{phys}(s) = \pm \sqrt{A_{z,phys} \beta_z(s)} \quad 1.41$$

The physical acceptance in vertical plane in Indus-2 was estimated using beta functions and uniform aperture of vacuum chamber  $a_z = 17 \text{ mm}$ . The physical acceptance in vertical plane in one unit cell of Indus-2 is shown in Figure 1.15.

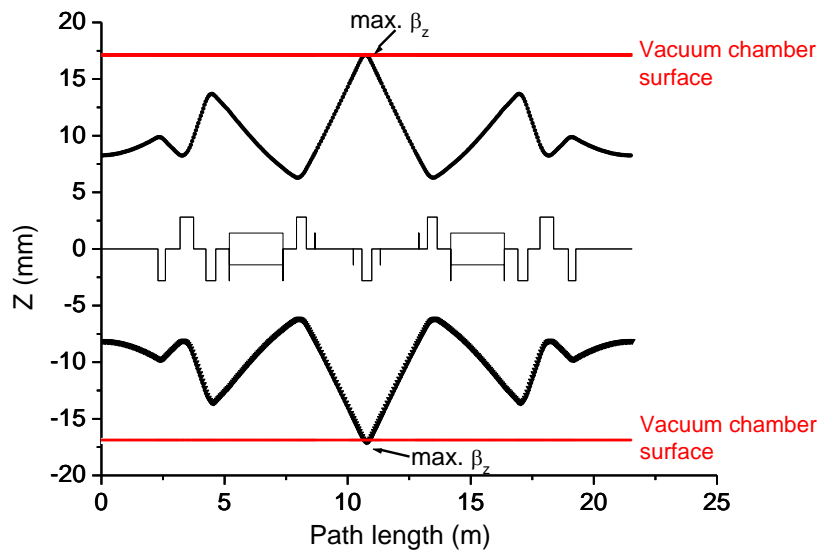


**Fig.1.15. Physical acceptance in vertical plane in Indus-2**

The above results show that electrons are lost in vertical plane at maximum  $\beta_z$  locations in the ring.

### 1.6.1.2 Dynamic aperture

The particle motion in an accelerator is linear if the lattice is made of perfect dipoles and quadrupoles. In a real storage ring, electrons are subjected to non-linear forces of the sextupole magnets and multipole field errors of dipoles, quadrupoles and sextupoles. With the increase in betatron amplitude, the motion of electrons becomes more and more non-linear due to the presence of such forces. The dynamic aperture is the smallest initial amplitude of the electron whose motion will cause its amplitude to increase until it is lost from the vacuum chamber. So the dynamic aperture is defined to be the maximum stable initial transverse amplitude in the presence of nonlinearities. A proper choice of tune point [30] helps in enhancing the dynamic aperture.

To find the dynamic aperture for on momentum electrons ( $\delta=0$ ) at the centre of long straight section in Indus-2, single particle tracking was carried out using particle tracking codes MAD-8 [31], ELEGANT [32] and RACETRACK [33]. The tracking was carried out up to 10,000 turns which is more than one damping time  $\tau_x$  at beam energy 2.5 GeV. The results of dynamic aperture using above code are shown in Figure 1.16(a-c). Figure 1.16(a) and (b) shows the dynamic aperture in presence of systematic errors using MAD-8 and ELEGANT code respectively whereas Figure 1.16(c) shows the dynamic aperture using RACETRACK code in presence of both systematic and random errors using 20 different random seeds.

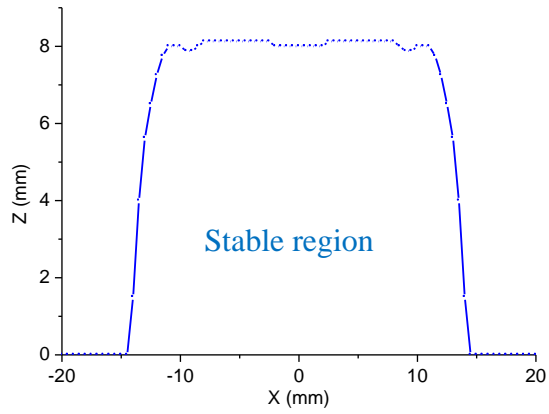


*Fig.1.16(a). Dynamic aperture using MAD-8 code with systematic multi-pole field errors*

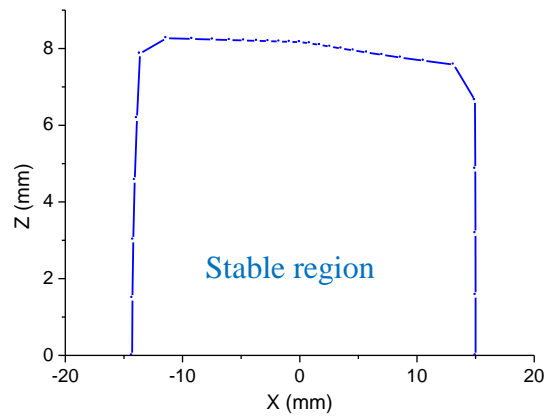


*Fig.1.16(b). Dynamic aperture using ELEGANT code with systematic multi-pole field errors*

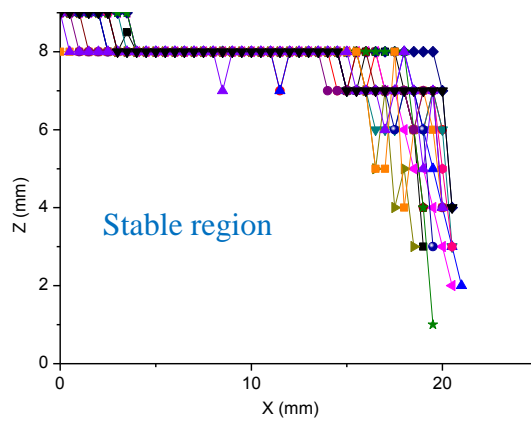


*Fig.1.16(c). Dynamic aperture using RACETRACK code*

The above results show that with aperture limitations in Indus-2, the dynamic aperture at the centre of long straight section is ~15 mm and ~6 mm in horizontal and vertical plane respectively. With these values of apertures, we can get apertures at other location in ring by normalizing it with  $\beta$  function (if  $\beta_x(s_0)$  and  $\beta_z(s_0)$  are the beta function at the centre of long straight section where the aperture is 15 mm and 6 mm respectively then the aperture at location  $s$  where the beta function is  $\beta_x(s)$  and  $\beta_z(s)$  will be  $\sqrt{\beta_x(s)/\beta_x(s_0)} \times 15 \text{ mm}$  and  $\sqrt{\beta_z(s)/\beta_z(s_0)} \times 6 \text{ mm}$  in horizontal and vertical plane respectively). All the three codes give nearly same results. Ideally the dynamic aperture should be more than or equal to the physical aperture.

### 1.6.1.3 Momentum aperture

Momentum aperture in the horizontal plane depends on the dispersion function and it varies along the circumference of the storage ring.

An on-axis electron that suffer a large angle electron-electron scattering or inelastic scattering with residual gas atoms at the ring location  $s_0$ , its momentum deviation changes to  $\delta_0$  moves on a different closed orbit and start executing oscillation around it with invariant  $A_x$ .

$$x(s) = \sqrt{A_x \beta_x(s)} \cos \psi_x(s) + \eta_x(s) \delta_0$$

$$A_x = \gamma_x(s_0) x^2(s_0) + 2\alpha_x(s_0) x(s_0) x'(s_0) + \beta_x(s_0) x'^2(s_0)$$

At location of scattering  $s_0$ ,  $x(s_0) = \eta_x(s_0) \delta_0$  and  $x'(s_0) = \eta'_x(s_0) \delta_0$ , we get phase ellipse as shown in Figure 1.6 above.

$$A_x = \left[ \gamma_x(s_0) \eta_x^2(s_0) + 2\alpha_x(s_0) \eta_x(s_0) \eta'_x(s_0) + \beta_x(s_0) \eta_x'^2(s_0) \right] \delta_0^2 = H(s_0) \delta_0^2$$

$$x(s) = \left[ \sqrt{H(s_0) \beta_x(s)} \cos \psi_x(s) + \eta_x(s) \right] \delta_0$$

The above equation shows induced betatron amplitude  $\sqrt{H(s_0)\beta_x(s)} \delta_0$  and consequently a maximum acquired horizontal displacement given by

$$x_{\max}(s) = \left[ \sqrt{H(s_0)\beta_x(s)} + \eta_x(s) \right] \delta_0$$

The transverse momentum acceptance is defined as the minimum momentum deviation such that there exist at least one location  $s_1$  along the ring where the electron hits the horizontal aperture either physical aperture or dynamic aperture whichever is less,  $x_{\max}(s_1) = \min [x_{phy}(s_1), x_{dyn}(s_1)]$ , so the transverse momentum acceptance [29] is given as

$$\varepsilon_{trans}(\delta_0) = \min_{s_1 \in [0, C]} \left[ \frac{x_{\max}(s_1)}{\sqrt{H(s_0)\beta_x(s_1)} + |\eta_x(s_1)|} \right] \quad 1.42$$

Using the above relation 1.42, estimating  $H$  function for different scattering locations and using lattice functions  $\beta_x$  and  $\eta_x$ , transverse momentum  $\varepsilon_{trans}$  was estimated and is shown in Figure 1.17.

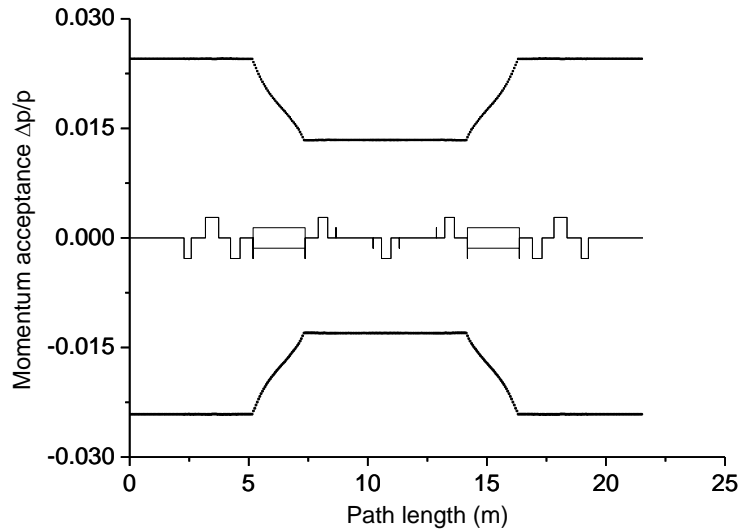


**Fig.1.17. Transverse momentum acceptance in one unit cell in Indus-2**

Momentum aperture in the longitudinal plane also known as RF momentum acceptance corresponds to the maximum particle momentum deviation at which the longitudinal motion remain stable due to RF field. The RF acceptance [25] is given as

$$\varepsilon_{rf} = \pm \left[ \frac{2U_0}{\pi \alpha_c h E_0} \left( \sqrt{\left( \frac{eV_{rf}}{U_0} \right)^2 - 1} - \cos^{-1} \left( \frac{U_0}{eV_{rf}} \right) \right) \right]^{1/2} \quad 1.43$$

Using Indus-2 parameters, energy 2.5 GeV, cavity voltage 1200 kV, RF acceptance was estimated and it is the same along the circumference of the ring. The variation in momentum acceptance in transverse and longitudinal plane in one unit cell of Indus-2 is shown in Figure 1.18.

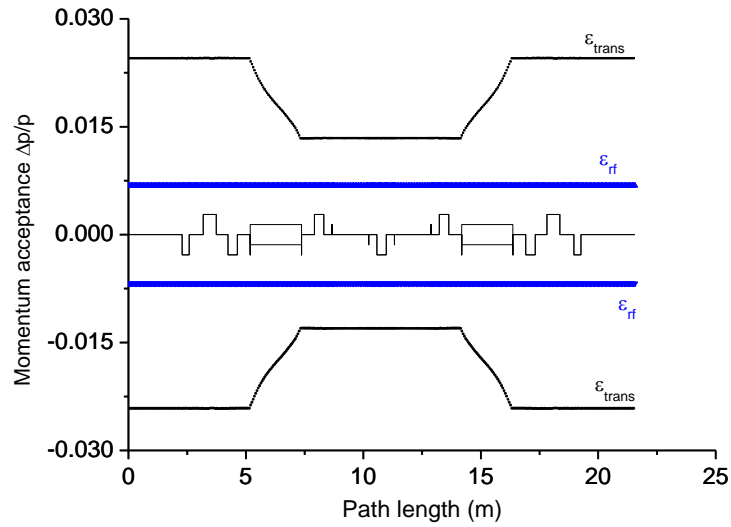


**Fig.1.18. Comparison of transverse and RF momentum acceptance in one unit cell in Indus-2**

Single particle tracking was also carried out to find the momentum aperture in transverse plane using 4D (4 Dimensional) particle tracking and momentum aperture using 6D (including longitudinal motion also) particle tracking using TRACY-3 particle tracking code [34].

The momentum acceptance results obtained by 4D and 6D particle tracking is shown in Figure 1.19.

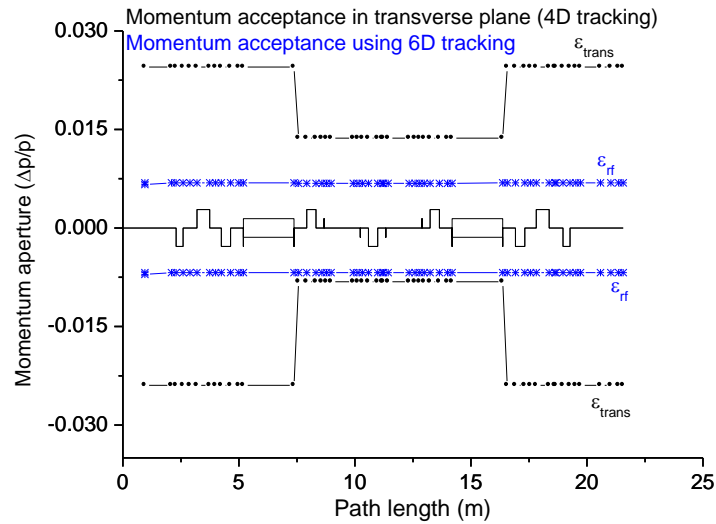


*Fig.1.19. Momentum acceptance in Indus-2 using tracking code*

The above results show that the momentum acceptance in Indus-2 is limited due to RF momentum acceptance.

## 1.7 Closed orbit distortion and its correction

In an electron storage ring, the reference closed orbit is defined by assuming perfect magnetic elements as well as perfect magnets alignment. In real practical conditions, unavoidable magnet imperfection will cause the trajectory of the closed orbit to deviate from this perfect closed orbit. The sources of closed orbit distortion (COD) are the dipole field errors and the errors due to magnetic element positioning in the ring. The most prominent effects come from the misalignment of quadrupole magnets where the resulting dipole field is proportional to both field gradient and alignment errors. If the electron beam is passing off centre in the sextupoles, it will generate a quadrupolar effect that can change the betatron tune and beta function. The beam offset in the sextupole should be minimized to make the storage ring optics near to linear optics.

For an angular kick  $\theta$  due to dipolar error at location  $s_0$  in ring, the closed orbit distortion at observation point  $s$  in the ring is given by [26]

$$y_{cod}(s) = \frac{\sqrt{\beta_y(s_0)\beta_y(s)}}{2\sin\pi\nu_y} \cos[\pi\nu_y - |\psi_y(s) - \psi_y(s_0)|] \theta(s_0) \quad 1.44$$

where  $y = x$  or  $z$  for horizontal and vertical plane,  $\beta_y(s_0)$  and  $\beta_y(s)$  are the beta function at the error point and observation point of COD respectively,  $\nu_y$  is the betatron tune,  $|\psi_y(s) - \psi_y(s_0)|$  is the phase difference between the point  $s_0$  and  $s_1$  in ring.

The uncorrected COD reduces the available aperture for the beam oscillations and hence beam lifetime. The COD correction is essential for the improvement of beam lifetime and also to minimise the feed down effect from the higher order magnetic elements such as sextupoles.

Usually the dipole correctors (horizontal and vertical steering magnets) for COD correction are distributed in the ring. The location and the number of correctors depend on the orbit correction methods. For monitoring the closed orbit in horizontal and vertical planes, beam position indicators (BPIs) are used. Normally, the number of correctors is less than that of the BPIs and if too many correctors are in use for orbit correction then there will be cross talk with them. Normally minimum four BPIs in one betatron tune are required for monitoring closed orbit correction in ring. In Indus-2, 56 BPIs are used for beam position monitoring.

The orbit correction magnets produce dipole kicks and have the same effects as dipole errors. The change of closed orbit at the BPI position  $s_j$  resulted due to the corrector kick  $\theta_i$  at position  $s_i$  is given as [26]

$$\Delta y(s_j) = \frac{\sqrt{\beta_y(s_j)}}{2\sin\pi\nu_y} \sum_{i=1}^N \theta_i \sqrt{\beta_y(s_i)} \cos[\pi\nu_y - |\psi(s_j) - \psi(s_i)|] \quad 1.45$$

It can be expressed in matrix form as

$$\overrightarrow{\Delta y}_m = R_{ji} \overrightarrow{\theta}_n \quad 1.46$$

where  $\overrightarrow{\Delta y}_m$ : the vector formed by the change of the orbit at  $m$  BPIs and  $\overrightarrow{\theta}_n$  is the  $n$  corrector vector,  $R_{ji}$  is the orbit change per unit corrector strength known as the response matrix and is given as

$$R_{ji} = \frac{\sqrt{\beta_y(s_j)}}{2 \sin \pi \nu_y} \sqrt{\beta_y(s_i)} \cos \left[ \pi \nu_y - |\psi_y(s_j) - \psi_y(s_i)| \right] \quad 1.47$$

For closed orbit correction, the response matrices are measured in electron storage ring. The objective of the orbit correction is to obtain the corrector strengths which give the minimum value of  $\overrightarrow{\Delta y}_m + R_{ji} \overrightarrow{\theta}_n$ . The distorted orbit can be corrected at least at the BPIs to the desired value so that  $\overrightarrow{\Delta y}_m = -\overrightarrow{\Delta u}_m$ , where  $\overrightarrow{\Delta u}_m$  is the difference between the measured orbit and the reference orbit with expression  $\overrightarrow{\theta}_n = R_{ji}^{-1} \overrightarrow{\Delta y}_m$ . Since the number of correctors  $n$  are not equal to the number of BPIs  $m$ , we cannot get an unique solution. Usually, some sophisticated methods are used in solving the least square problems to avoid the unnecessary large strengths in correctors for orbit correction. The correctors strength are estimated as

$\overrightarrow{\theta}_n = -(R^T R)^{-1} R^T \overrightarrow{\Delta u}_m$ , where  $R^T$  is the transpose operation on response matrix  $R$ . Some popular orbit correction methods are as follows:

### 1.7.1 MICADO method

The orbit minimization package MICADO is the first orbit control algorithm. In this method, we can find the single most effective corrector in the first iteration and then the second most effective corrector in the second iteration and so on. We can choose any number of correctors to be used in the ring.

### 1.7.2 Harmonic correction method

Placing correctors and BPIs at the location of high beta functions uniformly with respect to the betatron phase is an effective way to reduce the closed orbit distortion using harmonic method. We can choose two correctors with phase advance of  $\pi/2$  such that the strength of these two correctors can be adjusted independently to reduce the orbit stepwise. On the other hand once we have enough well distributed correctors and monitors, we can choose a few harmonics near the betatron tune to minimise the orbit with these correctors.

### 1.7.3 Local orbit bump method

For the correction of closed orbit locally in the ring we apply local orbit bump and the correction is effective in the local region whereas it does not affect other parts of the ring. Local bumps can be constructed using two, three or four orbit corrector magnets with angular kicks. For example, the condition for local orbit bump using three orbit corrector magnets with angular kicks  $\theta_i$  ( $i=1,2,3$ ) at locations 1, 2 and 3 is

$$\sum_{i=1}^3 R_{ki} \theta_i = 0 \text{ and } \sum_{i=1}^3 R_{ji} \theta_i = 0, \text{ where } j \text{ and } k \text{ are the monitors inside and outside the local}$$

orbit bump respectively and gives

$$\frac{\theta_1 \sqrt{\beta_1}}{\sin \psi_{32}} = \frac{\theta_2 \sqrt{\beta_2}}{\sin \psi_{13}} = \frac{\theta_3 \sqrt{\beta_3}}{\sin \psi_{21}} \text{ where } \psi_{ij} = \psi_i - \psi_j \quad 1.48$$

In this method, we need to minimize the residual of the sum of measured orbit and local bumped orbit stepwise and iteratively. The monitor errors and accuracy of lattice parameters are rather sensitive in this method.

### 1.7.2 Singular value decomposition (SVD) method

As seen above, for  $m$  beam position monitors and  $n$  closed orbit correctors, we get response matrix  $R$  of the order  $m \times n$ . A  $m \times n$  matrix  $R$  ( $m \geq n$ ) can be written as the product of a

$m \times m$  column-orthogonal matrix  $U$ , a  $m \times n$  diagonal matrix  $W$  (diagonal elements are called as singular values) with positive or zero elements and the transpose of an  $n \times n$  orthogonal matrix  $V$ . So the response matrix  $R$  can be written as

$$R = UWV^T, U^T U = U U^T = V V^T = V^T V = I, \text{ where } I \text{ is the identity matrix.} \quad 1.49$$

So the response matrix can be decomposed in to the product of the corrector eigen vector, the orbit eigen vector and the singular values connecting these eigen vectors. Small singular value  $w_j$  requires larger angular kick strength in order to produce a required orbit response.

The corrector strengths for the correction of the orbit to the desired value can be obtained as

$$\overrightarrow{\Delta\theta}_n = -R^{-1} \overrightarrow{u}_m = -V W^{-1} U^T \overrightarrow{u}_m = -V (\text{diag}(1/w_j)) U^T \overrightarrow{u}_m \quad 1.50$$

If  $1/w_j$  is above the threshold value, let  $(1/w_j) = 0$ . Rejection of the singular values or close to the singular values can reduce the rms value of the orbit correctors.

This method is very effective for closed orbit correction in electron storage ring and is in use in Indus-2.

Effect of closed orbit correction on beam lifetime in Indus-2 is presented in chapter 4 and 5.

## **1.8 Estimation of beam lifetime in Indus-2 storage ring**

For a stable beam in an electron storage ring, the most important processes of electron losses that decide the beam lifetime [35] are as follows:

1.8.1 Quantum lifetime due to emission of synchrotron radiation

1.8.2 Vacuum lifetime due to electron beam and gas atoms interaction

1.8.3 Touschek lifetime due to electron-electron interaction within a bunch

### **1.8.1 Estimation of Quantum lifetime**

The synchrotron radiation is emitted in discrete units. The discrete emission of synchrotron radiation induces noise on the beam which causes the electrons to diffuse. The equilibrium between the quantum excitation and the radiation damping determine the distribution of the

electrons. In principle, the tails of the distribution which is Gaussian in nature will extend to infinity. The vacuum chamber and the momentum acceptance will however truncate the distribution which leads to a constant loss of electrons. The resulting lifetime are known as quantum lifetime.

The quantum lifetime in vertical, horizontal and longitudinal plane in Indus-2 was estimated to find the sufficient aperture to overcome the electron loss due to aperture limitations.

The quantum lifetime [36] is given as

$$\tau_q = \tau_{x,z} \frac{e^u}{2u} \quad 1.51$$

where  $\tau_{x,z}$  is the damping time in horizontal and vertical plane and  $u = \frac{a_{x,z}^2}{2\sigma_{x,z}^2}$ ,  $a_{x,z}$  and  $\sigma_{x,z}$  are the aperture and beam size in horizontal and vertical plane respectively. In longitudinal plane the quantum lifetime is given as

$$\tau_q = \tau_\varepsilon \frac{e^u}{2u} \quad 1.52$$

where  $\tau_\varepsilon$  is the damping time in longitudinal plane and  $u = \frac{\varepsilon_{rf}^2}{2(\sigma_\varepsilon/E_0)^2}$  where  $\varepsilon_{rf}$  and  $\sigma_\varepsilon/E_0$  are the RF acceptance and energy spread of beam respectively.

The quantum lifetime in vertical, horizontal and longitudinal plane at beam energy 2.5 GeV in Indus-2 was estimated and is shown in figure 1.20 (a), (b) and (c) respectively.

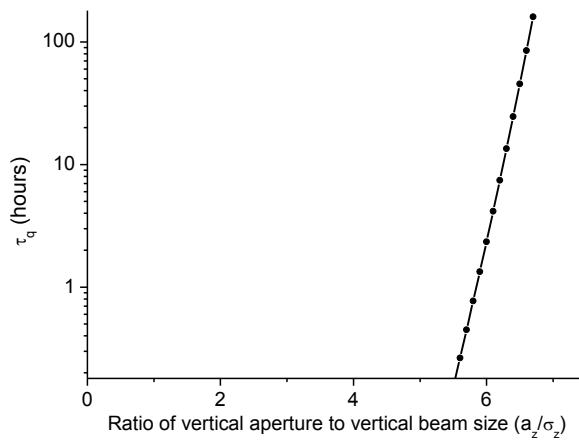


**Fig.1.20(a). Quantum lifetime with ratio of vertical aperture to vertical beam size**

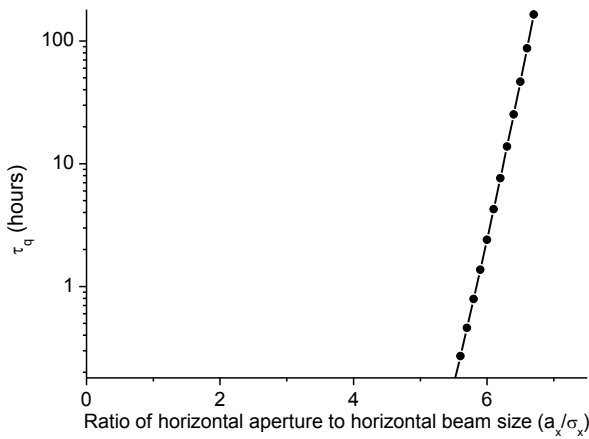


**Fig.1.20(b). Quantum lifetime with ratio of horizontal aperture to horizontal beam size**

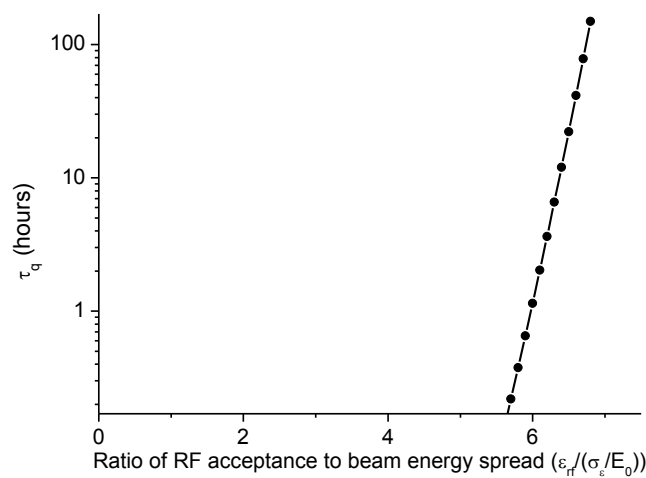


**Fig.1.20(c). Quantum lifetime with ratio of RF acceptance to beam energy spread**

From the above graph, we see that we get quantum lifetime of more than 100 hours for the aperture to beam size ratio in transverse plane  $\sim 7$ . Similarly in longitudinal plane, for RF acceptance to energy spread ratio  $\sim 7$ , we get quantum lifetime more than 100 hours. The quantum excitation effect in Indus-2 has been studied using beam scrapers and is discussed in chapter 5.

### 1.8.2 Estimation of vacuum lifetime due to beam-gas interaction

The electrons from the stored electron beam are lost by scattering of the residual gas molecules present in the vacuum chamber. The effect is controlled by providing sufficient pumping to reach low vacuum pressures and by careful construction of vacuum chamber to minimise photo induced desorption of gas molecules. There are mainly two processes [35] in beam-gas interaction which contribute in estimating vacuum lifetime which are as follows:

1.8.2.1 Elastic coulomb scattering between the electron and the nuclei of the residual gas

atom  $\tau_{el}$

1.8.2.2 Inelastic scattering between the electron and the nuclei of the residual gas atom  $\tau_{br}$

#### 1.8.2.1 Elastic coulomb scattering between the electron and the nuclei of the residual gas

atom  $\tau_{el}$

The elastic scattering of the electron on the nuclei of the residual gas atoms leads to an angular kick, which generates the betatron oscillation. If the increase in the amplitude of the betatron oscillation exceeds the transverse acceptance of the ring, the electron gets lost. The vacuum lifetime due to this process is given as [25, 35, 37]

$$\frac{1}{\tau_{el}} = \frac{2r_0^2 c \rho Z^2}{\gamma^2} \frac{1}{\theta_m^2} \quad 1.53$$

where  $r_0$  is the classical electron radius,  $c$  is the speed of light,  $\rho$  is the gas density,  $Z$  is the atomic number of residual gas atom,  $\gamma$  is the relativistic Lorentz factor and  $\theta_m$  is the

minimum scattering angle for the electron loss at beam loss location i.e. at maximum  $\beta_x$  in horizontal plane or at maximum  $\beta_z$  in vertical plane. For a rectangular chamber of horizontal aperture  $a$  and vertical aperture  $b$  at beam loss location, minimum scattering angle  $\theta_m$  is given as [25]

$$\frac{1}{\theta_m^2} = \frac{2\langle\beta_x\rangle\beta_{xm}}{a^2} \left[ \tan^{-1}\left(p\frac{b}{a}\right) + \frac{pab}{a^2 + p^2b^2} \right] + \frac{2\langle\beta_z\rangle\beta_{zm}}{b^2} \left[ \cot^{-1}\left(p\frac{b}{a}\right) + \frac{pab}{a^2 + p^2b^2} \right] \quad 1.54$$

where  $p = \sqrt{\frac{\langle\beta_x\rangle\beta_{xm}}{\langle\beta_z\rangle\beta_{zm}}}$ ,  $\beta_{xm}, \beta_{zm}$  are the  $\beta$  functions at the beam loss location,  $\langle\beta_x\rangle, \langle\beta_z\rangle$  are average  $\beta$  functions in the ring. These expressions are derived and discussed in chapter 2.

### 1.8.2.2 Inelastic scattering between the electron and the nuclei of the residual gas atom

$\tau_{br}$

The vacuum lifetime due to inelastic scattering between the electrons and nuclei of residual gas atoms also known as bremsstrahlung [37-40] lifetime is given as

$$\frac{1}{\tau_{br}} = \frac{16r_0^2c}{411} \left[ -\ln(\varepsilon) - \frac{5}{8} \right] \frac{P}{kT} \sum_i Z_i^2 N_i f_i \ln \left( \frac{183}{Z_i^3} \right) \quad 1.55$$

It depends on the vacuum pressure  $P$  and weakly depends on the momentum acceptance  $\varepsilon$  in the ring. The value of momentum acceptance  $\varepsilon$  is the minimum value either in transverse or in longitudinal directions.

Total vacuum lifetime  $\tau_v$  due to these processes are given as

$$\frac{1}{\tau_v} = \frac{1}{\tau_{el}} + \frac{1}{\tau_{br}} \quad 1.58$$

Using Indus-2 lattice parameters and assuming 1 nTorr nitrogen equivalent vacuum pressure in ring with dynamic aperture at beam loss location i.e. at maximum  $\beta_x$ ,  $a=20mm$  and at

maximum  $\beta_z$ ,  $b=12\text{ mm}$  (by normalizing the aperture with beta function), vacuum lifetime due to these processes were estimated at energy 550 MeV to 2500 MeV in steps of 100 MeV. As seen above that the momentum acceptance in longitudinal direction i.e. RF acceptance is minimum and is taken for estimation of vacuum lifetime at different beam energy. During the beam energy ramp from 550 MeV to 2500 MeV, betatron tune as well as synchrotron tune should remain constant so the value of  $\varepsilon_{rf}$  at different energy is taken considering synchrotron tune  $\nu_s=1.18\times 10^{-2}$  (20.5 kHz) constant. The RF cavity voltage and RF acceptance for constant synchrotron tune is shown in Figure 1.21. The variation in vacuum lifetime due to these processes and total vacuum lifetime at beam energy 550 MeV to 2500 MeV is shown in Figure 1.22.

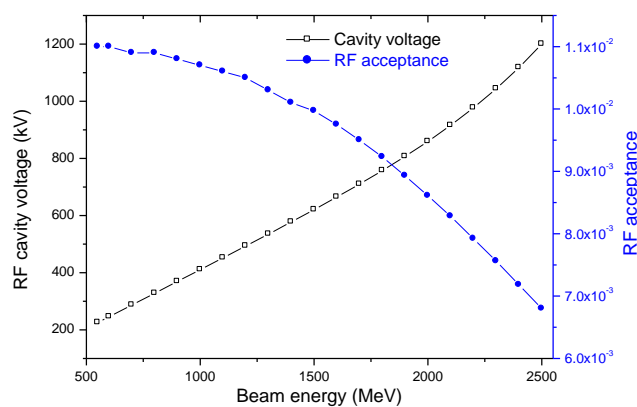


**Fig. 1.21. RF Cavity voltage and acceptance at different beam energy in Indus-2**

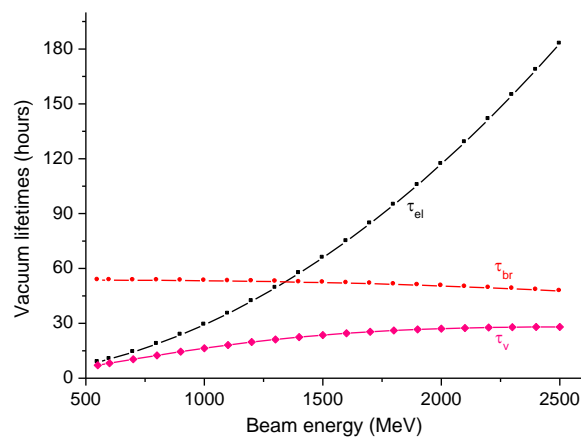


**Fig.1.22. Vacuum lifetime due to beam-gas atoms interaction at different beam energy**

From the above estimation, it is seen that the contribution of elastic scattering of electrons with the nuclei of residual gas atoms is dominant in total vacuum lifetime at low energy whereas at higher energy the contribution of inelastic scattering of electrons with nuclei of residual gas atoms is dominant in total vacuum lifetime. The elastic scattering strongly depends on the aperture and for small apertures it may compete with the bremsstrahlung at high energy also. So the contributions of elastic and inelastic scattering between the electrons and the nuclei of residual gas atoms are taken in the analysis of vacuum lifetime [35].

### 1.8.3 Estimation of Touschek lifetime due to electron-electron interaction within a bunch

If two electrons inside an electron bunch collide, the collisions occur in both transverse and longitudinal plane and there is a transfer of energy from transverse to the longitudinal plane and vice versa [41]. The energy transfers involved from the longitudinal plane to the transverse plane are insufficient to generate a betatron oscillation capable of leading to electron loss whereas the energy transfer involved from the transverse plane to the longitudinal plane are sufficient for loss of both colliding electrons. If all of the transverse momentum is transferred to longitudinal momentum, the longitudinal momentum would be approximately  $\gamma$  times the transverse momentum if observed in laboratory frame of reference which means the longitudinal momentum will receive a significant boost [42, 43]. The Touschek scattered electron can gain or lose longitudinal momentum from such a scattering process. If the momentum change experienced by the electron exceeds the momentum acceptance of the electron storage ring then the electron will be lost.

The Touschek lifetime  $\tau_{\text{tous}}$  due to electrons scattering within a bunch [25, 42] is given by

$$\frac{1}{\tau_{\text{tous}}} = -\frac{N}{\gamma^2} \frac{r_0^2 c}{8\pi \sigma_x \sigma_z \sigma_s} \frac{1}{(\Delta p/p)^3} D(\xi) \quad 1.59$$

For positive  $\delta_+$  ( $\Delta p/p = \text{positive}$ ) and negative  $\delta_-$  ( $\Delta p/p = \text{negative}$ ) energy deviation, the Touscheck loss rate along the circumference of ring is given as

$$\frac{1}{\tau_{\text{tous}}} = -\frac{N r_0^2 c}{8\pi \gamma \sigma_s^2} \frac{r_0^2 c}{8\pi \sigma_s \sigma_z \sigma_s} \left\langle \frac{1}{\sigma_x \sigma_z} \left( \frac{D(\xi_+)}{\delta_+^3} + \frac{D(\xi_-)}{\delta_-^3} \right) \right\rangle$$

where  $\xi_{\pm} = \left( \frac{\delta_{\pm} \beta_x}{\gamma \sigma_x} \right)^2$  and

$$D(\xi_{\pm}) = \xi_{\pm}^{1/2} \left[ -\frac{3}{2} e^{-\xi_{\pm}} + \frac{\xi_{\pm}}{2} \int_{\xi_{\pm}}^{\infty} \frac{\ln u}{u} e^{-u} du + \frac{1}{2} (3\xi_{\pm} - \xi_{\pm} \ln \xi_{\pm} + 2) \int_{\xi_{\pm}}^{\infty} \frac{e^{-u}}{u} du \right]$$

Where  $\sigma_x, \sigma_z$  and  $\sigma_s$ : horizontal, vertical and longitudinal rms beam size respectively,  $\delta = \Delta p/p$ : limiting momentum acceptance either in transverse or in longitudinal plane,  $N$  is the number of electrons per bunch.

These expressions are discussed in chapter 3. For the estimation of Touscheck lifetime, the particle tracking code ELEGANT [32], ZAP [44] was used. The variation in Touscheck lifetime of 100 mA stored current (0.34 mA per bunch) and at different beam energy using the cavity voltage as shown in Figure 1.21 with 0.5% and 1% betatron coupling using ELEGANT code is shown in Figure 1.23.

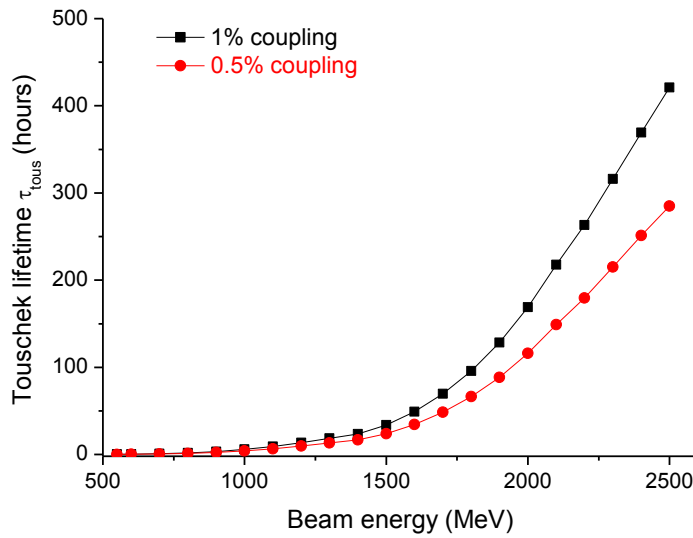


**Fig.1.23. Touschek lifetime at different beam energy**

The above results show that the Touschek scattering effect is significant at low beam energy whereas it is significantly reduced at higher beam energy. The Touschek scattering effects in Indus-2 are studied by storing electrons in single bunch and are discussed in chapter 5.

The total beam lifetime  $\tau_t$  was estimated using vacuum lifetime  $\tau_v$  and Touschek lifetime  $\tau_{\text{Touschek}}$  and is shown in Figure 1.24.

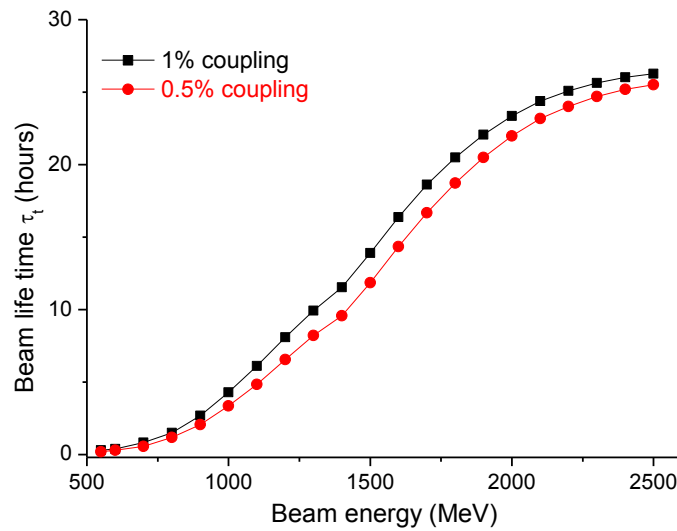


**Fig.1.24. Beam lifetime at different beam energy in Indus-2**

## CHAPTER 2

### DEPENDENCE OF ELECTRON LOSS ON THE SHAPE OF VACUUM CHAMBER

#### 2.1 Introduction

As discussed in chapter 1 that the beam lifetime in an electron storage ring is limited by the loss of the stored electrons due to the elastic coulomb scattering of electrons with the nuclei of residual gas atoms. The contribution of the beam lifetime due to this elastic scattering depends upon the shape of the vacuum chamber. Since in a real storage ring, vacuum pressure is not the same at all locations along its circumference, it is essential to know the shape factor at each location. In this chapter, analytical expressions for the shape factor for a rectangular and an elliptical vacuum chamber at a scattering location in a storage ring are derived using an approach in which the shape of the vacuum chamber at the focusing quadrupole is transformed to the location of defocusing quadrupole and vice versa to define the parts of the vacuum chamber, where the loss of electrons takes place at the quadrupoles. This method has enabled derivation of more accurate expressions for the two shapes. A comparative study of the value of average shape factor obtained from derived expressions and with the existing expressions is discussed using Indus-2 design lattice parameters and considering rectangular, elliptical, square and circular shapes of the chamber.

For the storage of an electron beam for a longer lifetime in an electron storage ring, average vacuum pressure of the order of  $1 \times 10^{-9}$  Torr is required in the vacuum chamber in which the electron beam circulates. The presence of residual gas species even at a low pressure of 1 nTorr, causes scattering of the electrons with the nuclei of residual gas atoms. The scattering may be elastic or inelastic. In the elastic scattering of electrons of the stored electron beam with the nuclei of residual gas atoms, the electrons are deflected from their path and the amplitude of betatron oscillation of electrons increases. If the amplitude of betatron

oscillation of an electron is more than the chamber aperture i.e. the acceptance of the ring, the electron is lost there. The rate of loss of electrons due to this process contributes to beam lifetime. The loss of electrons due to elastic coulomb scattering takes place at maximum  $\beta$  function in horizontal ( $X$ ) and vertical ( $Z$ ) planes, when the aperture of vacuum chamber is uniform in the ring. The loss of electrons depends on the aperture which is related to a parameter which we define the shape factor, which is governed by the shape and size of vacuum chamber. In deriving the expression it is assumed that the dynamic aperture is equal to or greater than the physical aperture of the chamber. In the electron storage rings, rectangular or elliptical shapes of the vacuum chamber are widely used. The average shape factor for a rectangular chamber is discussed in [25] and used for beam lifetime estimation in operating rings like MAX II [45], SPEAR3 [46], INDUS-2 [47] etc. The shape factor for elliptical chamber is given in [48] and used in estimating beam lifetime in SAGA-LS storage ring [49]. The derivation of shape factor [50] for different shapes of vacuum chambers has not been derived and discussed clearly in detail so the problem was re-visited for finding the exact analytical expressions.

Here, general expressions of the shape factor for a rectangular and an elliptical chamber for a given scattering location in a storage ring are derived starting from abinitio using linear beam dynamics. The motion of electrons is considered to be constrained by the physical aperture neglecting the non linear beam dynamical effects. To find the expression, the position of the electron at the focusing quadrupole is transformed to the position at defocusing quadrupole location based on the beta functions in horizontal and vertical planes and vice versa to define the part of the vacuum chamber at which the beam loss takes place at these locations. This approach has enabled derivation of exact expressions for the shape factor within the domain of linear beam dynamics. A theoretical estimation of shape factor at different scattering locations is also carried out using Indus-2 lattice parameters considering rectangular and

elliptical chambers. The average shape factor is also estimated for these shapes and compared with that calculated values using the existing expressions.

In section 2.2 we present the beam lifetime formulation due to elastic coulomb scattering of electrons with the nuclei of residual gas atoms in which the shape factor appears as a parameter. The approach for the derivation of expression for shape factor for a rectangular and elliptical shape of the vacuum chamber is discussed in section 2.3 and the average shape factor considering Indus-2 lattice parameters and a comparison with the estimated results obtained using the existing expressions is discussed in section 2.4.

## 2.2 Beam lifetime due to elastic coulomb scattering

The rate of loss of relativistic electrons due to elastic coulomb scattering of electrons with the nuclei of residual gas atom is given by [37, 51]

$$-\frac{1}{N} \frac{dN}{dt} = c \rho \sigma \quad 2.1$$

where  $N, c, \rho, \sigma$  are the number of electrons, speed of electrons, residual gas density of molecular gas species present in the vacuum chamber and scattering cross section of electrons respectively.

The rate of loss of electrons due to elastic coulomb scattering  $\tau_{el}$  varies from location to location in ring. So

$$\frac{1}{\tau_{el}} = \left\langle -\frac{1}{N} \frac{dN}{dt} \right\rangle = c \langle \rho \sigma \rangle \quad 2.2$$

where  $\langle \rho \sigma \rangle$  is the average of the product of residual gas density and scattering cross section of electrons at different scattering locations spread over the ring.

Differential scattering cross section of elastic coulomb scattering of a relativistic electron scattered by the nuclei of residual gas atom at a location  $j$  is given by [51]

$$\frac{d\sigma_j}{d\Omega} = \frac{Z_i^2 r_0^2}{4\gamma^2} \frac{1}{\sin^4\left(\frac{\theta}{2}\right)} \quad 2.3$$

where  $d\Omega = \sin\theta d\theta d\phi$  is the solid angle in which the electron is scattered,  $\theta$  and  $\phi$  are the scattering polar (range from 0 to  $\pi$ ) and azimuth (range from 0 to  $2\pi$ ) angle respectively,  $Z_i$  is the atomic number of the nucleus of the residual gas atom of species  $i$ ,  $r_0$  is the classical electron radius and  $\gamma$  is the relativistic Lorentz factor. The electrons will survive in the chamber up to minimum scattering angle  $\theta_m$  and will be lost for  $\theta$  above the value of  $\theta_m$ .

Integrating equation 2.3 with respect to  $\theta$  from limit  $\theta_m$  to  $\pi$ , we get

$$\sigma_j(\phi) = \frac{Z_i^2 r_0^2}{4\gamma^2} \frac{2\cos^2\left(\frac{\theta_m}{2}\right)}{\sin^2\left(\frac{\theta_m}{2}\right)} d\phi \quad 2.4$$

For small angle of scattering  $\theta_m \ll 1$  we get

$$d\sigma_j(\phi) = \frac{2Z_i^2 r_0^2}{\gamma^2} \frac{d\phi}{\theta_m^2} \quad 2.5$$

The survival chances of a scattered electron depend on the shape and size of the vacuum chamber. As shown in equations 2.3 and 2.4, the scattering cross-section has a dependence on angle  $\theta$ . The maximum allowed displacement for  $\theta$  will be different for different shapes and size of the vacuum chamber, therefore, the average scattering cross-section as it appears in equation 2.2, will be different for different shapes and sizes of the vacuum chamber.

The elastic scattering cross section, causing loss of an electron scattered at the location  $j$  in a storage ring is given as

$$\sigma_j = \frac{2Z_i^2 r_0^2}{\gamma^2} F_j \quad \text{where } F_j = \int_0^{2\pi} \frac{d\phi}{\theta_m^2(\phi)} \text{ is defined as the **shape factor**} \quad 2.6$$

Vacuum pressure or even the composition of residual gases varies from point to point in a storage ring, therefore it is important to know the shape factor  $F_j$  for each location in a storage ring. If the vacuum pressure and gas composition is uniform along the circumference, the equation 2.2 becomes

$$\frac{1}{\tau_{el}} = c \rho \langle \sigma \rangle \quad \text{where} \quad \langle \sigma \rangle = \frac{2Z_i^2 r_0^2}{\gamma^2} \langle F \rangle \quad \text{and} \quad \langle F \rangle = \frac{\sum_{j=1}^n F_j}{n} \quad 2.7$$

where  $\langle F \rangle$  is the average shape factor and  $n$  is the number of scattering locations spread over the ring at a uniform interval.

Obviously, the correct value of average shape factor  $\langle F \rangle$  is essential to estimate the beam lifetime due to elastic coulomb scattering between the electrons and the nuclei of residual gas atom.

### 2.3 Expressions for shape factor $F$

When an electron collides with a nucleus of a residual gas atom at location  $s_0$  in the ring, the electron gets deflected by an angle  $\theta$ . In spherical polar coordinates, for small scattering angle, the deflection is resolved in  $X$  plane as  $\theta_x = \theta \cos \phi$  and  $\theta_z = \theta \sin \phi$  in  $Z$  plane. The electrons are lost at maximum  $\beta_x$  or at maximum  $\beta_z$  as shown in Figure 2.1.

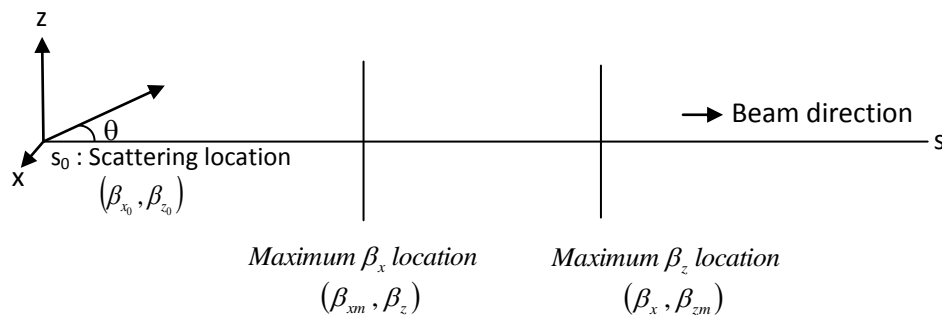


**Fig.2.1. Scattering and beam loss locations in ring**

If the electron at location  $s_1$  reaches the boundary of the vacuum chamber, its horizontal  $x$  and vertical  $z$  coordinates at  $s_1$  is given as

$$\begin{aligned} x &= \sqrt{\beta_x(s_0)\beta_x(s_1)} \theta_x = \sqrt{\beta_x(s_0)\beta_x(s_1)} \theta_m \cos \phi \\ z &= \sqrt{\beta_z(s_0)\beta_z(s_1)} \theta_z = \sqrt{\beta_z(s_0)\beta_z(s_1)} \theta_m \sin \phi \end{aligned} \quad 2.8$$

where  $\beta_x(s_0)$  and  $\beta_z(s_0)$  are  $\beta$  functions at the scattering location  $s_0$  in  $X$  and  $Z$  planes respectively and  $\beta_x(s_1)$  and  $\beta_z(s_1)$  are  $\beta$  functions at beam loss location  $s_1$  in  $X$  and  $Z$  planes respectively and  $\theta_m$  is the minimum scattering angle. In equation 2.8, maximum betatron displacements are considered taking the betatron phase term equal to one because here we consider the electrons, which are lost from the ring. Substituting  $x$  and  $z$  from equation 2.8 into equation 2.6, the expression for shape factor at scattering location  $j$  i.e.  $F_j$  becomes

$$\begin{aligned} F_j &= \int_0^{2\pi} \frac{d\phi}{\theta_m^2(\phi)} = \int_0^{2\pi} \frac{\beta_x(j)\beta_x(s_1)\cos^2\phi + \beta_z(j)\beta_z(s_1)\sin^2\phi}{x^2 + z^2} d\phi \\ &\text{where } \tan\phi = \sqrt{\frac{\beta_x(j)\beta_x(s_1)}{\beta_z(j)\beta_z(s_1)}} \frac{z(s_1)}{x(s_1)} \end{aligned} \quad 2.9$$

Dependence of the shape factor  $F_j$  on  $x$  and  $z$  indicates that it is governed by the shape of the vacuum chamber. We consider that the storage ring has a vacuum chamber of uniform cross section all along the circumference. In such a ring, the beam loss will takes place either at the location where  $\beta_x$  is maximum or the location where  $\beta_z$  is maximum. The derivation of expressions for the shape factors for a rectangular and an elliptical vacuum chamber is given in the following paragraph.

### 2.3.1 Shape factor for rectangular vacuum chamber

Let the horizontal and vertical dimensions of the rectangular vacuum chamber be  $a$  and  $b$  respectively. In order to find out the domain of azimuth angle  $\phi$  for electron loss in  $X$  and

Z plane, we assume that at maximum  $\beta_z$  location, the electrons lie on the boundary of vacuum chamber. The electron, which, is at  $P(a,b)$  at maximum  $\beta_z$  location, will be at

$$P'' \left( \sqrt{\frac{\beta_{xm}}{\beta_x}} a, \sqrt{\frac{\beta_z}{\beta_{zm}}} b \right) \text{ at maximum } \beta_x \text{ location as shown in Figure 2.2(a), where}$$

$\beta_{xm}$  and  $\beta_z$  are  $\beta$  functions at maximum  $\beta_x$  location in X and Z planes respectively,

$\beta_x$  and  $\beta_{zm}$  are  $\beta$  functions at maximum  $\beta_z$  location in X and Z planes respectively. The

electrons which lie on the boundary of the chamber at maximum  $\beta_z$  will, accordingly, follow

the dotted rectangle as shown in Figure 2.2(a) whereas the solid rectangle shows the actual

aperture at maximum  $\beta_x$  location.

Similarly, we assume that at maximum  $\beta_x$  location, electrons are on the boundary of the

vacuum chamber. Referring to Figure 2.2(b), the electron, which is at  $P(a,b)$  at maximum

$$\beta_x \text{ location will be at } P'' \left( \sqrt{\frac{\beta_x}{\beta_{xm}}} a, \sqrt{\frac{\beta_{zm}}{\beta_z}} b \right) \text{ at maximum } \beta_z \text{ location. The electrons which}$$

lie on the boundary of the chamber at maximum  $\beta_x$  will follow the dotted rectangle as shown

in Figure 2.2(b) whereas the solid rectangle shows the actual aperture at maximum  $\beta_z$

location.

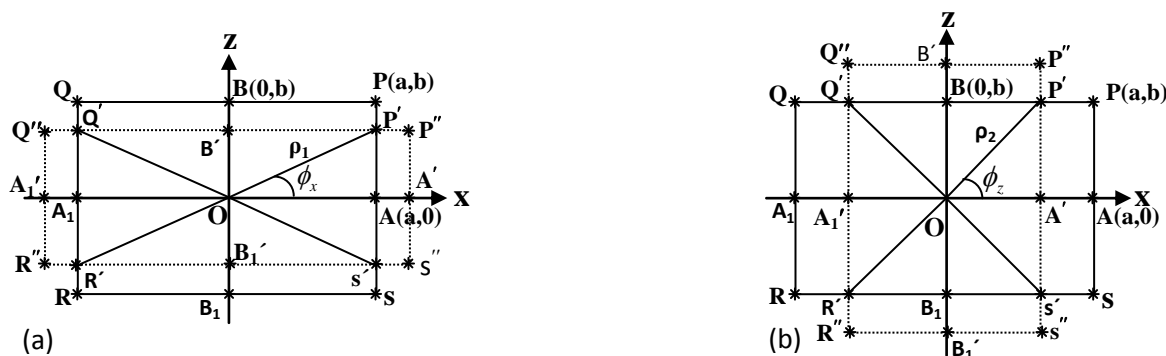


**Fig.2.2. Electron Positions (a) at maximum  $\beta_x$  (dotted rectangle) with respect to their positions on the boundary of chamber at maximum  $\beta_z$  and (b) at maximum  $\beta_z$  (dotted rectangle) with respect to their positions on the boundary of chamber at maximum  $\beta_x$ .**

From Figure 2.2(a), it is seen that at the location of maximum  $\beta_x$ , electrons, which have the magnitude of horizontal displacement  $a$  or greater and also vertical displacement magnitude up to  $OB' \left( \sqrt{\frac{\beta_z}{\beta_{zm}}} b \right)$  are lost on the  $P'AS'$  and  $Q'A_1R'$  parts of the vacuum chamber.

Electrons, having the magnitude of vertical displacement greater than to  $OB'$  are lost at the maximum  $\beta_z$  location.

Similarly, from Figure 2.2(b), it is understood that at the location of maximum  $\beta_z$ , electrons, which have the magnitude of vertical displacement  $b$  or greater and also magnitude of horizontal displacement up to  $OA' \left( \sqrt{\frac{\beta_x}{\beta_{xm}}} a \right)$  are lost on the  $P'BQ'$  and  $S'B_1R'$  parts of the

vacuum chamber. Electrons having the magnitude of horizontal displacement greater than to  $OA'$  are lost at the maximum  $\beta_x$  location.

In order to obtain the shape factor, we consider only the first quadrant of the vacuum chamber taking advantage of four fold symmetry. First, we consider the maximum  $\beta_x$  location and for this we refer to Figure 2.2(a). Here, the electrons are lost on the aperture boundary  $P'A$ . The azimuth angle  $\phi$  varies from 0 to an angle  $\phi_{xm}$  which is related to the angle  $\phi_x$  at this location.

Similarly at the maximum  $\beta_z$  location, electrons are lost on boundary  $P'B$  of Figure 2.2(b). The azimuth angle  $\phi$  here varies from  $\phi_{zm}$  to  $\pi/2$  which is related to the angle  $\phi_z$  at this location.

From Figure 2.2(a), the coordinate of the electron at the location  $P'$  is  $\left( a, \sqrt{\frac{\beta_z}{\beta_{zm}}} b \right)$ , where

$\beta_{zm} > \beta_z$ . From equation 2.8, the coordinate of  $P'(x, z)$  at maximum  $\beta_x$  location is given as

$$x = \sqrt{\beta_{x_0} \beta_{xm}} \theta_m \cos \phi$$

$$z = \sqrt{\beta_{z_0} \beta_z} \theta_m \sin \phi$$

$$\tan \phi = \sqrt{\frac{\beta_{x_0} \beta_{xm}}{\beta_{z_0} \beta_z}} \frac{z}{x} \quad 2.10$$

The maximum value of  $\phi$  i.e.  $\phi_{xm}$  is obtained at location  $P'$  of electron loss,

$$x = a \text{ and } z = \sqrt{\frac{\beta_z}{\beta_{zm}}} b, \text{ so}$$

$$\tan \phi_{xm} = \sqrt{\frac{\beta_{x_0} \beta_{xm}}{\beta_{z_0} \beta_z}} \sqrt{\frac{\beta_z}{\beta_{zm}}} \frac{b}{a} \Rightarrow \tan \phi_{xm} = \sqrt{\frac{\beta_{x_0} \beta_{xm}}{\beta_{z_0} \beta_{zm}}} \frac{b}{a} \Rightarrow \phi_{xm} = \tan^{-1} \left( \frac{pb}{a} \right) \quad 2.11$$

where  $p = \sqrt{\frac{\beta_{x_0} \beta_{xm}}{\beta_{z_0} \beta_{zm}}}$

From Figure 2.2(a),  $\tan \phi_x = \frac{z}{x} \Rightarrow \tan \phi = p_1 \tan \phi_x$  where  $p_1 = \sqrt{\frac{\beta_{x_0} \beta_{xm}}{\beta_{z_0} \beta_z}}$  (using eq. 2.10) 2.12

Similarly from Figure 2.2(b), the coordinate of the electron at point  $P'$  is  $\left( \sqrt{\frac{\beta_x}{\beta_{xm}}} a, b \right)$ ,

where  $\beta_{xm} > \beta_x$ . The coordinate of  $P'(x, z)$  at maximum  $\beta_z$  location is given as

$$x = \sqrt{\beta_{x_0} \beta_x} \theta_m \cos \phi$$

$$z = \sqrt{\beta_{z_0} \beta_{zm}} \theta_m \sin \phi$$

$$\tan \phi = \sqrt{\frac{\beta_{x_0} \beta_x}{\beta_{z_0} \beta_{zm}}} \frac{z}{x}$$

Using the coordinate of  $P'$ ,  $x = \sqrt{\frac{\beta_x}{\beta_{xm}}} a$  and  $z = b$ , the maximum value of  $\phi$  i.e.  $\phi_{zm}$  is

$$\tan \phi_{zm} = \sqrt{\frac{\beta_{x_0} \beta_x}{\beta_{z_0} \beta_{zm}}} \sqrt{\frac{\beta_{xm}}{\beta_x}} \frac{b}{a} \Rightarrow \tan \phi_{zm} = \sqrt{\frac{\beta_{x_0} \beta_{xm}}{\beta_{z_0} \beta_{zm}}} \frac{b}{a} \Rightarrow \phi_{zm} = \tan^{-1} \left( \frac{pb}{a} \right) \quad 2.13$$

$$\text{where } p = \sqrt{\frac{\beta_{x_0} \beta_{xm}}{\beta_{z_0} \beta_{zm}}}$$

$$\text{From Figure 2.2(b), } \tan \phi_z = \frac{z}{x} \Rightarrow \tan \phi = p_2 \tan \phi_x \text{ where } p_2 = \sqrt{\frac{\beta_{x_0} \beta_x}{\beta_{z_0} \beta_{zm}}} \quad 2.14$$

It is clear from equations 2.11 and 2.13 that  $\phi_{xm} = \phi_{zm} = \phi_m$ . In brief, for  $\phi$  varying from 0 to  $\phi_m$ , the electrons are lost at maximum  $\beta_x$  location on  $P'A$  (Figure 2.2(a)) and from  $\phi_m$  to  $\pi/2$  at maximum  $\beta_z$  on  $P'B$  (Figure 2.2(b)).

The shape factor  $F_j$  taking into consideration the four fold symmetry of chamber is

$$F_j = \int_0^{2\pi} \frac{d\phi}{\theta_m^2(\phi)} = 4 \int_0^{\pi/2} \frac{d\phi}{\theta_m^2(\phi)}$$

In this integral, in first quadrant, electrons scattered into azimuth angle  $\phi$  between 0 to  $\phi_m$  will be lost at maximum  $\beta_x$  and those scattered between  $\phi_m$  to  $\pi/2$  will be lost at maximum  $\beta_z$  location.

$$\int_0^{\pi/2} \frac{d\phi}{\theta_m^2(\phi)} = \int_0^{\phi_m} \frac{\beta_{x_0} \beta_{xm} \cos^2 \phi + \beta_{z_0} \beta_z \sin^2 \phi}{\rho_1^2} d\phi + \int_{\phi_m}^{\pi/2} \frac{\beta_{x_0} \beta_x \cos^2 \phi + \beta_{z_0} \beta_{zm} \sin^2 \phi}{\rho_2^2} d\phi$$

From Figure 2.2(a),  $\rho_1^2 = a^2 + a^2 \tan^2 \phi_x$ , putting in first integral and from Figure 2.2(b),

$\rho_2^2 = b^2 + b^2 \cot^2 \phi_z$ , putting in second integral and using relation 2.12 and 2.14, we get

$$F_j = \frac{2\beta_{x_0} \beta_{xm}}{a^2} \left[ \phi_m + \frac{1}{2} \sin 2\phi_m \right] + \frac{2\beta_{z_0} \beta_{zm}}{b^2} \left[ \frac{\pi}{2} - \phi_m + \frac{1}{2} \sin 2\phi_m \right]$$

$$F_j = \frac{2\beta_{x_0}\beta_{xm}}{a^2} \left[ \tan^{-1}\left(\frac{pb}{a}\right) + \frac{pab}{a^2 + p^2b^2} \right] + \frac{2\beta_{z_0}\beta_{zm}}{b^2} \left[ \cot^{-1}\left(\frac{pb}{a}\right) + \frac{pab}{a^2 + p^2b^2} \right]$$

where  $p = \sqrt{\frac{\beta_{x_0}\beta_{xm}}{\beta_{z_0}\beta_{zm}}}$  2.15

The above expression, which gives the contribution to the shape factor due to the elastic coulomb scattering at location  $j$  is the similar to that given for the average shape factor in [25] as below

$$\langle F \rangle = \frac{2\langle\beta_x\rangle\beta_{xm}}{a^2} \left[ \tan^{-1}\left(\frac{pb}{a}\right) + \frac{pab}{a^2 + p^2b^2} \right] + \frac{2\langle\beta_z\rangle\beta_{zm}}{b^2} \left[ \cot^{-1}\left(\frac{pb}{a}\right) + \frac{pab}{a^2 + p^2b^2} \right]$$

where  $p = \sqrt{\frac{\langle\beta_x\rangle\beta_{xm}}{\langle\beta_z\rangle\beta_{zm}}}$ ,  $\langle\beta_x\rangle$  and  $\langle\beta_z\rangle$  are average values of  $\beta$  function in the ring 2.16

The expression 2.16 is derived by assuming the average value of minimum scattering angle  $\theta_x$  and  $\theta_z$  avoiding point to point calculation of shape factor in the ring which we have considered in deriving expression 2.15 by using above approach.

### 2.3.2 Shape factor for elliptical vacuum chamber

We follow the same approach as that used for a rectangular chamber to find out an expression for the shape factor of an elliptical chamber. Here also we assume that at maximum  $\beta_z$  location, electrons are on the boundary of chamber surface. The position of these electrons at maximum  $\beta_x$  location will be as shown in Figure 2.3(a) by the dotted ellipse, whereas the solid ellipse is the boundary of vacuum chamber surface at maximum  $\beta_x$  location. Similarly we assume that the electrons at maximum  $\beta_x$  location are on the boundary of vacuum chamber, these electrons at maximum  $\beta_z$  location will lie on the dotted ellipse as shown in Figure 2.3(b) whereas the solid ellipse here shows the boundary of the vacuum chamber at maximum  $\beta_z$  location.

From Figure 2.3(a), it is clear that at maximum  $\beta_x$  location, electrons are lost on the *PAS* and *QCR* parts of the vacuum chamber. Similarly Figure 2.3(b) indicates that at maximum  $\beta_z$  location, electrons are lost on *QBP* and *RDS* parts of the vacuum chamber.

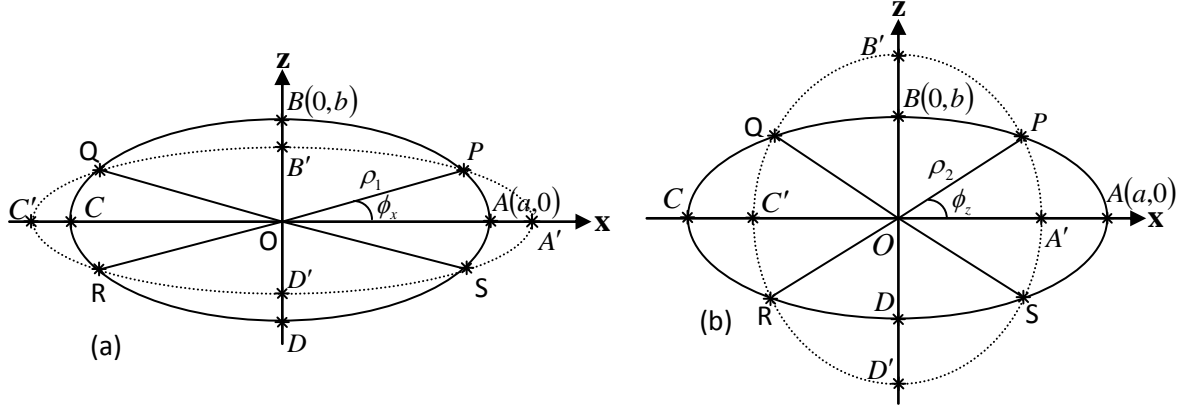


**Fig.2.3. Electron positions (a) at maximum  $\beta_x$  (dotted ellipse) with respect to their positions on the boundary of chamber at maximum  $\beta_z$  and (b) at maximum  $\beta_z$  (dotted ellipse) with respect to their positions on the boundary of chamber at maximum  $\beta_x$**

From Figure 2.3(a), equation of solid ellipse representing the vacuum chamber is  $\frac{x^2}{a^2} + \frac{z^2}{b^2} = 1$

and that of the dotted ellipse is  $\frac{x^2}{a_1^2} + \frac{z^2}{b_1^2} = 1$ , where  $a_1 = \sqrt{\frac{\beta_{xm}}{\beta_x}} a$  and  $b_1 = \sqrt{\frac{\beta_z}{\beta_{zm}}} b$ . Let

$\beta_{x_0}$  and  $\beta_{z_0}$  be the  $\beta$  functions at the location  $s_0$  where scattering of electron with gas atom takes place. At location  $s_0$ , the electron gets kick of angle  $\theta_m$ , the position coordinates  $P(x, z)$  at the location of maximum  $\beta_x$  is given as

$$x = \sqrt{\beta_{x_0} \beta_{xm}} \theta_m \cos \phi$$

$$z = \sqrt{\beta_{z_0} \beta_z} \theta_m \sin \phi$$

From this equation, we get  $\tan \phi = \sqrt{\frac{\beta_{x_0} \beta_{xm}}{\beta_{z_0} \beta_z}} \frac{z}{x}$  2.17

In Figure 2.3(a), point P is intersection of two ellipses so on solving these, we get

$$\frac{z}{x} = \sqrt{\frac{\beta_z (\beta_{xm} - \beta_x)}{\beta_{xm} (\beta_{zm} - \beta_z)}} \frac{b}{a}$$

Accordingly from equation 2.17, the maximum value of  $\phi$  at the location of electron loss  $\phi_{xm}$  is,

$$\tan \phi_{xm} = \sqrt{\frac{\beta_{x_0} (\beta_{xm} - \beta_x)}{\beta_{z_0} (\beta_{zm} - \beta_z)}} \frac{b}{a} \Rightarrow \phi_{xm} = \tan^{-1} \left( \frac{pb}{a} \right) \text{ where } p = \sqrt{\frac{\beta_{x_0} (\beta_{xm} - \beta_x)}{\beta_{z_0} (\beta_{zm} - \beta_z)}} \quad 2.18$$

Let the coordinate of point P on ellipse in Figure 2.3(a) be  $(\rho_1 \cos \phi_x, \rho_1 \sin \phi_x)$  so, we get

$$\frac{1}{\rho_1^2} = \frac{\cos^2 \phi_x}{a^2} + \frac{\sin^2 \phi_x}{b^2}, \quad \tan \phi_x = \frac{z}{x} \Rightarrow \tan \phi = p_1 \tan \phi_x \text{ where } p_1 = \sqrt{\frac{\beta_{x_0} \beta_{xm}}{\beta_{z_0} \beta_z}} \text{ (using eq. 2.17)} \quad 2.19$$

Similarly from Figure 2.3(b), equation of solid ellipse representing the vacuum chamber is  $\frac{x^2}{a^2} + \frac{z^2}{b^2} = 1$  and that of dotted ellipse is  $\frac{x^2}{c_1^2} + \frac{z^2}{d_1^2} = 1$ , where  $c_1 = \sqrt{\frac{\beta_x}{\beta_{xm}}} a$  and  $d_1 = \sqrt{\frac{\beta_{zm}}{\beta_z}} b$ . The position coordinates  $P(x, z)$  at the location of maximum  $\beta_z$  is given as

$$x = \sqrt{\beta_{x_0} \beta_x} \theta_m \cos \phi$$

$$z = \sqrt{\beta_{z_0} \beta_{zm}} \theta_m \sin \phi$$

In Figure 2.3(b), point P is the intersection of two ellipses, so on solving these, we get

$$\frac{z}{x} = \sqrt{\frac{\beta_{zm} (\beta_{xm} - \beta_x)}{\beta_x (\beta_{zm} - \beta_z)}} \frac{b}{a}$$

The maximum value of  $\phi$  at the location of electron loss  $\phi_{zm}$  is given as

$$\tan \phi_{zm} = \sqrt{\frac{\beta_{x_0} (\beta_{xm} - \beta_x)}{\beta_{z_0} (\beta_{zm} - \beta_z)}} \frac{b}{a} \Rightarrow \phi_{zm} = \tan^{-1} \left( \frac{pb}{a} \right) \text{ where } p = \sqrt{\frac{\beta_{x_0} (\beta_{xm} - \beta_x)}{\beta_{z_0} (\beta_{zm} - \beta_z)}} \quad 2.20$$

It is clear from equations 2.18 and 2.20 that  $\phi_{xm} = \phi_{zm} = \phi_m$ . In brief for  $\phi$  varying from 0 to  $\phi_m$ , the electrons are lost at maximum  $\beta_x$  location and from  $\phi_m$  to  $\pi/2$ , they are lost at the maximum  $\beta_z$  location.

Let the coordinate of point P on ellipse in Figure 2.3(b) be  $(\rho_2 \cos \phi_z, \rho_2 \sin \phi_z)$  so

$$\frac{1}{\rho_2^2} = \frac{\cos^2 \phi_z}{a^2} + \frac{\sin^2 \phi_z}{b^2}, \quad \tan \phi_z = \frac{z}{x} \Rightarrow \tan \phi = p_2 \tan \phi_z \quad \text{where } p_2 = \sqrt{\frac{\beta_{x_0} \beta_x}{\beta_{z_0} \beta_{zm}}} \quad 2.21$$

Shape factor  $F_j$  is given as

$$F_j = \int_0^{2\pi} \frac{d\phi}{\theta_m^2(\phi)} = 4 \int_0^{\pi/2} \frac{d\phi}{\theta_m^2(\phi)}$$

$$\int_0^{\pi/2} \frac{d\phi}{\theta_m^2(\phi)} = \int_0^{\phi_m} \frac{\beta_{x_0} \beta_{xm} \cos^2 \phi + \beta_{z_0} \beta_z \sin^2 \phi}{\rho_1^2} d\phi + \int_{\phi_m}^{\pi/2} \frac{\beta_{x_0} \beta_x \cos^2 \phi + \beta_{z_0} \beta_{zm} \sin^2 \phi}{\rho_2^2} d\phi$$

Using  $\rho_1^2$  from equation 2.19 and  $\rho_2^2$  from equation 2.21, we get

$$\int_0^{\pi/2} \frac{d\phi}{\theta_m^2(\phi)} = \int_0^{\phi_m} (\beta_{x_0} \beta_{xm} \cos^2 \phi + \beta_{z_0} \beta_z \sin^2 \phi) \left( \frac{\cos^2 \phi_x}{a^2} + \frac{\sin^2 \phi_x}{b^2} \right) d\phi +$$

$$\int_{\phi_m}^{\pi/2} (\beta_{x_0} \beta_x \cos^2 \phi + \beta_{z_0} \beta_{zm} \sin^2 \phi) \left( \frac{\cos^2 \phi_z}{a^2} + \frac{\sin^2 \phi_z}{b^2} \right) d\phi$$

Using equation 2.19,  $\tan \phi = p_1 \tan \phi_x$  in first integral and equation 2.21,  $\tan \phi = p_2 \tan \phi_z$  in second integral, we get

$$F_j = \frac{2 \beta_{x_0} \beta_{xm}}{a^2} \left( \phi_m + \frac{1}{2} \sin 2\phi_m \right) + \frac{2 \beta_{z_0} \beta_z}{b^2} \left( \phi_m - \frac{1}{2} \sin 2\phi_m \right) +$$

$$\frac{2 \beta_{z_0} \beta_{zm}}{b^2} \left( \frac{\pi}{2} - \phi_m + \frac{1}{2} \sin 2\phi_m \right) + \frac{2 \beta_{x_0} \beta_x}{a^2} \left( \frac{\pi}{2} - \phi_m - \frac{1}{2} \sin 2\phi_m \right) \quad 2.22$$

where  $\phi_m = \tan^{-1} \left( \sqrt{\frac{\beta_{x_0} (\beta_{xm} - \beta_x)}{\beta_{z_0} (\beta_{zm} - \beta_z)} \frac{b}{a}} \right)$

$$F_j = \frac{2 \beta_{x_0} \beta_{xm}}{a^2} \left( \tan^{-1} \left( \frac{pb}{a} \right) + \frac{pab}{a^2 + p^2 b^2} \right) + \frac{2 \beta_{x_0} \beta_x}{a^2} \left( \cot^{-1} \left( \frac{pb}{a} \right) - \frac{pab}{a^2 + p^2 b^2} \right) +$$

$$\frac{2 \beta_{z_0} \beta_{zm}}{b^2} \left( \cot^{-1} \left( \frac{pb}{a} \right) + \frac{pab}{a^2 + p^2 b^2} \right) + \frac{2 \beta_{z_0} \beta_z}{b^2} \left( \tan^{-1} \left( \frac{pb}{a} \right) - \frac{pab}{a^2 + p^2 b^2} \right) \quad 2.23$$

where  $p = \left( \sqrt{\frac{\beta_{x_0} (\beta_{xm} - \beta_x)}{\beta_{z_0} (\beta_{zm} - \beta_z)}} \right)$

This is a new expression of the shape factor for an elliptical shape of vacuum chamber which has not been reported so far in the literature.

An expression of average shape factor for an elliptical chamber is reported in literature [48, 49] as below.

$$F = \pi \left[ \frac{\langle \beta_x \rangle \beta_{xm}}{a^2} + \frac{\langle \beta_z \rangle \beta_{zm}}{b^2} \right] \quad 2.24$$

where  $\langle \beta_x \rangle$  and  $\langle \beta_z \rangle$  are the average  $\beta$  function in  $X$  and  $Z$  planes,  $\beta_{xm}$  and  $\beta_{zm}$  are the maximum  $\beta$  function in  $X$  and  $Z$  planes respectively.

The expression 2.24 has been derived considering the loss of electrons at the location where both  $\beta_x$  as well as  $\beta_z$  are maximum. The derivation is given in Appendix A. From the relation A.4 from APPENDIX A, the shape factor at location  $j$  is given as

$$F_j = \pi \left[ \frac{\beta_x(s_0) \beta_{xm}}{a^2} + \frac{\beta_z(s_0) \beta_{zm}}{b^2} \right] \quad 2.25$$

A comparison in the point by point shape factor in one unit cell of Indus-2 using derived relation 2.23 and existing relation 2.25 is shown in Figure 2.4.

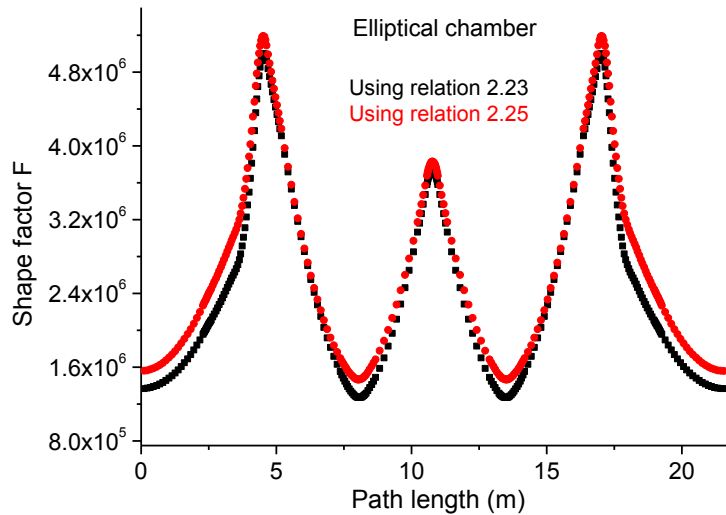


**Fig.2.4. Shape factor variation for elliptical shape of chamber**

The percentage increase in shape factor from relation 2.23 to relation 2.25 is shown in Figure 2.5.

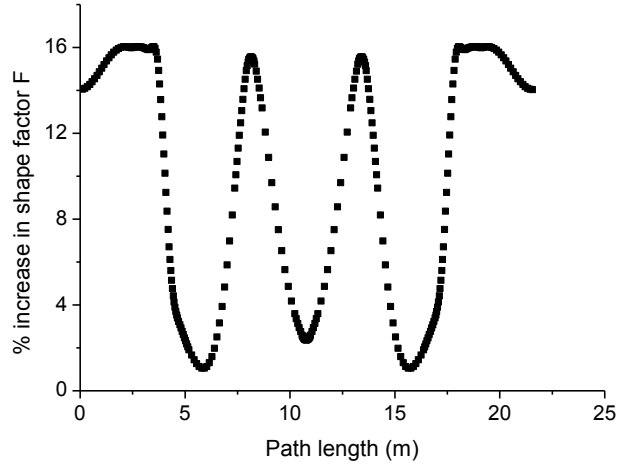


**Fig.2.5. Increase in the shape factor along the circumference in ring**

It shows that in case of Indus-2, the difference between the shape factors obtained from derived and existing expressions is more than 16% at some locations which are significant.

#### **2.4 Estimation of shape factor**

The shape factor  $F_j$  is estimated by using Indus-2 lattice parameters of design lattice for rectangular and elliptical shape of the vacuum chamber.

Considering  $\beta_{xm} = 21.1m$ ,  $\beta_{zm} = 18.7m$ ,  $\beta_x = 3.9m$ ,  $\beta_z = 5.4m$ ,  $\langle \beta_{x_0} \rangle = 8.0m$  and  $\langle \beta_{z_0} \rangle = 7.7m$ , shape factor was estimated using expression 2.15 and 2.23 at different scattering locations at uniform interval along the beam path using value of aperture  $a$  and  $b$ , for rectangular and elliptical vacuum chamber. The point by point variation of shape factor in one unit cell of Indus-2 for rectangular ( $a = 30mm, b = 15mm$ ), elliptical ( $a = 30mm, b = 15mm$ ) chamber shapes is shown in Figure 2.6.

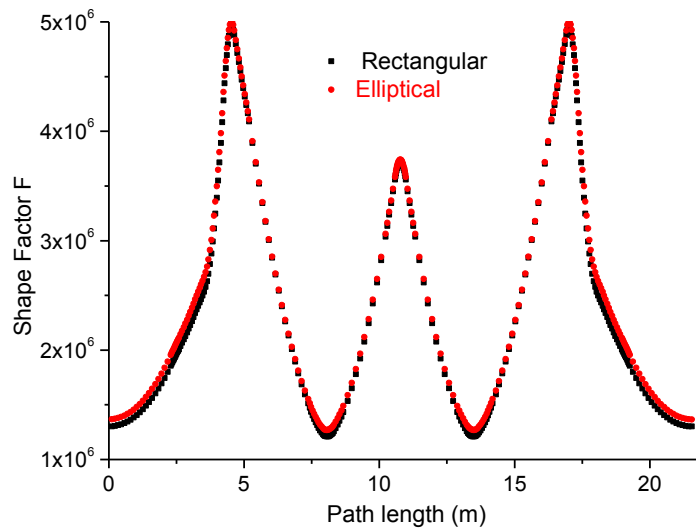


**Fig.2.6. Comparison in shape factor in one unit cell for rectangular and elliptical shape of chamber in case Indus-2**

The percentage increase in the shape factor at all scattering locations was estimated and is shown in Figure 2.7.

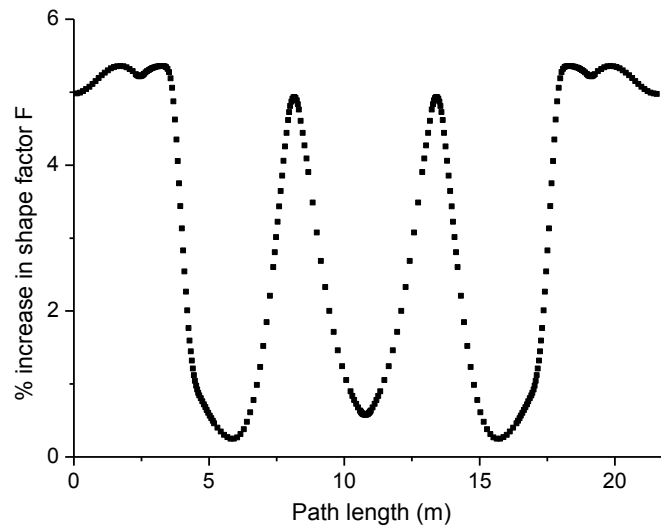


**Fig.2.7. Increase in the shape factor from rectangular to elliptical shape**

From the expression of shape factor for rectangular and elliptical shape, the shape factor for square ( $a = 30\text{mm}, b = 30\text{mm}$ ) and circle ( $\text{radius} = 30\text{mm}$ ) was estimated point by point in one unit cell of Indus-2, a comparison of shape factor is shown in Figure 2.8.

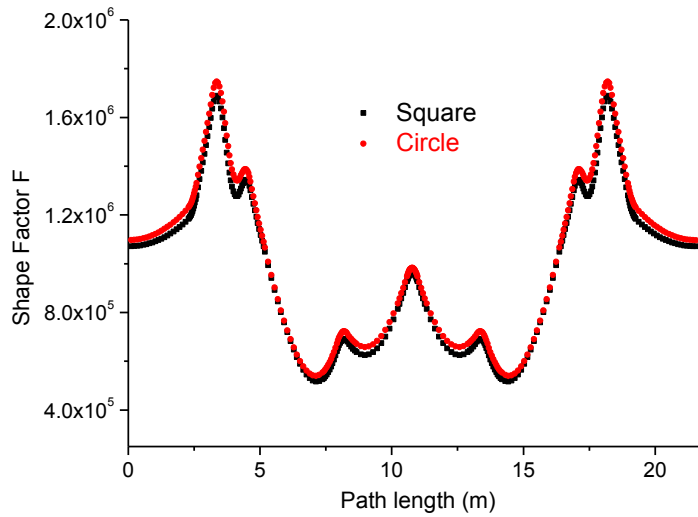


**Fig.2.8. Comparison in shape factor in one unit cell for square and circular shape of chamber**

The percentage increase in the shape factor at all scattering locations was estimated and is shown in Figure 2.9.

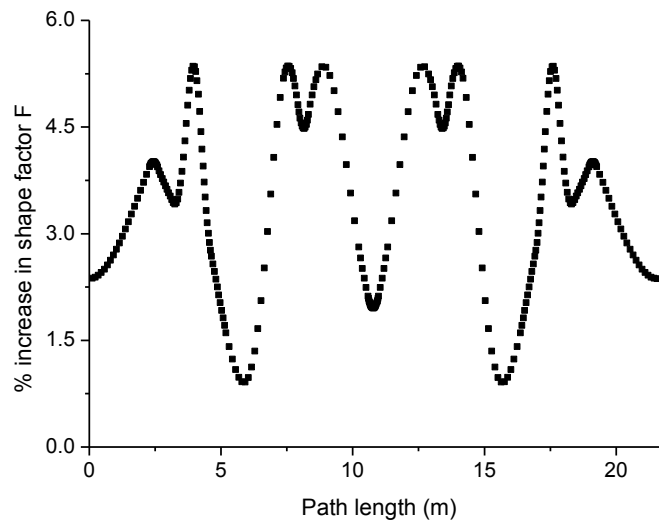


**Fig.2.9. Increase in the shape factor from square to circular shape**

Using the derived expression 2.23 of shape factor for elliptical shape and with existing expression 2.25, point by point shape factor was estimated for circular shape of chamber and the results are shown in Figure 2.10.

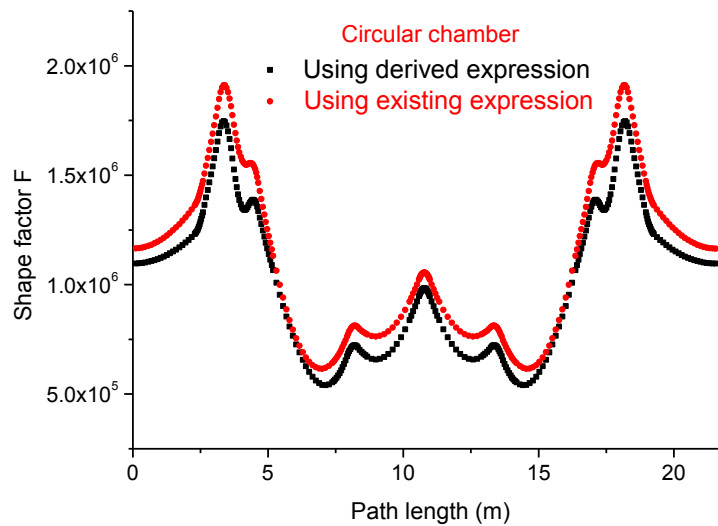


**Fig.2.10. Comparison in shape factor in one unit cell for circular shape of chamber**

The percentage increase in the shape factor for circular shape at all scattering locations was estimated and is shown in Figure 2.11.

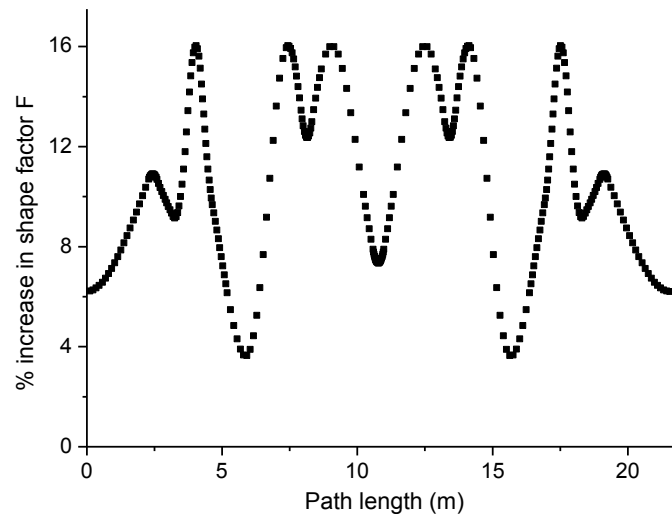


**Fig.2.11. Increase in the shape factor for circular shape**

### 2.4.1 Estimation of average shape factor

From the value of shape factor at different locations, average shape factor is estimated using equation 2.7. The average value of shape factor for rectangular ( $a = 30mm, b = 15mm$ ), square ( $a = 30mm, b = 30mm$ ), ellipse ( $a = 30mm, b = 15mm$ ) and circular ( $radius = 30mm$ ) shape of chamber using derived expression 2.15 and 2.23 and existing expression 2.16 and 2.24 is given in Table 2.1. The estimated values of average shape factor obtained from derived and existing expressions are also compared.

Table 2.1. Comparison of estimated average shape factor using derived and existing expressions for different shapes of chamber

Chamber shape	Dimensions (mm)	Average shape factor using eq. (2.7) and expressions (2.15) and (2.23) ( $F_1 \times 10^6$ )	Average shape factor from existing expression (2.16) and (2.24) ( $F_2 \times 10^6$ )	% difference $(F_2 - F_1) \times 100 / F_2$
Rectangular	a=30, b=15	2.35	2.26	-4.0
Elliptical	a=30, b=15	2.41	2.61	+7.6
Square	a=30, b=30	0.96	0.90	-6.7
Circle	Radius= 30	0.99	1.09	+9.1

From the table, if we compare the change in average shape factor from rectangular to elliptical shape ( $a = 30mm, b = 15mm$ ), the increase in shape factor from the derived expression is ~2.5% whereas it increases to ~15.5% if we use the existing expression. Similarly as reported in [25], the average shape factor increase from square to circle is ~22% (from  $0.9 \times 10^6$  to  $1.09 \times 10^6$ ) whereas from the derived expression, the increase is ~3.3% (from  $0.96 \times 10^6$  to  $0.99 \times 10^6$ ). The result for a rectangular shape closely matches with the existing

expression [25]. The small difference is attributed to the fact that in [25], an approximation has been made in the derivation of the average shape factor by using average values of the minimum scattering angles. The expressions for the shape factor developed in this chapter are required for estimation of the lifetime due to scattering of electrons with nuclei because the vacuum pressure in a storage ring is normally not the same everywhere. The expression 2.15 for the shape factor for the rectangular chamber looks similar to the expression 2.16 for the average shape factor available in the literature. It shows that the approach for the derivation is appropriate. This approach has resulted in a new expression 2.23 for the shape factor for the elliptical shape, which has evolved after considering the effect of the shape accurately.

## CHAPTER 3

### STUDIES OF ELECTRON-ELECTRON INTERACTION WITHIN A BUNCH

#### 3.1 Introduction

In an electron storage ring, circulating electrons are scattered and lost through collision with residual gas atoms present in the vacuum chamber. In addition, the electrons within a bunch collide with each other via transverse betatron oscillations and longitudinal synchrotron oscillations [25, 26]. As explained in section 1.8.3 of chapter 1, the beam loss due to electron-electron scattering within a bunch is due to Touschek effect, it was first explained by Bruno Touschek [41] after observations of the beam lifetime on Frascati storage ring ADA at Orsay, France. The Touschek effect is one of the limiting beam loss mechanisms in present day low emittance and high brilliance [52, 53] synchrotron radiation sources.

To understand the beam loss mechanism [42, 54] we consider the motion of electrons in a frame which moves with them. The betatron motion in this frame is purely transverse and a collision will transfer momentum into the longitudinal plane. Transforming back to the laboratory frame the transferred momentum is boosted by a factor  $\gamma$ . The process is shown in the Figure 3.1.

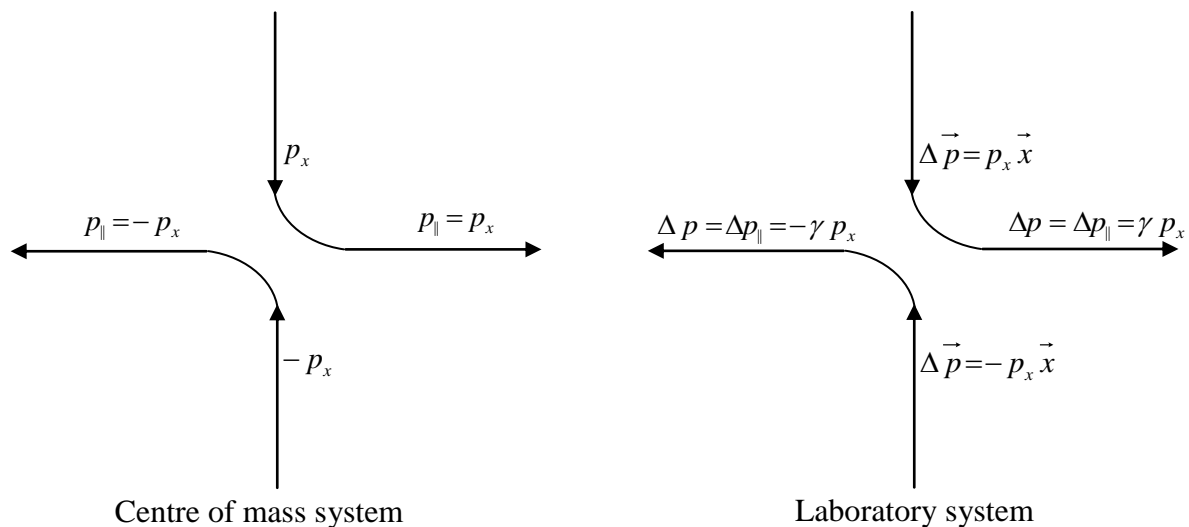


**Fig.3.1. Coulomb scattering of two electrons in centre of mass and laboratory system**

### 3.2 Expression of Touschek lifetime

The loss rate of electrons due to Touschek scattering ( $1/\tau_{tous}$ ) between electrons within a bunch is given as [25, 42, 54]

$$\frac{1}{\tau_{tous}} = -\frac{N}{\gamma^2} \frac{r_0^2 c}{8\pi \sigma_x \sigma_z \sigma_s} \frac{1}{(\Delta p/p)^3} D(\xi) \quad 3.12$$

$$\text{where } D(\xi) = \xi^{1/2} \left[ -\frac{3}{2} e^{-\xi} + \frac{\xi}{2} \int_{\xi}^{\infty} \frac{\ln u}{u} e^{-u} du + \frac{1}{2} (3\xi - \xi \ln \xi + 2) \int_{\xi}^{\infty} \frac{e^{-u}}{u} du \right] \quad 3.13$$

$$\xi = \left( \frac{\Delta p/p}{\gamma} \frac{\beta_x}{\sigma_x} \right)^2$$

The integral  $D(\xi)$  was evaluated numerically, the variation in  $D(\xi)$  with  $\xi$  is shown in Figure 3.2. The sign marked in Figure 3.2 is the value of  $D(\xi)$  for Indus-2.

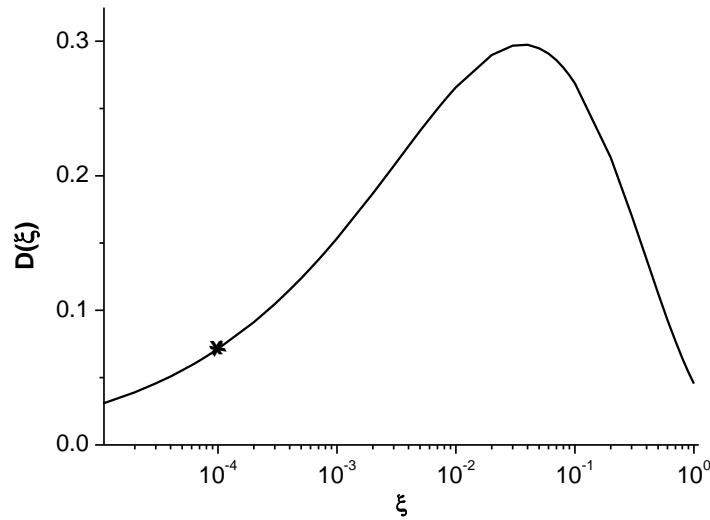


**Fig.3.2. The variation of  $D(\xi)$  with  $\xi$**

From Figure 3.5, we see that the function  $D(\xi)$  varies slowly with parameter  $\xi$ .  $\tau_{tous}$  given by the relation 3.12 gives half lifetime  $\tau_{1/2}(s)$  due to Touschek scattering at one point  $s$  in the ring. So the overall Touschek lifetime is obtained by taking the average over the whole

circumference of ring  $\tau_{1/2} = \langle \tau_{1/2}(s) \rangle$ . To convert it to  $\tau_{1/e}$  required for the estimation of total beam lifetime, the value of  $\tau_{1/2}$  is divided by  $\ln 2$ .

### 3.3 Methods for the enhancement of Touschek lifetime

In a low emittance electron storage ring operating at an average vacuum pressure  $1 \times 10^{-9}$  Torr, the beam lifetime is limited due to the electron-electron scattering within a high density electron bunch. As seen from relation 3.12 and 3.13, the Touschek lifetime is

- a) Proportional to the cube of beam energy ( $\tau_{tous} \propto \gamma^3$ ).
- b) Proportional to the square of the momentum acceptance ( $\tau_{tous} \propto (\Delta p/p)^2$ ).
- c) Proportional to beam sizes in horizontal ( $\sigma_x$ ), vertical ( $\sigma_z$ ) and longitudinal ( $\sigma_s$ ) plane ( $\tau_{tous} \propto \sigma_x \sigma_z \sigma_s$ ).
- d) Inversely proportional to the number of electrons in a bunch  $N$  ( $\tau_{tous} \propto (1/N)$ ).

To increase the Touschek lifetime, we have to increase the momentum acceptance. The momentum acceptance in transverse plane is optimised while designing the lattice and the RF acceptance is increased by increasing the RF cavity voltage. There are alternate methods for the enhancement of Touschek lifetime which are described in next section.

#### 3.3.1 Vertical beam size in Indus-2

Another way to reduce the Touschek scattering is by increasing the vertical beam size because in an electron storage ring the beam is nearly flat. As we know, in a normal quadrupole, the force experienced by the electron displaced in horizontal plane is in horizontal direction and similarly for electron displaced in vertical plane, the force is in vertical direction. If there is rotation error in normal quadrupole along the longitudinal axis then the electron displaced in horizontal plane experience a force in vertical plane and for electron displaced in vertical plane experience a force in horizontal plane. So, due to the rotational error in normal quadrupoles about the beam direction, there is coupling between

horizontal and vertical motion and it give rise to vertical emittance in storage ring. The rotated quadrupoles in dispersion region ( $\eta_x \neq 0$ ) will give rise to vertical dispersion and due to this vertical dispersion, there is also vertical emittance in ring. So, the vertical size of the electron beam in Indus-2 is mainly defined by two processes, first is betatron coupling between vertical and horizontal motion and second is due to the residual vertical dispersion function.

Main sources of vertical beam emittance [55-64] is

- a) Betatron coupling due to rotation error in normal quadrupoles along beam axis and vertical closed orbit distortion at sextupole location
- b) Residual Vertical dispersion (generated due to dipole rotation error, quadrupole transverse displacement, quadrupole rotation in dispersion region, sextupole transverse displacement)

### 3.3.1.1 Measurement of betatron coupling in Indus-2

In the presence of betatron coupling, the horizontal oscillatory motion of a beam can be transferred to the vertical motion, thereby increasing the vertical beam size. It is necessary to measure the degree of coupling in the storage ring.

Under the influence of linear coupling, the ratio of vertical beam emittance ( $\varepsilon_z$ ) to the horizontal beam emittance ( $\varepsilon_x$ ) known as coupling ratio is given by [65]

$$\kappa = \frac{\varepsilon_z}{\varepsilon_x} = \frac{|\Delta\nu_{\min}/\Delta_1|^2}{(2 + |\Delta\nu_{\min}/\Delta_1|^2)} \quad 3.14$$

where  $\Delta\nu_{\min}$  is the minimum tune separation at coupling resonance and  $\Delta_1 = \nu_x - \nu_z - p$ .

The coupling ratio  $\kappa$  is measured by driving the tunes across the coupling resonance. By changing current in one of the quadrupole power supplies, the betatron tunes are changed and when the tunes are close to the coupling resonance, the horizontal motion is transferred to the

vertical plane and vice versa which leads to a coupling between horizontal and vertical motion. In Indus-2, the strength of Q3D family of quadrupoles was changed gradually at the same rate and betatron tune in both horizontal and vertical plane was measured. Q3D family quadrupoles were chosen for measurement because it is in a non-dispersion region and the change in betatron tune in both planes with change in quadrupole current is less as compared to the other quadrupoles like Q1D and Q2F which are also in the non dispersion region. Figure 3.3 shows the measured horizontal and vertical betatron tunes as a function of the quadrupole current in Q3D family of quadrupoles [66].

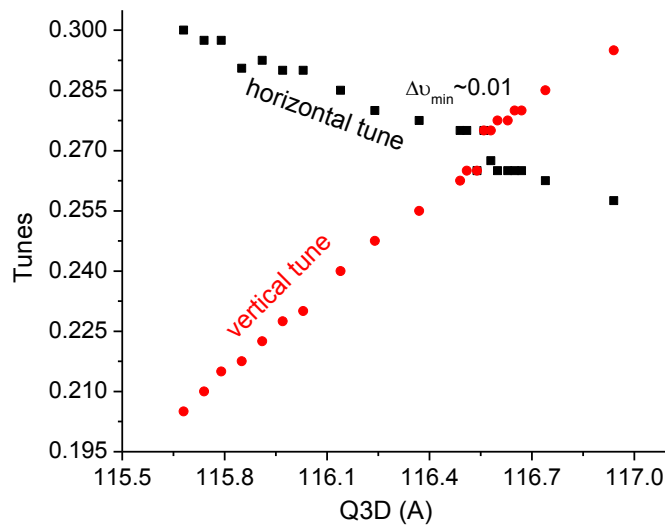


**Fig.3.3. Measured horizontal and vertical fractional betatron tunes with change of current in Q3D family of quadrupoles**

From Figure 3.6, the value of minimum tune separation at coupling resonance is  $\Delta\nu_{\min} \sim 0.01$ . From relation 3.14, the coupling ratio is 0.0049 (0.49%).

### 3.3.1.2 Measurement of vertical dispersion in Indus-2

By changing the RF frequency up to 8 kHz in steps of 2 kHz, change in vertical closed orbit at all beam position indicators was observed. If with frequency change  $\Delta f_{rf}$ , there is change in orbit  $\Delta z$  in vertical plane, then the vertical dispersion is given as  $\eta_z = \Delta z / (\Delta p / p)$  where

change in momentum or energy is  $\frac{\Delta p}{p} = \frac{1}{\alpha_c} \frac{\Delta f_{rf}}{f_{rf}}$  where  $\alpha_c$  is the momentum compaction factor and  $f_{rf}$  is the RF frequency and  $\Delta f_{rf}$  is the change in RF frequency.

Change in energy was estimated considering  $\alpha_c = 0.00732$ . The measured value of vertical dispersion at BPIs location with RF frequency change  $\Delta f_{rf} = 8 \text{ KHz}$  is shown in Figure 3.4.

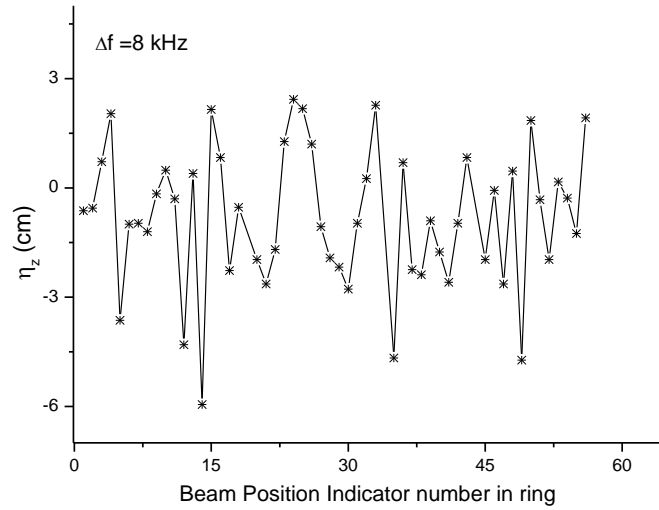


**Fig.3.4. Measured vertical dispersion at all BPI locations in Indus-2**

The vertical beam size  $\sigma_z$  is given by  $\sigma_z(s) = \sqrt{\varepsilon_z \beta_z(s) + \eta_z^2(s) (\sigma_\varepsilon / E_0)^2}$

### 3.3.1.3 Beam size measurement at beamline-16

The coupling measurement was complemented with the technique of beam size measurement at one of the dipole beamlines. The beam sizes were measured at micro focus X-ray fluorescence beamline (XRF-microprobe beamline-16) [67] which is connected at 5° port of one of the dipole magnets. The measured horizontal and vertical beam sizes are  $\sigma_x(FWHM) = 7.5 \mu\text{m}$  and  $\sigma_z(FWHM) = 4.3 \mu\text{m}$  respectively. These beam sizes were measured at ~17 m away from the source point in storage ring. After applying the demagnification factors of 118 in horizontal plane and 54 in vertical plane, the horizontal and vertical beam size at the source point are 885  $\mu\text{m}$  and 232.2  $\mu\text{m}$  respectively.

The electron beam sizes in horizontal and vertical planes at the source point are given by

$$\sigma_x = \sqrt{\varepsilon_x \beta_x + \eta_x^2 (\sigma_\varepsilon / E_0)^2}$$

$$\sigma_z = \sqrt{\varepsilon_z \beta_z + \eta_z^2 (\sigma_\varepsilon / E_0)^2}$$

For the operating lattice, the optical functions  $\beta_x, \beta_z, \eta_x$  at the source point are 0.636m, 6.362m, 0.00123m respectively, for which  $\eta_x^2 (\sigma_\varepsilon / E_0)^2 \ll \varepsilon_x \beta_x$  and measured value of vertical dispersion at source is  $\sim 1.2$ cm, so  $\eta_z^2 (\sigma_\varepsilon / E_0)^2 \approx 7 \times 10^{-11}$  is very small. It leads to simple formula for the coupling ratio  $\kappa$  as

$$\kappa = \frac{\varepsilon_z}{\varepsilon_x} \approx \frac{\beta_x}{\beta_z} \frac{\sigma_z^2}{\sigma_x^2} \quad 3.15$$

Using the measured beam sizes and the lattice function in relation 3.15, the coupling ratio comes out to be 0.0066 (0.66%). This value is very close to the coupling ratio obtained using minimum tune separation method. So by increasing betatron coupling, Touschek lifetime in an electron storage ring can be increased.

### 3.3.2 RF phase modulation

Touschek lifetime can be enhanced by decreasing the density of electron bunches. This can be done by applying RF phase modulation in main RF which has been applied in other synchrotron radiation sources such as KEK photon factory [68, 69], ASTRID [70], LNLS [71], PLS [72], TLS [73] ring for the improvement in Touschek lifetime. A theoretical simulation study of the application of RF phase modulation of nearly one and two times of synchrotron oscillation frequency in main RF of Indus-2 ring at beam energy 2.5 GeV was carried out.

#### 3.3.2.1 Longitudinal beam dynamics under RF Phase modulation

Considering the longitudinal motion of a single electron under RF phase modulation and neglecting the beam loading effect, let  $\tau$  be the longitudinal time advance of an electron

away from the position of synchronous particle and  $\delta$  be the relative energy deviation from that of the synchronous particle, the equations of motion [68] for electron are given as

$$\frac{d\tau}{dt} = -\alpha_c \delta \quad 3.14$$

$$\frac{d\delta}{dt} = \frac{eV_{rf} \cos(\phi_s - \omega\tau + \phi_m) - U_0}{T_0 E_0} - 2\gamma_\varepsilon \delta \quad 3.15$$

where  $\alpha_c$  is the momentum compaction factor,  $e$  is the electron charge,  $V_{rf}$  is the RF cavity peak voltage,  $\phi_s$  is the synchronous phase,  $\omega$  is the angular RF frequency,  $U_0$  is the synchrotron radiation loss per turn for the synchronous particle,  $T_0$  is the revolution time,  $E_0$  is the energy of the synchronous particle,  $\gamma_\varepsilon$  is the radiation damping rate in longitudinal plane and  $\phi_m$  is the phase modulation. The simulation is carried out with RF phase modulated at the one and twice of the synchrotron oscillation frequency  $\omega_s$ .

$$\phi_m = \phi_{m0} \cos(\omega_s t) \text{ and } \phi_m = \phi_{m0} \cos(2\omega_s t)$$

where  $\phi_{m0}$  is the modulation amplitude and  $\omega_s$  is the unperturbed synchrotron frequency which is given as

$$\omega_s = \sqrt{\frac{\alpha_c \omega e V_{rf} \sin \phi_s}{T_0 E_0}}$$

### 3.3.2.2 Criterion for RF phase modulation

In order that the cavity field can follow any modulation in the input RF wave, the bandwidth of the cavity which is the ratio of cavity resonant frequency to the loaded quality factor should be comparable to or wider than the modulation frequency. In Indus-2, cavity bandwidth is about ~50 kHz, so the cavity can follow the phase modulation up to about this frequency with certain amplitude and phase response due to the cavity impedance.

### 3.3.2.3 Effect of the RF phase modulation on distribution of electrons in a bunch

A simulation study of the effect of RF phase modulation on the distribution of electrons in a bunch was carried out using particle tracking code ELEGENT [32]. The particle tracking equation is given as

$$\tau_{n+1} = \tau_n - \alpha \delta_n T_0$$

$$\delta_{n+1} = (1 - 2\gamma_\epsilon T_0) \delta_n + \frac{[eV_{rf} \cos(\phi_s - \omega\tau_n + \phi_m) - U_0]}{E_0}$$

where  $n$  is the number of turns of electron motion

Particle tracking considering 5000 electrons in a bunch was carried out in longitudinal plane for 10,000 turns with nearly one and two times of synchrotron frequency and with different modulation amplitude. With applied RF modulation frequency of 20.5 kHz, 41 kHz and modulation amplitude of  $3^\circ$ , the longitudinal phase space of electrons at the start of tracking i.e. 0 turn, after 1000 turns and 10000 turns are shown in Figure 3.5(a)-(c) and 3.6(a)-(c) respectively, where  $\gamma$  on y-axis is the relativistic factor. The tracking results show that by applying the RF phase modulation of nearly two times of synchrotron oscillation frequency, the distribution of electrons in a bunch in phase space changes. In low emittance storage ring, the density of electrons in a Gaussian bunch is higher at the centre. Due to high density of electron at the bunch centre, there is a large scattering which causes loss of electrons and decrease in beam lifetime. As seen in Figure 3.6(c), the density of the electrons at the centre of the bunch become lesser and the distribution is divided in two parts by applying RF phase modulation so there is less scattering. The electrons execute two states of stable oscillations, the phases of which are opposite to each other, there arises a quadrupole mode longitudinal oscillation of the electrons and it leads to increase in bunch length [68, 74] which causes the increase in Touschek lifetime. The studies show that it is not happening if we apply phase modulation of frequency near to synchrotron frequency as shown in Figure 3.5(c).

Modulation with synchrotron frequency

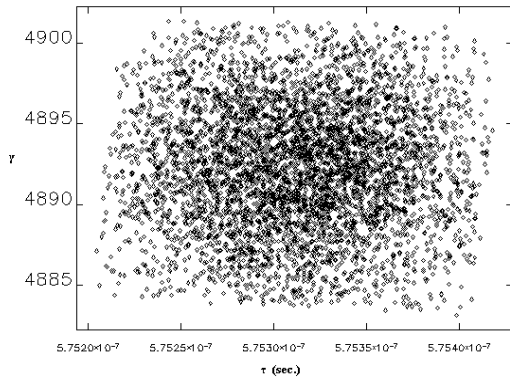


*Fig.3.5(a). Electron distribution at the start of tracking*

Modulation with two times of synchrotron frequency

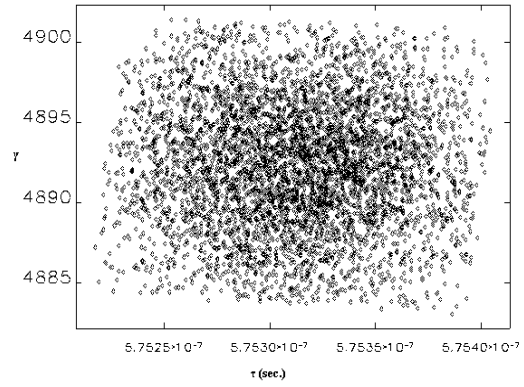


*Fig.3.6(a). Electron distribution at the start of tracking*

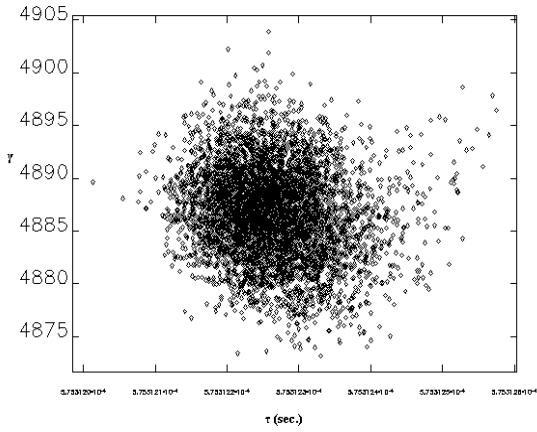


*Fig.3.5(b). Electron distribution after 1000 turns*

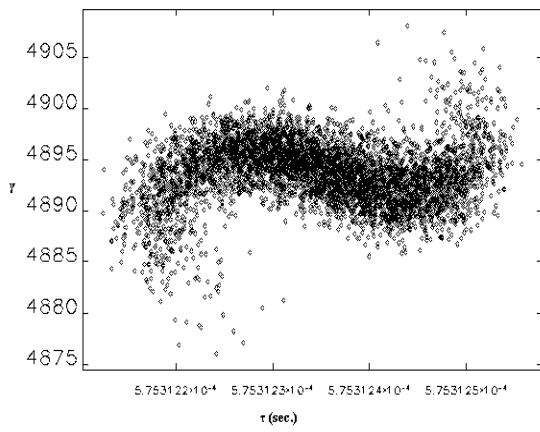


*Fig.3.6(b). Electron distribution after 1000 turns*

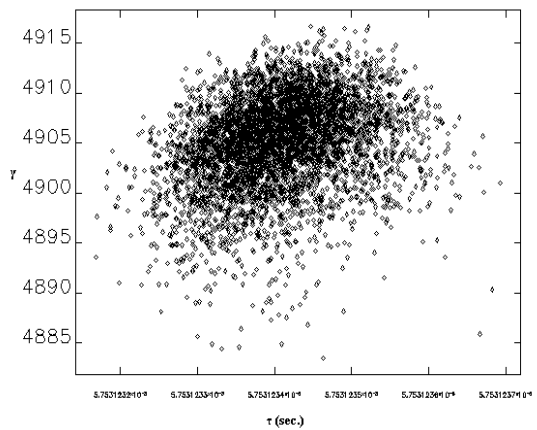


*Fig.3.5(c). Electron distribution after 10,000 turns*

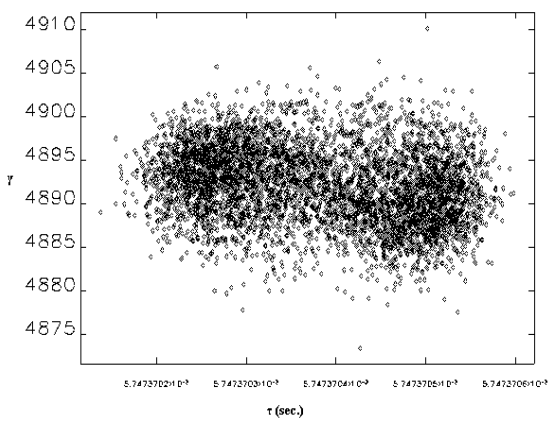
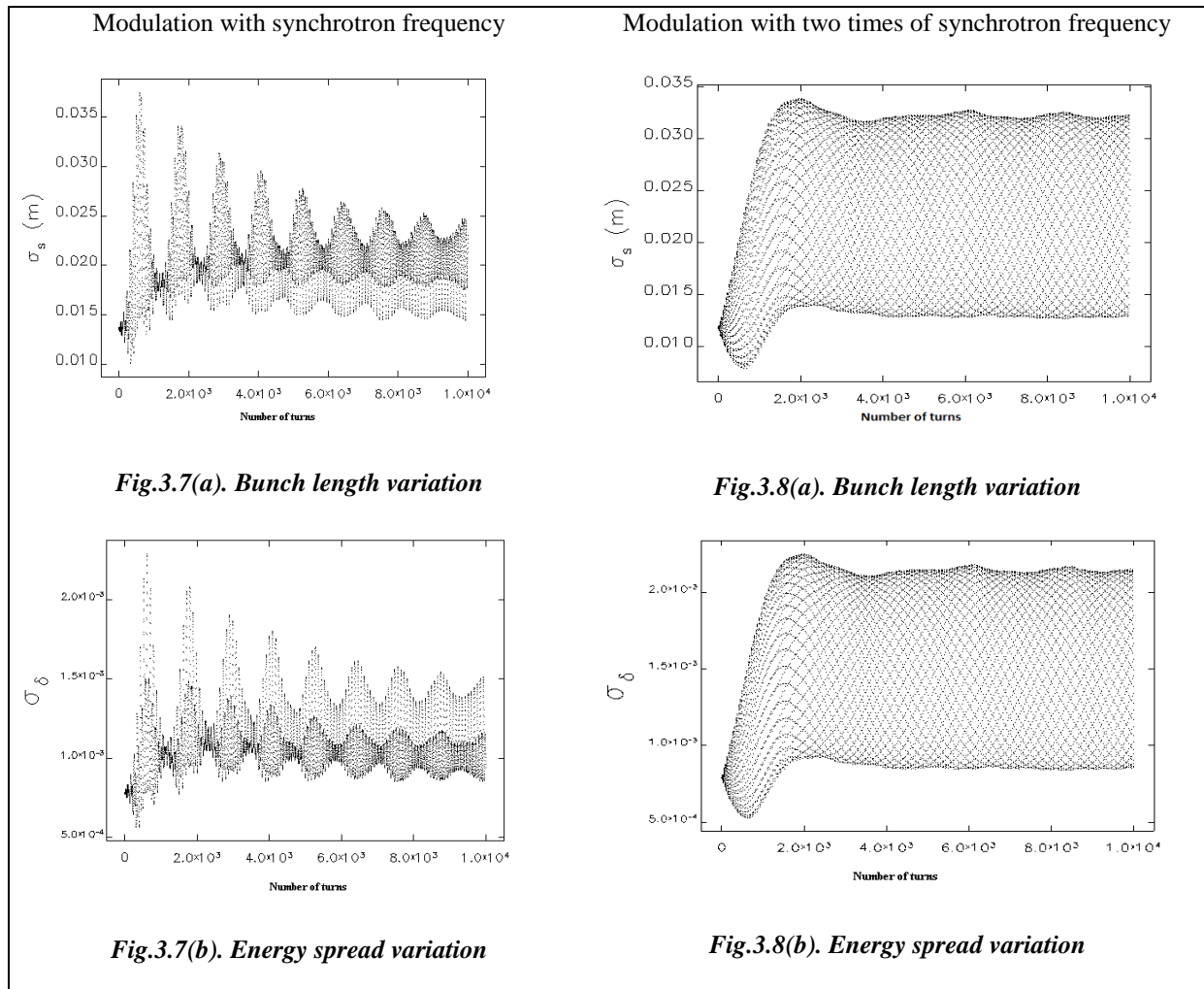


*Fig.3.6(c). Electron distribution after 10,000 turns*

### 3.3.2.4 Effect of RF phase modulation on longitudinal beam parameters

To study the effect of RF phase modulation on bunch length  $\sigma_s$  and energy spread  $\sigma_\delta$ , particle tracking of 5000 electrons in a bunch was carried out for 10,000 turns. The tracking results are shown in Figure 3.7(a, b) and 3.8(a, b) respectively.



The bunch length and energy spread in Indus-2 at beam energy 2.5 GeV and cavity voltage 1200 kV without RF phase modulation are 1.53 cm and  $9 \times 10^{-4}$  respectively. The tracking results show that by applying RF phase modulation of nearly two times of synchrotron frequency, the bunch length is increased on an average from 1.53 cm to 2.0 cm and increase in energy spread is from  $9 \times 10^{-4}$  to  $1.1 \times 10^{-3}$ .

Touschek lifetime is proportional to the bunch length. The increase in bunch length by the application of RF phase modulation [74] gives rise to increase in Touschek lifetime. If the beam lifetime is Touschek limited then by the application of RF phase modulation, the overall beam lifetime will increase.

### **3.3.2.5 Implementation of RF phase modulation in Indus-2**

A schematic diagram of RF phase modulation implemented in Indus-2 ring is shown in Figure 3.9. An experiment was conducted to study the effect of RF phase modulation in present operating condition. The applied RF cavity peak voltage was ~1200 kV. Beam spectrum was observed on a spectrum analyzer and a signal of main RF was observed at operating frequency ~505.812 MHz. The estimated synchrotron frequency at RF voltage 1200 kV is 20.5 kHz.

RF phase modulation of frequency ~41 kHz was made ON with  $0^\circ$  modulation amplitude. No signal of modulation frequency was observed on beam spectrum. By increasing the modulation amplitude, the modulated frequency signal was seen at a separation of ~41 kHz from the main RF signal. As the modulation amplitude was increased, the modulated signal amplitude on beam spectrum also increased. The beam spectrum without applying RF phase modulation and for RF modulated frequency ~41 kHz and modulation amplitude  $3^\circ$  is shown in Figure 3.10(a) and (b) respectively.

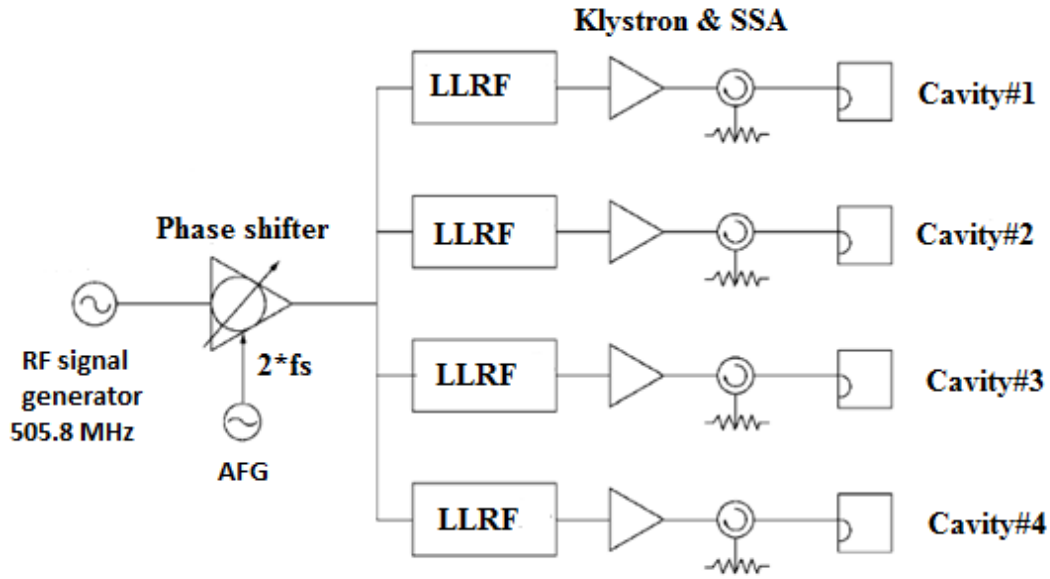
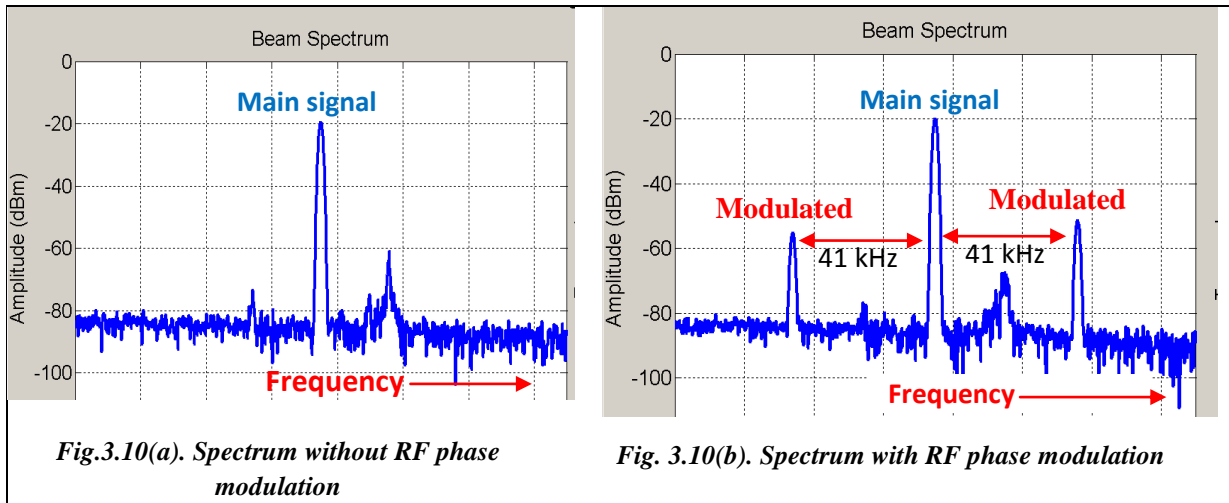


*Fig.3.9. RF phase modulation in Indus-2, AFG is arbitrary frequency generator,  $f_s$  is synchrotron frequency, LLRF is Low Level RF system, SSA is solid state amplifier*



The stored beam current in the ring at the time of experiment was  $\sim 100$  mA at beam energy 2.5 GeV. From the beam spectrum showing the phase modulated signal, we found that the beam has undergone the RF phase modulation. The beam lifetime at stored current 100 mA before and after applying the phase modulation was observed and found nearly same. It shows that the beam lifetime is not Touschek lifetime limited in Indus-2.

## CHAPTER 4

### EXPERIMENTAL STUDIES OF BEAM LIFETIME IN INDUS-2

#### 4.1 Introduction

Beam lifetime measurements and its theoretical analysis using measured vacuum pressure and applied radio frequency (RF) cavity voltage in Indus-2 electron storage ring at beam energy 2 GeV were carried out. Experimental studies of the effect of RF cavity voltage and bunched beam filling pattern on beam lifetime were also carried out. An equation of stable beam current decay is evolved and this equation closely follows the observed beam current decay pattern. It shows that the beam is stable and the beam current decay is mainly due to the beam-residual gas interaction and electron-electron interaction within a bunch. The estimated vacuum, Touschek and total beam lifetimes from analytical formulations are also compared with the measured beam lifetime.

The pressure in the ring has gradually reduced (at 100 mA stored current, average pressure:  $1.2 \times 10^{-9}$  Torr) due to cleaning of the surface of vacuum chamber by synchrotron radiation. The pressure reduction, closed orbit correction [75] and optimization of RF phase with electron beam have led to the improvement in beam lifetime from ~1.5 hours to ~22 hours at stored beam current 100 mA.

Experiments were conducted to study the beam lifetime and loss mechanism during the beam current decay from 100 mA to 50 mA at beam energy 2 GeV. Experiments were also conducted to study the effect of RF cavity voltage on beam lifetime to find the limiting momentum acceptance in transverse as well as in the longitudinal plane. There are 291 RF buckets available for electron beam accumulation in Indus-2 storage ring. To study the effect of bunch filling pattern on beam lifetime, experiments were conducted by accumulating electron beam current uniformly in all 291 RF buckets and also accumulating same amount of current in two-third RF buckets keeping the rest one-third empty. During all these

experiments, safety shutters of all working beam lines (open for synchrotron radiation users) were kept closed to avoid any variation in storage ring pressure through beam lines.

An analysis was carried out using analytical formulations to estimate the vacuum, Touschek and total beam lifetimes with existing vacuum pressure and applied RF cavity voltages. The estimated vacuum, Touschek and total beam lifetimes are compared with the measured beam lifetimes.

As regards the number of bunches in the circulating current, there is a provision to fill [76] all the RF buckets uniformly or fill part of RF buckets in succession keeping the remaining RF buckets empty or to fill only one RF bucket leading to a single bunch. The experimental results of beam lifetime studies carried out at beam energy 2 GeV in multi-bunch mode are presented in this chapter.

#### **4.2 Effect on beam lifetime due to the emission of synchrotron radiation**

At the start of operation of Indus-2 at beam energy 2 GeV, the measured beam lifetime at 100 mA stored beam current was ~1.5 hours. Short beam lifetime is attributed to increase in pressure (at 100mA stored current, average pressure in the ring:  $1.3 \times 10^{-8}$  Torr) resulting from the photo-induced desorption of gases from the vacuum chamber caused by the incident synchrotron radiation emitted from the circulating electron beam. With cleaning of the vacuum chamber surface due to emission of synchrotron radiation, the reduction in vacuum pressure was observed and this led to an increase in beam lifetime. A comparison in beam current decay from 100 mA to 50 mA with time was observed and is shown in Figure 4.1.

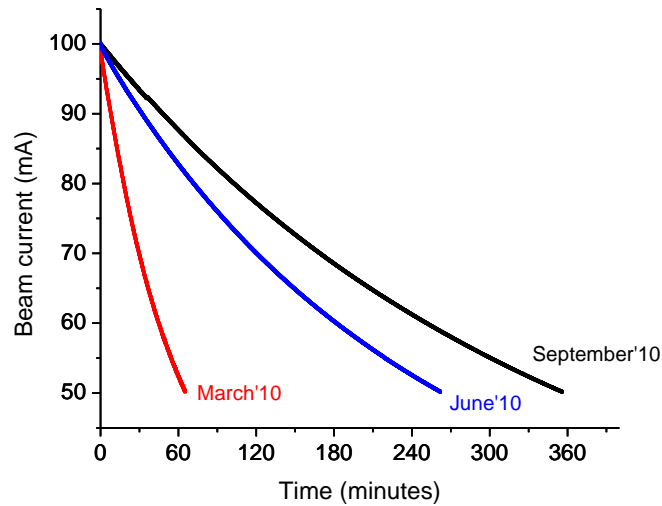


**Fig.4.1. Comparison in beam current decay with time**

During the beam current decay as shown in Figure 4.1, vacuum pressure and beam lifetime was measured. Vacuum pressure was measured from Bayard Alpert Gauges (BAGs) installed in ring. The systematic diagram of one unit cell in Indus-2 with vacuum pumps and BAGs are shown in Figure 4.2 [77, 78]. A DC Current Transformer (DCCT) installed in long straight section 7 (LS-7) is used for the measurement of average beam current circulating in the storage ring.

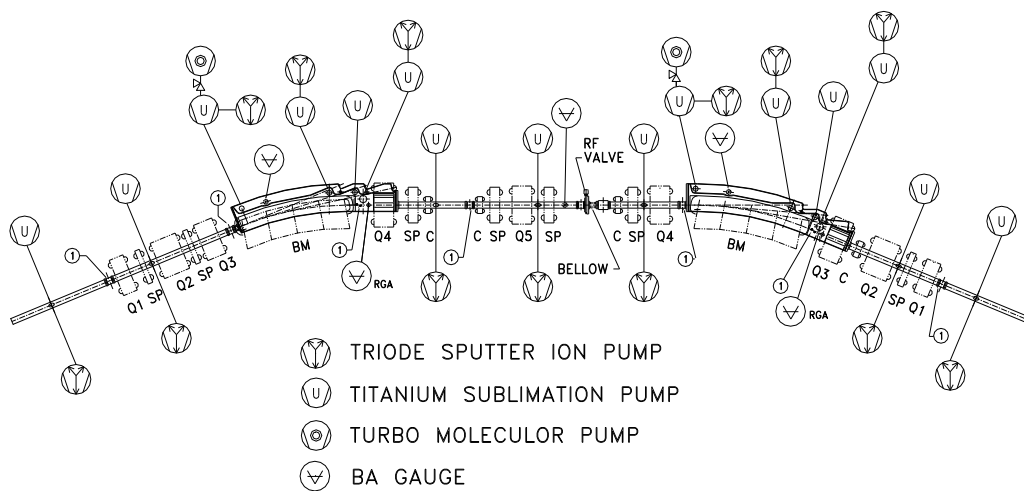


**Fig.4.2. BAGs and vacuum pumps location in one unit cell of Indus-2**

The average vacuum pressure and beam lifetime with different stored beam current during beam current decay is shown in Figure 4.3.

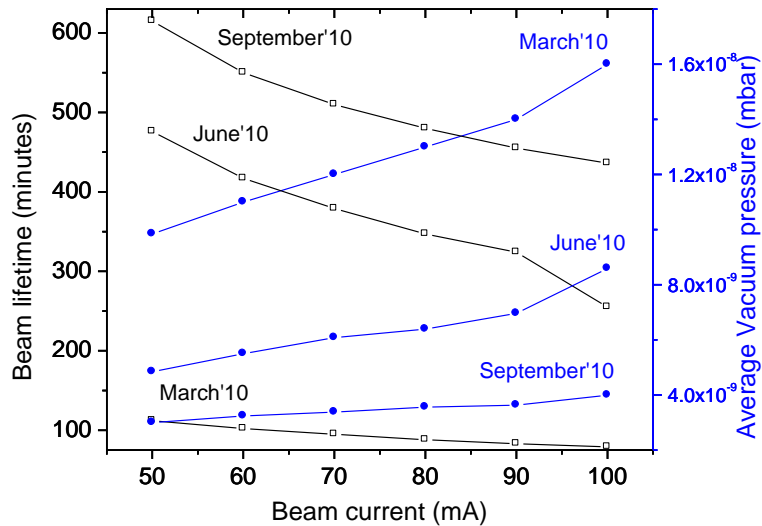


*Fig.4.3. Average vacuum pressure and beam lifetime during beam current decay*

During the above measurements, all other parameters in the storage ring were same except the vacuum pressure. So, due to the reduction in pressure with time, an increase in beam lifetime was observed.

### 4.3 Effect of aperture on beam lifetime

The total displacement of the beam from the ideal design orbit is given by

$$x = x_{cod} + x_{\beta} + x_{\eta} \quad 4.1$$

where  $x_{cod}$  is displacement due to closed orbit distortion,  $x_{\beta}$  due to betatron oscillation and  $x_{\eta}$  due to off momentum electrons. As explained in section 1.7 in chapter 1 that due to dipolar field error, there is distortion in ideal closed path of electrons in the ring so the aperture available for beam motion is reduced this lead to decrease in beam lifetime. Beam experiments were conducted to study the effect of aperture on the beam lifetime. For the first experiment, a beam current 100 mA at beam energy 2 GeV was stored and beam current

decay with time was taken without applying closed orbit correction. Next experiment was conducted with the same condition but with applying closed orbit correction. The closed orbit in horizontal plane was corrected by energizing 48 horizontal steering magnets and in vertical plane using 40 vertical steering magnets. The horizontal and vertical closed orbit was monitored and corrected at 56 beam position indicators. The beam current decay without and with closed orbit correction is shown in Figure 4.4.

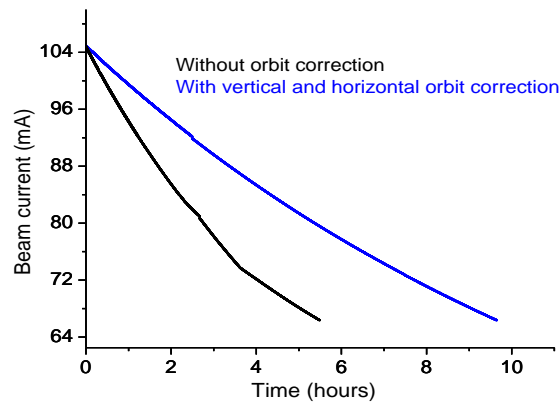
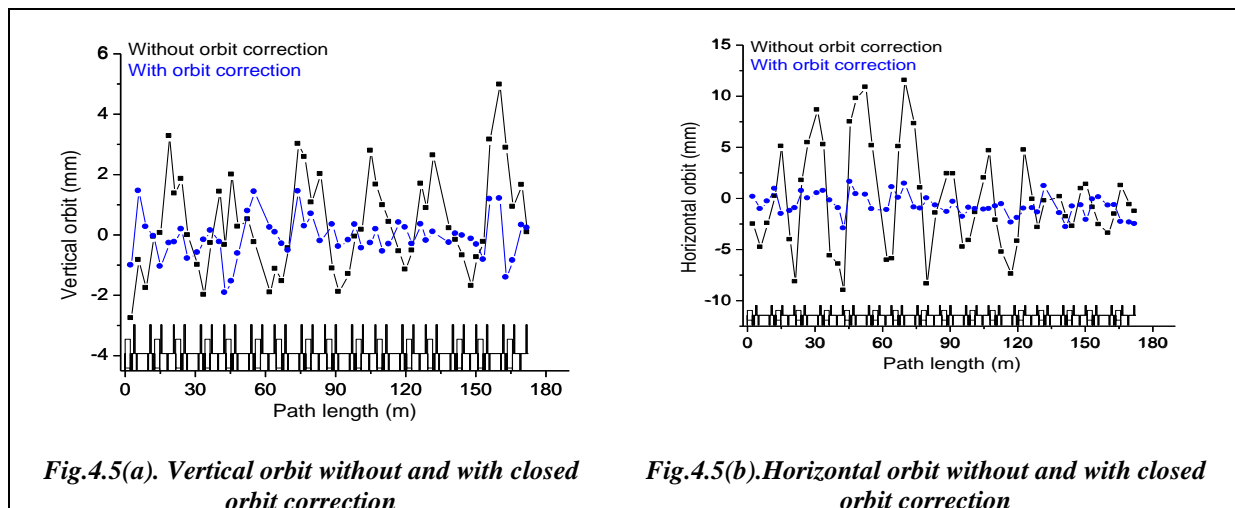
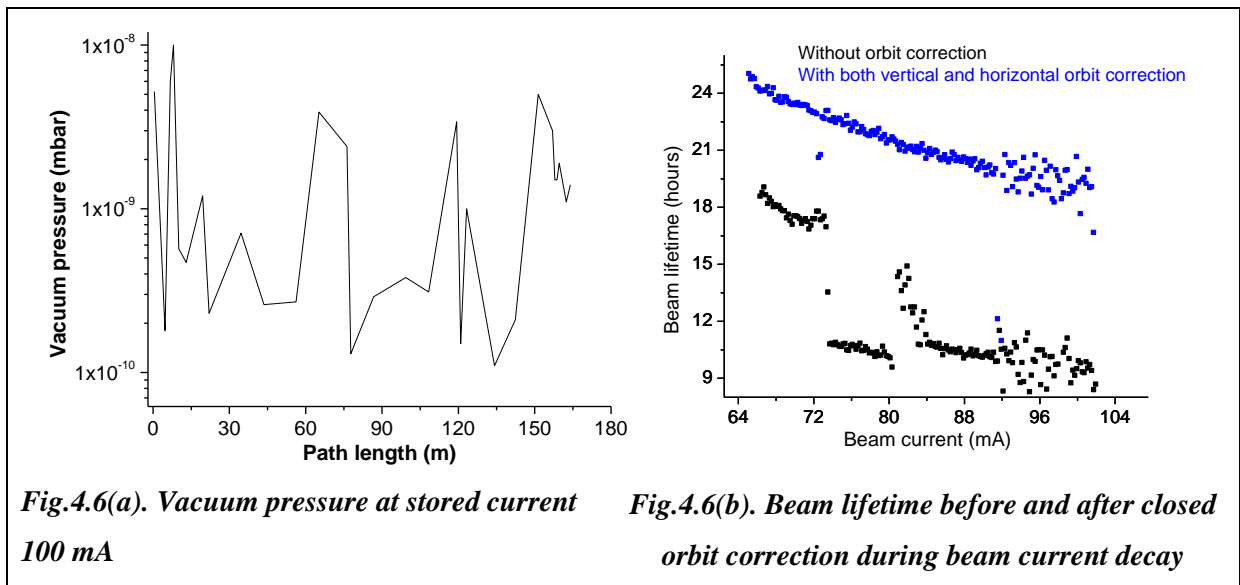


**Fig.4.4. Beam current decay without and with closed orbit correction**

The vertical and horizontal closed orbit without and with closed orbit correction is shown in Figure 4.5(a) and (b) respectively. Uncorrected rms horizontal and vertical orbit at beam position indicators were 5 mm and 1.7 mm respectively whereas the corrected rms horizontal and vertical orbit reduced to 1.3 mm and 0.7 mm respectively.



Vacuum pressure along the beam path was also monitored; the pressure along the beam path is shown in Figure 4.6(a). From the beam current decay data, beam current decay rate  $dI/dt$  was estimated for a short duration and from this beam lifetime was estimated. The beam lifetime during beam current decay without and with closed orbit correction is shown in Figure 4.6(b). The results show that without closed orbit correction, the beam lifetime suddenly reduced at beam current 80 mA and it was observed several times but this phenomenon was not observed when closed orbit correction was applied. It shows that without closed orbit correction, the aperture available for beam motion is reduced so the distance of beam centre from the vacuum chamber wall also reduced and beam undergoes unstable motion. So after applying closed orbit correction, beam instabilities may be suppressed and significant improvement in beam lifetime was achieved.



#### 4.4 Equation of beam current decay with time

As electrons circulate in an electron storage ring they collide within the bunch and also with residual gas atoms. The rate of electron loss can be written as [79]

$$-\frac{dI}{dt} = I^2 \sigma_T + I \rho \sigma_B + I \rho \sigma_C \quad 4.2$$

Where  $I$  is total beam current,  $\rho$  is the residual gas density and  $\sigma_{T,B,C}$  are the effective scattering cross sections of the electron loss due to Touschek, inelastic or bremsstrahlung and elastic coulomb scattering respectively. If we include the dynamic pressure response  $\rho = \rho_0 + \rho'_0 I$  and put in equation 4.2, we get

$$-\frac{dI}{dt} = I^2 [\sigma_T + \rho'_0 (\sigma_C + \sigma_B)] + I [\rho_0 (\sigma_C + \sigma_B)]$$

It has the form  $-\frac{dI}{dt} = a.I + b.I^2$  4.3

where  $a = \rho_0 (\sigma_C + \sigma_B)$  and  $b = \sigma_T + \rho'_0 (\sigma_C + \sigma_B)$  are the arbitrary constants.

After integration of equation 4.3, we get

$$I(t) = \frac{I_0}{e^{at} + \frac{b}{a} I_0 (e^{at} - 1)}$$
 4.4

where  $I_0$  is the Initial stored beam current at time  $t = 0$ .

#### 4.5 Beam current decay and lifetime with 900 kV RF cavity voltage

Beam current  $\sim 100$  mA at beam energy 2 GeV was stored with total RF cavity peak voltage of 900 kV by energizing all four RF cavities at the same voltage. In this condition, electron beam was accumulated uniformly in all 291 RF buckets ( $\sim 0.34$  mA, equivalent to  $1.23 \times 10^9$  electrons in a bunch per bucket). Beam current decay from stored beam current 100 mA to 50 mA was measured and is shown in the Figure 4.7(a). During the beam current decay, vacuum pressure in the ring was also measured. Betatron and synchrotron tunes during the beam current decay remained unchanged. It shows that the beam optics also remains unchanged during the experiments. From the beam current decay data, decay rate ( $-dI/dt$ ) and instantaneous beam lifetime [ $-I/(dI/dt)$ ] were estimated. The beam lifetime at different stored beam current is shown in the Figure 4.7(b).

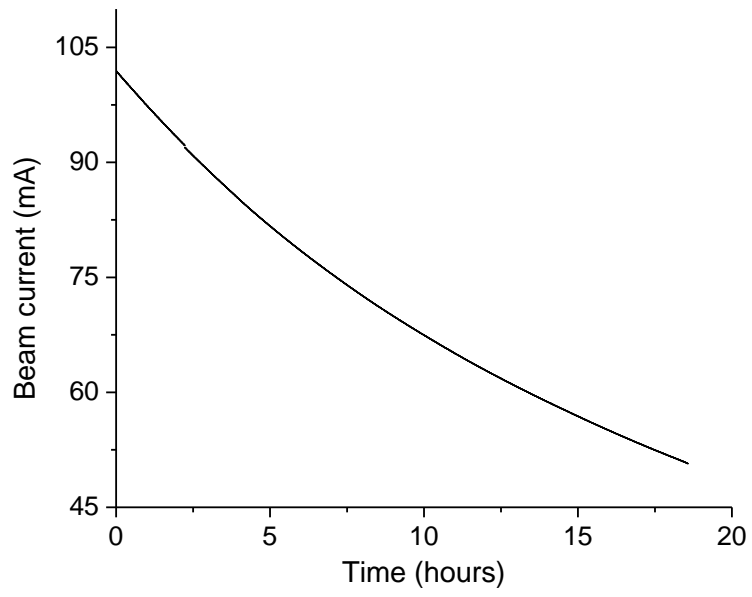


***Fig.4.7(a). Measured beam current decay***

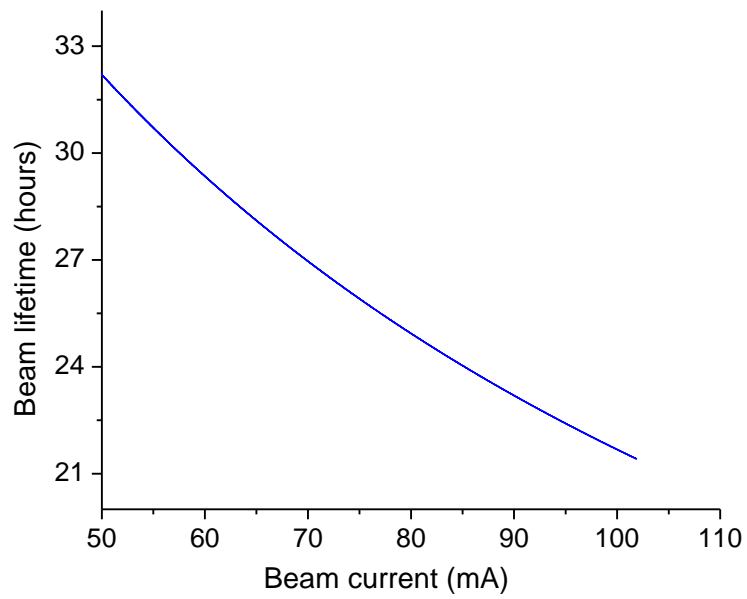


***Fig.4.7(b). Beam lifetime at different stored beam current during beam current decay***

#### 4.5.1 Beam current decay and lifetime with 750 kV RF cavity voltage

To study the limiting momentum acceptance, an experiment was conducted with RF cavity peak voltage 750 kV. In this condition, a comparison in beam current decay and beam lifetime from 102 to 85 mA with RF voltage of 750 and 900 kV are shown in the Figure 4.8(a) and 4.8(b) respectively. In this condition, all 291 RF buckets were filled uniformly. It shows that by increasing cavity voltage, RF acceptance increases that leads to increase in beam lifetime.

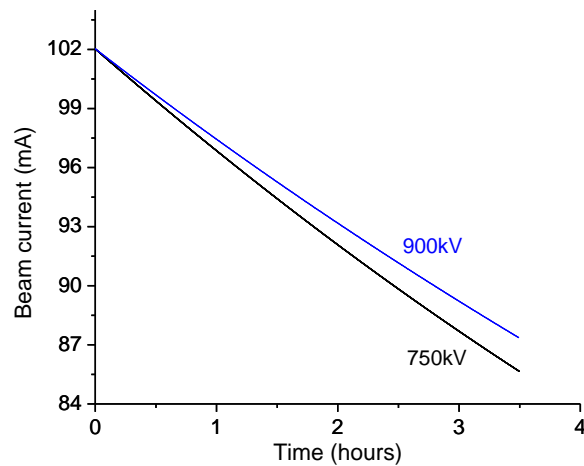


*Fig.4.8(a). Beam current decay at different RF voltages*

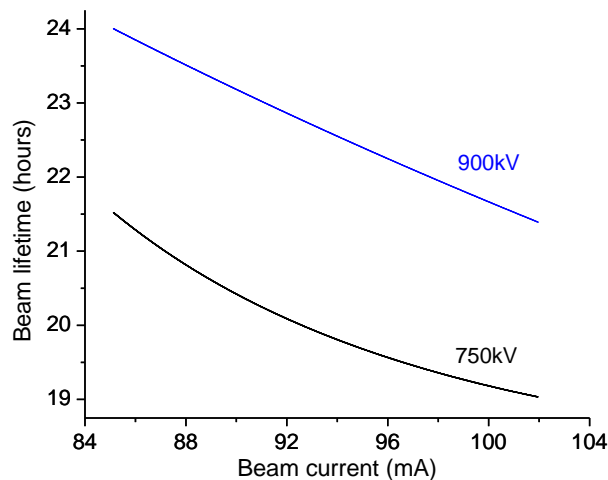


*Fig.4.8(b). Beam lifetime at different stored current at different RF voltages*

#### 4.6 Beam current decay and lifetime in different bunch filling pattern

To study the effect of increase in number of electrons in a bunch assuming that the volume of the bunch remains same (increase in bunch density i.e. number of electrons in a bunch/volume), beam current was stored uniformly in two-third RF buckets (194) and the rest one-third (97) were kept empty. Stored beam current  $\sim 100$  mA was filled uniformly in 194 RF buckets ( $\sim 0.51$  mA, equivalent to  $1.85 \times 10^9$  electrons in a bunch per bucket). The applied cavity peak voltage was 750 kV. The wall current monitor signal stored on the CRO indicating the bunch filling pattern for all 291 and 194 RF buckets filled are shown in the Figures 4.9(a) and 4.9(b) respectively. The beam current decay and beam lifetime in both cases at same RF cavity peak voltage of 750 kV were compared and are shown in the Figures 4.10(a) and 4.10(b) respectively. The vacuum pressure during the beam current decay was measured at all BAGs and found to be the approximately same at the same stored beam current in both the cases as shown in Figure 4.11.

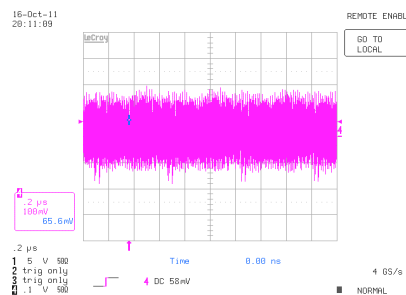


**Fig.4.9(a). Wall current monitor signal at 100mA stored current when all 291 RF buckets are filled**

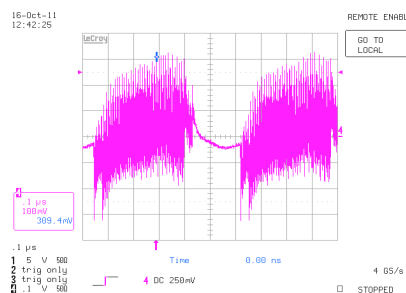


**Fig.4.9(b). Wall current monitor signal at 100mA stored current when two-third RF buckets are filled**

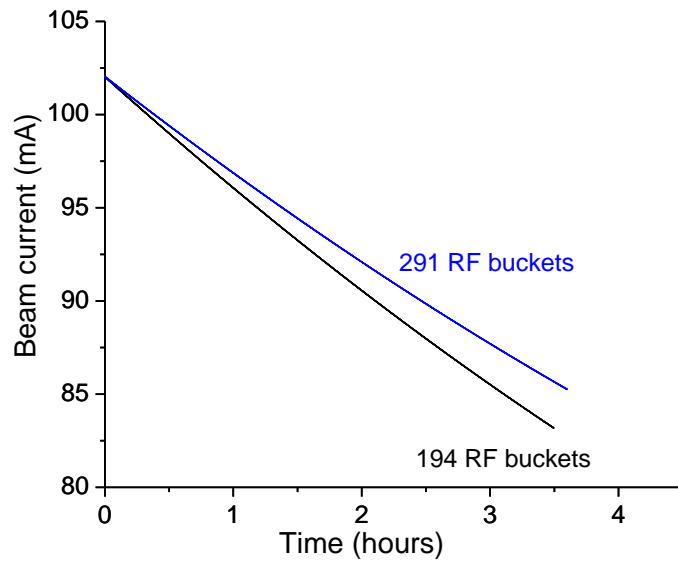


**Fig.4.10(a). Beam current decay for two different RF buckets fill pattern**

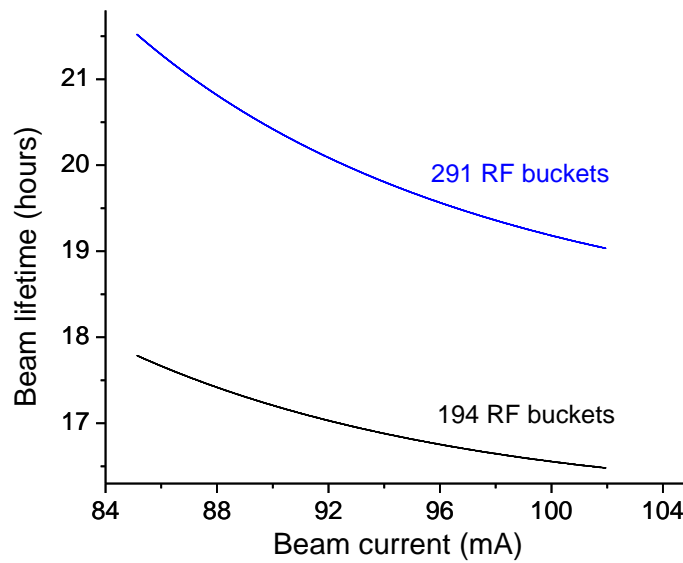


**Fig.4.10(b). Beam lifetime for two different RF buckets fill pattern**

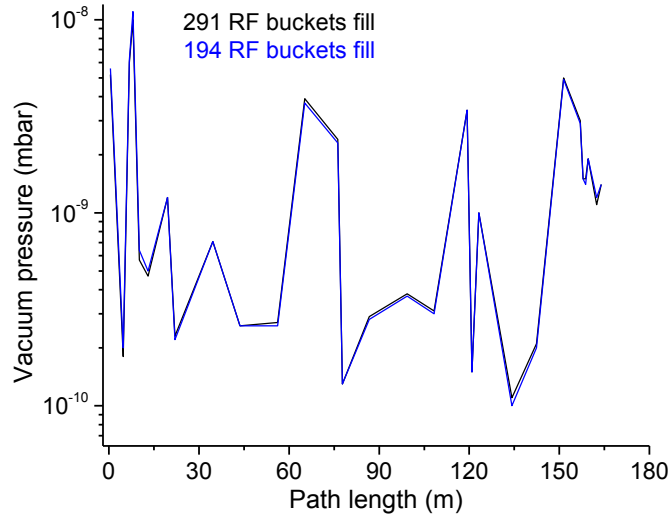


**Fig.4.11.** Measured pressure at all BAGs for two different filling pattern at stored current 100 mA

#### 4.7 Analysis of measured beam lifetime

From the measured beam current decay curve Figure 4.7(a), it was tried to obtain an equation that follows the beam current decay pattern. Let us assume that the beam current decay is due to the beam-gas scattering and Touschek scattering, so the beam current decay rate should follow equation 4.3.

We take 100 data points of measured stored beam current  $I_i$  ( $i = 1, 2, \dots, 100$ ) and its decay

rate  $-\frac{dI_i}{dt}$  (say  $d_i$ ). Using the data of stored beam current and decay rate, a curve fitting of

the form  $d_i = a.I_i + b.I_i^2$  was generated.

To estimate the coefficients  $a$  and  $b$  we use least square minimization method as follows:

$$\text{error } \chi^2(a, b) = \sum_{i=1}^{100} \left[ \frac{1}{\sigma_i} (d_i - a.I_i - b.I_i^2) \right]^2 \quad 4.5$$

where  $\sigma_i$  is the uncertainty in measured data.

For minimization of  $\chi^2$ , put  $\frac{\partial \chi^2}{\partial a} = 0$  and  $\frac{\partial \chi^2}{\partial b} = 0$ , we find coefficients  $a, b$  as

$$\begin{bmatrix} a \\ b \end{bmatrix} = \begin{bmatrix} \sum_{i=1}^{100} \frac{I_i^2}{\sigma_i^2} & \sum_{i=1}^{100} \frac{I_i^3}{\sigma_i^2} \\ \sum_{i=1}^{100} \frac{I_i^3}{\sigma_i^2} & \sum_{i=1}^{100} \frac{I_i^4}{\sigma_i^2} \end{bmatrix}^{-1} \begin{bmatrix} \sum_{i=1}^{100} \frac{d_i \cdot I_i}{\sigma_i^2} \\ \sum_{i=1}^{100} \frac{d_i \cdot I_i^2}{\sigma_i^2} \end{bmatrix}$$

$$\begin{bmatrix} a \\ b \end{bmatrix} = \frac{1}{\Delta} \times \begin{bmatrix} \sum_{i=1}^{100} \frac{I_i^4}{\sigma_i^2} & -\sum_{i=1}^{100} \frac{I_i^3}{\sigma_i^2} \\ -\sum_{i=1}^{100} \frac{I_i^3}{\sigma_i^2} & \sum_{i=1}^{100} \frac{I_i^2}{\sigma_i^2} \end{bmatrix} \times \begin{bmatrix} \sum_{i=1}^{100} \frac{d_i \cdot I_i}{\sigma_i^2} \\ \sum_{i=1}^{100} \frac{d_i \cdot I_i^2}{\sigma_i^2} \end{bmatrix}$$

$$\Delta = \begin{vmatrix} \sum_{i=1}^{100} \frac{I_i^2}{\sigma_i^2} & \sum_{i=1}^{100} \frac{I_i^3}{\sigma_i^2} \\ \sum_{i=1}^{100} \frac{I_i^3}{\sigma_i^2} & \sum_{i=1}^{100} \frac{I_i^4}{\sigma_i^2} \end{vmatrix} = \sum_{i=1}^{100} \frac{I_i^2}{\sigma_i^2} \sum_{i=1}^{100} \frac{I_i^4}{\sigma_i^2} - \left( \sum_{i=1}^{100} \frac{I_i^3}{\sigma_i^2} \right)^2$$

From this expression we get  $a$  and  $b$  as

$$a = \frac{1}{\Delta} \times \left[ \sum_{i=1}^{100} \frac{I_i^4}{\sigma_i^2} \sum_{i=1}^{100} \frac{d_i \cdot I_i}{\sigma_i^2} - \sum_{i=1}^{100} \frac{I_i^3}{\sigma_i^2} \sum_{i=1}^{100} \frac{d_i \cdot I_i^2}{\sigma_i^2} \right] \quad 4.6$$

$$b = \frac{1}{\Delta} \times \left[ \sum_{i=1}^{100} \frac{I_i^2}{\sigma_i^2} \sum_{i=1}^{100} \frac{d_i \cdot I_i^2}{\sigma_i^2} - \sum_{i=1}^{100} \frac{I_i^3}{\sigma_i^2} \sum_{i=1}^{100} \frac{d_i \cdot I_i}{\sigma_i^2} \right] \quad 4.7$$

We take beam current data using the same DC Current Transformer (DCCT) so uncertainty in all measurement is assumed to be same so  $\sigma_i = \sigma$  and is given [80] as

$$\sigma^2 = \frac{1}{N - m} \sum_{i=1}^{100} [d_i - a \cdot I_i - b \cdot I_i^2]^2 \quad 4.8$$

where  $N - m$  is the number of degrees of freedom and is equal to the number of measurements minus the number of parameters determined from the fit. In this case  $N = 100$ ,  $m = 2$  so number of degree of freedom is 98.

Putting the measured data in equations 4.6, 4.7 and 4.8, we get

$$\sigma = 1.6788 \times 10^{-5} \text{ mA./sec ond}$$

$$a = 4.3943 \times 10^{-6} \text{ /sec ond}$$

$$b = 8.4766 \times 10^{-8} \text{ /mA.sec ond}$$

$$\chi^2 = 98$$

#### 4.7.1 Estimation of uncertainties in the coefficients $a$ and $b$

In order to find out the uncertainty in the estimation of the coefficients  $a$  and  $b$ , error propagation method [80] is used. Uncertainty is given as

$$\sigma_a^2 = \sum_{i=1}^{100} [\sigma_i^2 (\partial a / \partial d_i)^2] \text{ and } \sigma_b^2 = \sum_{i=1}^{100} [\sigma_i^2 (\partial b / \partial d_i)^2]$$

Estimating partial derivative of  $a$  and  $b$  with respect to  $d_i$ , we get

$$\sigma_a^2 = \frac{1}{\Delta} \times \sum_{i=1}^{100} \frac{I_i^4}{\sigma_i^2} \quad 4.9$$

$$\sigma_b^2 = \frac{1}{\Delta} \times \sum_{i=1}^{100} \frac{I_i^2}{\sigma_i^2} \quad 4.10$$

Using the measured data we get uncertainty  $\sigma_a$  and  $\sigma_b$  in  $a$  and  $b$  respectively.

$$\sigma_a = \pm 1.2829 \times 10^{-7} \text{ /sec.}$$

$$\sigma_b = \pm 1.5524 \times 10^{-9} \text{ /mA.sec.}$$

Equation of beam current decay with uncertainty in coefficients  $a$  and  $b$  [81] is written as

$$-\frac{dI_i}{dt} = (4.3943 \times 10^{-6} \pm 1.2829 \times 10^{-7}) \times I_i + (8.4766 \times 10^{-8} \pm 1.5524 \times 10^{-9}) \times I_i^2 \quad 4.11$$

The instantaneous beam lifetime  $\tau_i$  is estimated as  $[-I_i / (dI_i / dt)]$  from measured beam current decay data. Due to uncertainty in coefficients  $a$  and  $b$ , there is uncertainty in measured beam lifetime of ~2.5%.

The measured beam current decay rate and fitted decay rate curve with coefficients  $a$  and  $b$  at different stored beam currents is shown in the Figure 4.11(a).

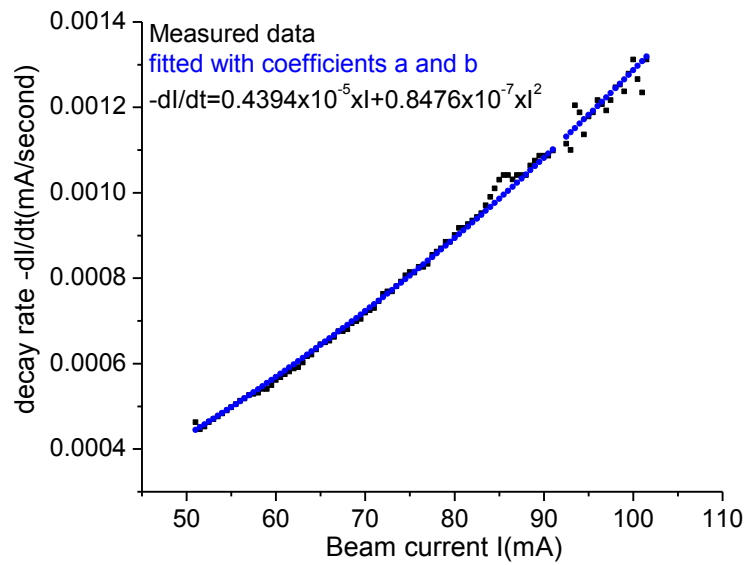


**Fig.4.11(a). Measured beam current decay rate and fitted curve at different beam current**

Substituting the value of coefficients *a* and *b* in equation 4.4 and initial beam current  $I_0 = 102\text{mA}$ , the measured beam current decay and current decay curve using coefficients *a* and *b* with time is shown in the Figure 4.11(b).

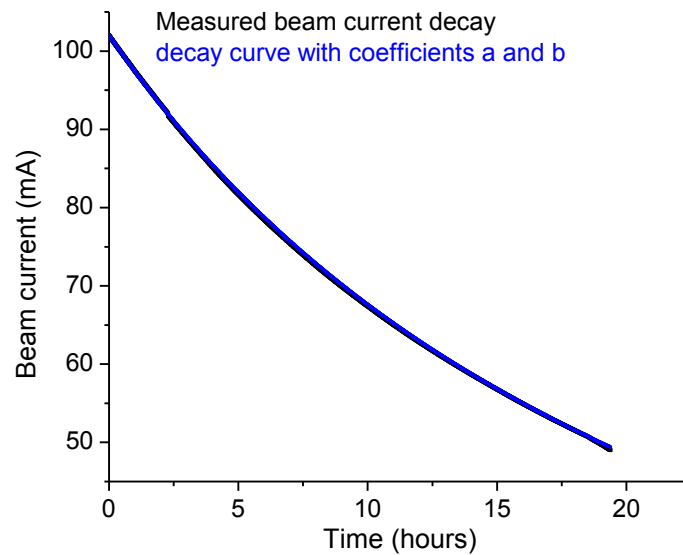


**Fig.4.11(b). Measured beam current decay and curve with coefficients a and b**

It is seen from Figure 4.11(a) and 4.11(b) that all the points in the measured beam current decay curve closely satisfies the fitted equation of the curve with coefficients  $a$  and  $b$ . So the measured beam decay is due to the beam-gas scattering and Touschek scattering only.

A theoretical estimation of the contribution of beam lifetime due to the vacuum lifetime and Touschek lifetime is as follows:

## **4.8 Estimation of Vacuum lifetime**

For the estimation of vacuum lifetime as explained in chapter 1, there are two main processes that contribute in beam-gas interaction. One is elastic scattering of electron beam with the nuclei of the residual gas atoms and other is inelastic scattering of beam with the nuclei of the residual gas atoms.

### **4.8.1 Vacuum lifetime due to elastic scattering**

The vacuum lifetime due to elastic scattering is given by expression 1.53 as given in chapter 1. It depends on aperture available, lattice functions  $\beta_x$  and  $\beta_z$  and vacuum pressure in the ring. Because the vacuum pressure in Indus-2 ring is not uniform along the circumference of ring so it is essential to estimate  $\beta_x.P$  and  $\beta_z.P$  for the estimation of vacuum lifetime due to elastic gas scattering.

### **4.8.2 Vacuum lifetime due to inelastic scattering**

Due to inelastic scattering of electrons with nuclei of residual gas atoms, there is a change in the momentum of electrons. If the change in momentum of an electron is more than the momentum acceptance  $\varepsilon$  of the storage ring, it gets lost. Using the expression 1.55 of  $\tau_{br}$  as given in 1.8.2.2 of chapter 1, the vacuum lifetime due to inelastic scattering (bremsstrahlung) of the stored electrons with the nuclei of the residual gas atoms was estimated. In the expression of  $\tau_{br}$ ,  $\varepsilon = \Delta E / E_0$  ( $\Delta E = E - E_0$ ,  $E_0$ : energy of synchronous electrons) is the limiting momentum acceptance either in transverse or in longitudinal plane,  $P$ : average

pressure in storage ring. From the experiment of the effect of RF voltage on beam lifetime, it is clear that by increasing cavity voltage from 750 kV to 900 kV, there is an increase in beam lifetime so the momentum acceptance due to RF (longitudinal plane) is a limiting factor for electrons loss. For 900kV, calculated RF acceptance  $\varepsilon = \pm 0.9\%$  was used for beam lifetime estimation. The RF acceptance reduced to 0.76% for RF voltage 750 kV.

For the estimation of vacuum lifetime due to elastic and inelastic scattering, average pressure  $P$ , average of  $\beta_x.P$  and  $\beta_z.P$  over the whole ring was estimated as follows:

#### 4.8.3 Estimation of average pressure $\bar{P}$ and average of $\beta_x.P$ and $\beta_z.P$

The residual gas pressure in Indus-2 was measured using thirty Bayard Alpert Ionization Gauges (BAGs) calibrated for nitrogen equivalent gas pressure installed in the storage ring.

From the measured vacuum pressure data at thirty BAGs in the ring, a vacuum pressure profile along the beam path was generated. From the pressure profile, average pressure  $\bar{P}$

was estimated as 
$$\bar{P} = \frac{\sum_{i=1}^n P_i \cdot l_i}{\sum_{i=1}^n l_i} \quad i = 1, 2, 3, \dots, n$$
 where  $P_i$  is measured pressure at location  $i$

representing the vacuum condition over the length  $l_i$ . Here from  $-\frac{l_i}{2}$  to  $+\frac{l_i}{2}$  over which  $P_i$  is

taken constant. The average pressure during beam current decay from 100mA to 50mA in steps of 10mA is shown in the Figure 4.12. The linear curve fit of average pressure graph

shows that the average pressure without beam ( $I = 0$ ) is  $0.55 \times 10^{-9}$  Torr, which is close to the

real measured value  $0.60 \times 10^{-9}$  Torr in the storage ring. The horizontal and vertical beta

functions  $\beta_x$  and  $\beta_z$  of the operating lattice were measured using quadrupole scan method

[82]. The measured beta function in the ring was found to be very close to the theoretical

operating value, so we have used the theoretical value of beta functions for the analysis. From

pressure profile and beta functions, average value of  $\beta_x.P$  and  $\beta_z.P$  in whole ring was calculated. The average value of  $\beta_x.P$  and  $\beta_z.P$  during beam current decay is shown in the Figure 4.13.

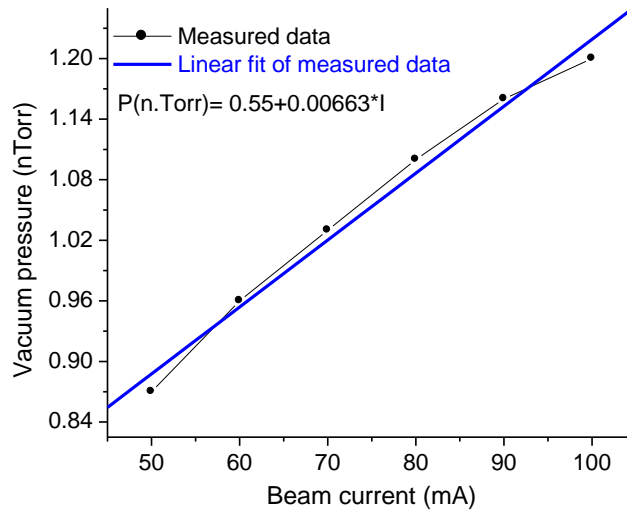


**Fig.4.12. Measured vacuum pressure during beam current decay**

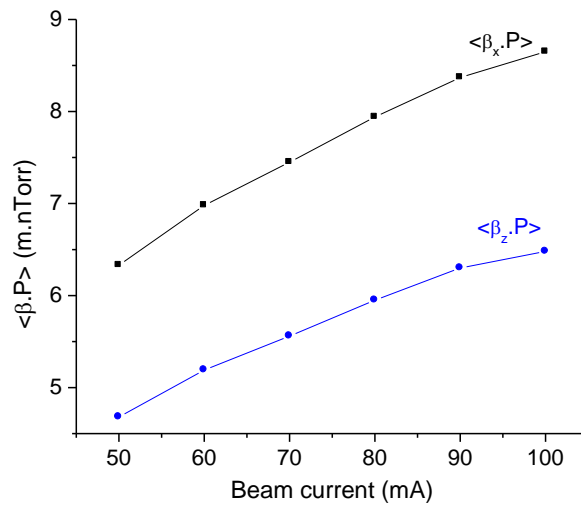


**Fig.4.13. Variation of  $\langle \beta_x.P \rangle$ ,  $\langle \beta_z.P \rangle$  during beam current decay**

#### 4.8.4 Estimation of available aperture for beam motion

The physical aperture available in vacuum chamber of Indus-2 is  $\pm 32\text{mm}$  (outward and inward from the centre of beam axis) in the horizontal plane and  $\pm 17\text{mm}$  (upward and downward from the centre of beam axis) in the vertical plane. Due to the presence of sextupoles, magnet multipole errors and magnet misalignment errors, aperture available for stable motion of the electrons is reduced. The tracking studies as discussed in chapter 1, show that aperture available at  $\beta_{\text{max}}$  location including closed orbit distortion (closed orbit was corrected to less than 1mm rms in both horizontal and vertical plane) is  $\pm 20$  and  $\pm 12$  mm in horizontal and vertical plane respectively. By using these values of the dynamic apertures, vacuum lifetime due to elastic scattering was estimated.

The estimation of vacuum lifetime due to elastic scattering  $\tau_{el}$  and due to inelastic scattering  $\tau_{br}$  was carried and from these lifetimes, total vacuum lifetime was estimated.

$$\text{Total vacuum lifetime } \tau_v \text{ is given by } \frac{1}{\tau_v} = \frac{1}{\tau_{el}} + \frac{1}{\tau_{br}} \quad 4.13$$

The estimated total vacuum lifetime  $\tau_v$  along with the contribution of elastic  $\tau_{el}$ , inelastic scattering  $\tau_{br}$ , assuming nitrogen equivalent gas pressure during beam current decay is shown in the Figure 4.14.

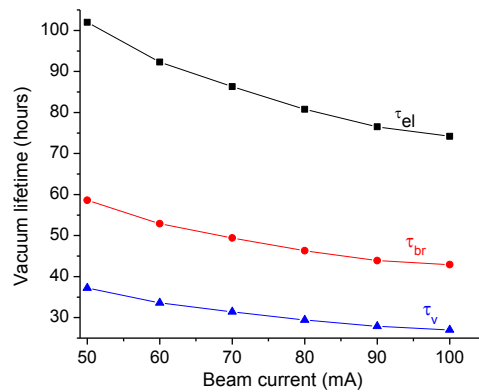


**Fig.4.14. Vacuum lifetime during beam current decay**

#### 4.9 Estimation of Touschek Lifetime $\tau_{tous}$

The Touschek lifetime ( $\tau_{tous}$ ) due to electrons scattering within a bunch is given by relation 1.59 in chapter 1.

For the estimation of Touschek lifetime, the particle tracking code ELEGANT [32] was used. For Indus-2, the momentum acceptance for positive and negative off momentum electrons was estimated by six-dimension (6D) particle tracking. The tracking result shows that the momentum acceptance is limited by RF acceptance, for RF voltage 900 kV,  $\epsilon$  is  $\pm 0.9\%$ . It was also confirmed experimentally by studying the effect of RF voltage on beam lifetime.

The motion of the electrons is stable inside the RF bucket. If the momentum change during Touschek scattering in two electrons is more than the RF acceptance  $\epsilon$ , the electrons will come out of the RF bucket and is lost. The synchronous phase  $\phi_s$  is the phase of right energy

electron called synchronous electron,  $\phi_s = \text{Sin}^{-1}\left(\frac{U_0}{eV_{rf}}\right)$  where  $U_0$ : energy loss per turn due to

synchrotron radiation and  $V_{rf}$  is applied RF cavity peak voltage. For RF cavity voltage 900 kV,  $\phi_s$  is  $163.7^\circ$  whereas for 750 kV it is  $160.5^\circ$ . The RF buckets in Indus-2 at RF cavity voltage 750 and 900 kV is shown in the Figure 4.15.

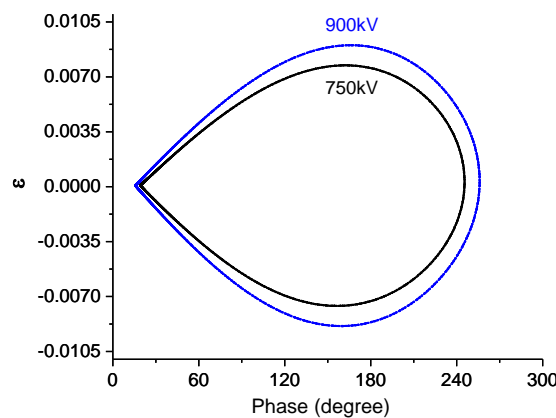


**Fig.4.15. RF buckets for two different RF voltages**

For estimating vertical beam size  $\sigma_z$ , betatron coupling was measured using minimum tune separation method [82] and found to be  $\sim 0.5\%$  as discussed in chapter 3. Using RF momentum acceptance  $0.9\%$  and measured betatron coupling  $0.5\%$ , the estimated Touschek lifetime for beam current decay from  $100\text{ mA}$  to  $50\text{ mA}$  using formula 1.59 is shown in the Figure 4.16.

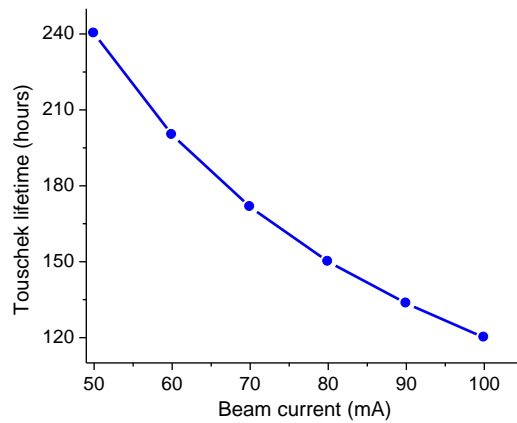


**Fig.4.16. Touschek lifetime during beam current decay**

The total beam lifetime  $\tau_t$  is given by 
$$\frac{1}{\tau_t} = \frac{1}{\tau_v} + \frac{1}{\tau_{Tous}}$$
 4.14

A comparison of estimated beam lifetime and measured beam lifetime during beam current decay is shown in the Figure 4.17.

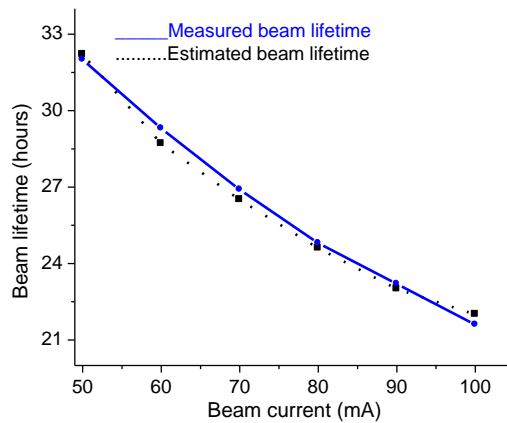


**Fig.4.17. Comparison of estimated and measured beam lifetime**

The theoretical analysis shows that the estimated beam lifetime using analytical formulations is close to the measured beam lifetime at different stored beam current during its natural decay.

#### 4.10 Estimation of vacuum and Touschek lifetime from measured beam lifetime

From the measured beam lifetime, the contribution of vacuum and Touschek lifetime [83, 84] was determined by using measured vacuum pressure. In the above experiment, we have taken beam current decay from 102 mA to 50 mA, the measured beam lifetime at 100 mA was 21.6 hours and at 50 mA it was 32 hours.

Let  $(\tau_{tous})_{100mA}$  and  $(\tau_{tous})_{50mA}$  be the Touschek lifetime at stored beam current 100 mA and 50 mA respectively. From Touschek lifetime formula 1.59, we see that if volume of the bunch is same (no change in horizontal, vertical rms beam size and rms bunch length during beam current decay) then Touschek lifetime is inversely proportional to the number of electrons in the bunch. The number of electrons in one bunch at 50 mA beam current will be half the number of electrons at current 100 mA. So the Touschek lifetime at 50 mA stored current will be twice of the Touschek lifetime at stored current 100 mA and

$$(\tau_{tous})_{50mA} = 2 \times (\tau_{tous})_{100mA} \quad 4.15$$

Let  $(\tau_v)_{100mA}$  and  $(\tau_v)_{50mA}$  be the vacuum lifetime at stored beam current 100 mA and 50 mA respectively. The measured average vacuum pressure at 100 mA ( $P_{100mA}$ ) is 1.2 nTorr and at 50 mA ( $P_{50mA}$ ) is 0.87 nTorr.

We know that the vacuum lifetime  $\tau_v$  is inversely proportional to the pressure in ring. So

$$\frac{(\tau_v)_{100mA}}{(\tau_v)_{50mA}} = \frac{P_{50mA}}{P_{100mA}} = \frac{0.87}{1.2} = 0.725 \Rightarrow (\tau_v)_{100mA} = 0.725 \times (\tau_v)_{50mA} \quad 4.16$$

If  $\tau_{100mA}$  and  $\tau_{50mA}$  be the total beam lifetime at stored beam current 100 mA and 50 mA respectively then

$$\frac{1}{\tau_{100mA}} = \frac{1}{(\tau_v)_{100mA}} + \frac{1}{(\tau_{tous})_{100mA}} \quad \text{and}$$

$$\frac{1}{\tau_{50mA}} = \frac{1}{(\tau_v)_{50mA}} + \frac{1}{(\tau_{tous})_{50mA}} \quad 4.17$$

Using the conditions  $(\tau_{tous})_{50mA} = 2 \times (\tau_{tous})_{100mA}$  and  $(\tau_v)_{100mA} = 0.725 \times (\tau_v)_{50mA}$ , we find that

$$(\tau_v)_{100mA} = 27.7 \text{ hours and } (\tau_{tous})_{100mA} = 98 \text{ hours and}$$

$$(\tau_v)_{50mA} = 38.2 \text{ hours and } (\tau_{tous})_{50mA} = 196 \text{ hours}$$

The vacuum lifetime and Touschek lifetime estimated for 50 and 100 mA stored current are close to the values estimated from analytical formulations using measured vacuum pressure, cavity voltage and horizontal and vertical aperture.

Accumulating electron beam in different bunch filling pattern was also carried out to find the contribution of Touschek and vacuum lifetime in total measured beam lifetime. It was found experimentally that at the same stored current, average pressure remains the same either all or two-third RF buckets are filled. So the vacuum lifetime at the same stored beam current in both the cases is same. From the measured beam lifetime at 100mA in both cases and considering vacuum lifetime same, vacuum and Touschek lifetime at 100mA stored current was estimated using formula 4.14 and found to be close to the estimated results from analytical formulations.

## CHAPTER 5

### MEASUREMENTS OF APERTURE AND BEAM LIFETIME USING BEAM SCRAPERS IN INDUS-2

#### 5.1 Introduction

The measurements of vertical and horizontal apertures which are available for stable beam motion in Indus-2 at beam energy 2.5 GeV using movable beam scrapers are presented and discussed in this chapter. These beam scrapers are installed in one of the long straight sections in the ring. With the movement of beam scrapers towards the beam centre, the beam lifetime is measured. The beam lifetime data obtained from the movement of vertical and horizontal beam scrapers is analyzed. The contribution of beam loss due to vacuum lifetime and Touschek lifetime is separated from the measured beam lifetime at different positions of the beam scrapers. Vertical and horizontal beam sizes at scrapers location are estimated from the scraper movement towards the beam centre in quantum lifetime limit and their values closely agree with measured value obtained using X-ray diagnostic beamline. From the analysis of aperture measurement data, further experiments were carried out for the improvement of beam lifetime in Indus-2 at operating energy 2.5 GeV. Beam lifetime in single bunch storage at low and higher beam energy in Indus-2 is also discussed.

Beam experiments in Indus-2 were conducted to measure the vertical and horizontal aperture at scraper location which are available for a stable beam motion at beam energy 2.5 GeV with stored beam current 100 mA. The main purpose of these studies is to choose an appropriate aperture for undulators which are planned to be installed in long straight sections and also to understand the contribution of beam loss which are mainly due to the scattering between electrons and residual gas atoms and electron-electron scattering within a bunch. For aperture measurements, vertical and horizontal beam scrapers, installed in one of the long straight

sections are used. A DC Current Transformer (DCCT) also installed in that section is used for the measurement of average beam current and beam lifetime of circulating beam in the storage ring.

A set of experiments were conducted to measure the vertical and horizontal aperture [85-91] at the scrapers location at beam energy 2.5 GeV with stored beam current 100 mA. Similar studies have been carried out in other electron storage rings like MAX II [45], SPEAR3 [46] and SAGA-LS [49] etc. The vertical beam scraper in Indus-2 has two rectangular blades with 50 mm width and 10 mm thickness which can move vertically in or out independently or simultaneously using stepper motors. Similarly the horizontal beam scraper has two blades with 30 mm width and 8 mm thickness which can move horizontally in or out independently or simultaneously using stepper motors. To study the beam off-set and beam instabilities in vertical plane as reported in MAX II ring, three experiments of beam lifetime with vertical scraper movement towards the beam centre were conducted which are as follows:

1. Measurement of beam lifetime by moving upper blade of vertical scraper towards the beam centre while lower blade was fixed at its extreme lower end.
2. Measurement of beam lifetime by moving lower blade of vertical scraper towards the beam centre while upper blade was fixed at its extreme upper end.
3. Measurement of beam lifetime by moving both the upper and lower blades simultaneously towards the beam centre.

Similar experiments were also carried out for the measurement of horizontal aperture with the movement of horizontal scraper blades towards the beam centre. The experimental set-up of beam scrapers in Indus-2 ring is described in the next section. During the vertical and horizontal scraper blade movement, vacuum pressure in the ring was observed at all Bayard Alpert Gauges (BAGs) installed in the ring whereas particular attention was paid to the BAGs

which are installed near the beam scraper location. We also monitored the radiation dose using radiation area monitors which are placed near the location of beam scrapers during the movement of scraper blades to know whether the beam is lost at the scraper location when scraper blade is inserted and lifetime starts decreasing. The scraper movement experiments were conducted within 5% beam current decay. A computer program has been developed and is in use to acquire the continuous beam current samples from beam current measurement system i.e. DC Current Transformer (DCCT) for the measurement of beam lifetime. During the beam scraper movement, beam lifetime decreases which depends on the position of scraper blade from the beam centre, so the time of beam current decay for beam lifetime measurement at different position of beam scrapers is calculated under the condition that the uncertainty in the beam lifetime measurement [46] is within 5%. The curve fitting and mathematical operation required for beam lifetime measurement is performed using MATLAB function for efficient computation. During the scraper movement, the program suitably selects the number of data point within the uncertainty of measured beam lifetime. The beam lifetime obtained at different positions of scrapers is analyzed using theoretical formulations. For analysis of vacuum lifetime, mass spectra of the residual gas molecules present in the vacuum chamber obtained from a quadrupole mass analyzer are used. Using the measured partial pressures of residual gases and applied RF cavity voltage, beam lifetime due to elastic coulomb scattering and bremsstrahlung is calculated using analytic expressions. A theoretical estimation of Touschek lifetime due to momentum aperture limitation during horizontal scraper movement is also carried out using the particle tracking code ELEGANT. The theoretical results of vacuum and Touschek lifetimes are verified by measuring the beam lifetime with partial beam bunch fill. The vertical and horizontal beam sizes are estimated by moving the scraper blade towards the beam centre up to the limit which is nearly six times of beam sizes, where quantum lifetime also contributes to the beam lifetime. The beam sizes in

both planes corresponding to theoretical  $\beta$  functions at scraper location closely agree with the beam sizes measured at X-ray diagnostic beamline set-up at  $10^\circ$  port of a dipole magnet in the ring. To study the Touschek lifetime, beam lifetime was measured with different beam bunch fill pattern. Bunch length in different bunch filling patterns was measured at visible diagnostic beamline set-up at  $5^\circ$  port of the same dipole magnet used for X-ray diagnostic beamline in the ring.

## **5.2 Experimental set-up for aperture measurement**

The movable vertical and horizontal scrapers reduce the physical aperture in the vertical and horizontal directions. The vertical and horizontal scrapers are close to each other and installed in a long straight section as shown in Figure 5.1. Operation of a scraper [92, 93] requires movement of blades in and out for vertical and horizontal movement. It requires a precise and ultrahigh vacuum compatible actuation mechanism, which can transmit the motion across the vacuum air interface. As shown in Figure 5.1, the blades are bolted to a movable flange, which is guided by precision ball bushes running over a cylindrical guide to ensure linear motion. A ball screw provides a low friction and precise means to convert rotary motion of stepper motor to linear motion of blades. The position of the beam scrapers relative to the beam centre is known with an accuracy of  $50\mu\text{m}$ .

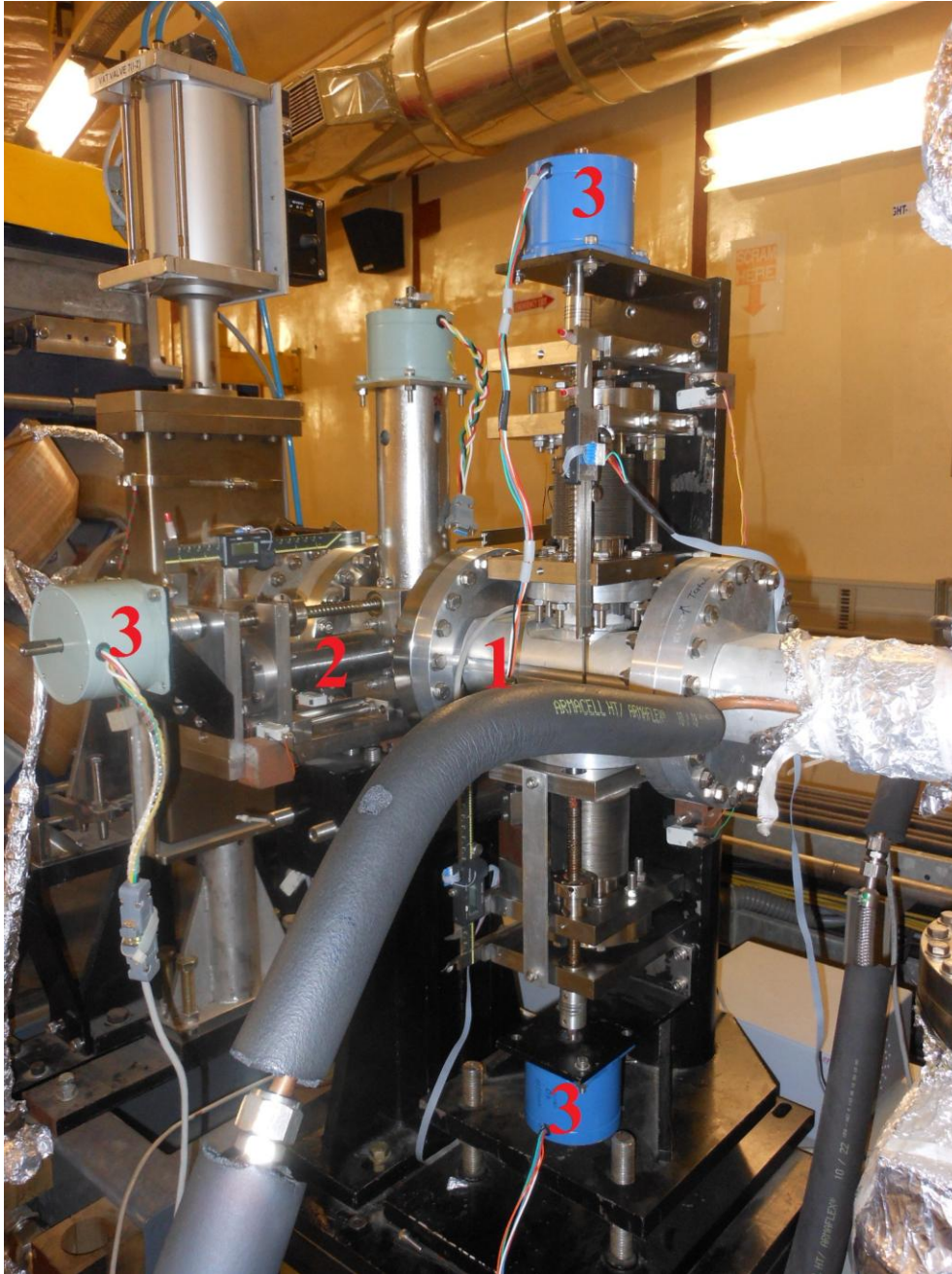


*Fig.5.1. Vertical and horizontal scrapers in the ring, mark (1) vertical scraper, (2) horizontal scraper, (3) stepper motors for vertical and horizontal movement of scraper blades*

### **5.3 Measurement of beam lifetime with scraper movement**

#### **5.3.1 Beam lifetime with vertical scraper movement**

The physical aperture available in vertical plane at scraper location is  $\pm 18$  mm. During the normal operation, the upper blade of scraper is at +18 mm and lower blade is at -18 mm from

the centre of the vacuum chamber pipe. For lifetime measurement, lower blade was moved gradually towards the beam centre using a stepper motor while upper blade was fixed at its extreme end. The experiments of beam lifetime measurement with scraper movement were carried out during beam current decay from 100 mA to 95 mA. Similar experiment was carried out with upper blade movement towards the beam centre, while lower blade position fixed. The same experiment was also carried out by the movement of both the upper and lower blade towards the beam centre simultaneously. The measured beam lifetime at different upper blade positions towards the beam centre is shown in Figure 5.2. Similar results were obtained in other two cases. The results show that, during beam scraper movement up to 4.1 mm from the beam centre, there is no change in beam lifetime and it remains ~13 hours. The lifetime starts decreasing, when the scraper position from beam centre becomes less than 4.1 mm. There was no change in vacuum pressure during the movement of scraper blades. During the beam scraper movement, no beam instabilities were observed as was reported in MAX II ring. The experimental results indicate that the measured vertical aperture is the same whether the upper or lower blade move independently or simultaneously. The aperture was measured by filling Indus-2 ring with a beam current of 100 mA in all 291 RF buckets as well as with 10% and 33% bunch gap uniformly. In all cases the measured aperture was found to be the same. Figure 5.2 shows the measurement of beam lifetime when all 291 RF buckets were filled uniformly. It shows that the aperture available in vertical plane at scraper location is  $\pm 4.1$  mm. When the scraper position from beam centre becomes  $\pm 0.58$  mm, a sudden loss of beam takes place.

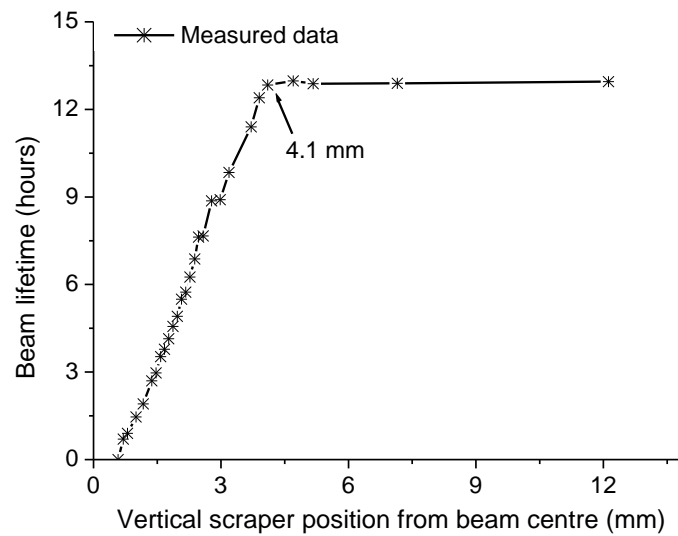


*Fig.5.2. Beam lifetime with vertical scraper movement towards the beam centre*

### 5.3.2 Beam lifetime with horizontal scraper movement

Similar procedure was followed to measure beam lifetime with the horizontal scraper. The physical aperture available at the scraper location is  $\pm 42$  mm. During the normal operation, the left blade of the scraper is at  $+42$  mm and right blade is at  $-42$  mm from the centre of vacuum chamber pipe. For lifetime measurement left blade was moved gradually towards the beam centre using a stepper motor and right blade was fixed at its extreme end. Similar experiment was carried out by keeping left blade fixed and right blade was moved. The same experiment was also carried out by the movement of both the left and right blades towards the beam centre simultaneously. The measured beam lifetime with left scraper movement towards the beam centre is shown in Figure 5.3. The experimental results indicate that when the horizontal scraper is at  $\pm 12.45$  mm from the beam centre, the beam lifetime start decreasing before it there was no change in beam lifetime. It shows that the aperture available for beam motion in horizontal plane at scraper location is  $\pm 12.45$  mm. When the scraper position from the beam centre becomes  $\pm 7.6$  mm, very fast beam current decay takes place.

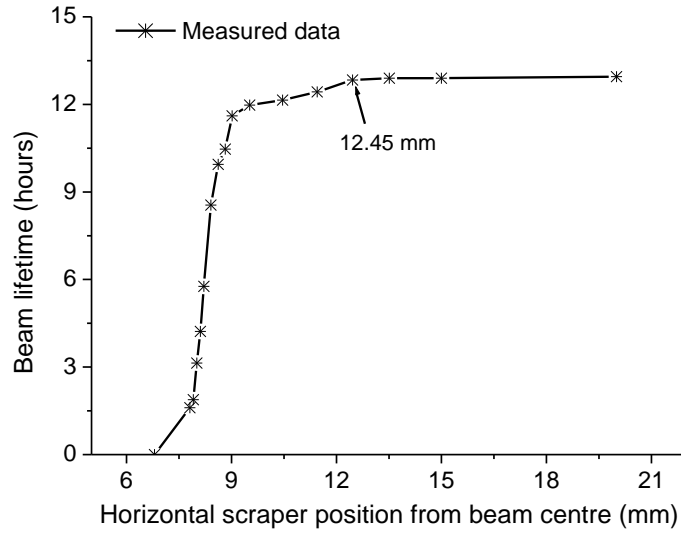


*Fig.5.3. Beam lifetime with horizontal scraper movement towards the beam centre*

#### 5.4 Analysis of measured beam lifetime with movement of vertical and horizontal scrapers

As discussed before that the lifetime of stored electron beam  $\tau_t$  in a storage ring is mainly governed by elastic coulomb scattering between the electrons and the nuclei of residual gas atoms  $\tau_{el}$ , inelastic scattering between electrons and the nuclei of residual gas atoms known as bremsstrahlung lifetime  $\tau_{br}$ , electron-electron scattering within a beam bunch known as Touschek lifetime  $\tau_{tous}$  and due to emission of synchrotron radiation known as quantum lifetime  $\tau_q$  and is given as

$$\frac{1}{\tau_t} = \frac{1}{\tau_{el}} + \frac{1}{\tau_{br}} + \frac{1}{\tau_{tous}} + \frac{1}{\tau_q} \quad 5.1$$

##### 5.4.1 Beam lifetime due to elastic coulomb scattering $\tau_{el}$

As discussed in chapter 2, the beam lifetime due to elastic coulomb scattering between the electrons and nuclei of a residual gas atoms is given by relation 1.53.

For a rectangular chamber of horizontal aperture  $a$  and vertical aperture  $b$  at the scraper location, minimum scattering angle  $\theta_m$  is given as

$$\frac{1}{\theta_m^2} = \frac{2\langle\beta_x\rangle\beta_{xs}}{a^2} \left[ \tan^{-1}\left(p\frac{b}{a}\right) + \frac{pab}{a^2 + p^2 b^2} \right] + \frac{2\langle\beta_z\rangle\beta_{zs}}{b^2} \left[ \cot^{-1}\left(p\frac{b}{a}\right) + \frac{pab}{a^2 + p^2 b^2} \right] \quad 5.2$$

where  $p = \sqrt{\frac{\langle\beta_x\rangle\beta_{xs}}{\langle\beta_z\rangle\beta_{zs}}}$ ,  $\beta_{xs}, \beta_{zs}$  are the  $\beta$  functions at the scraper location,  $\langle\beta_x\rangle, \langle\beta_z\rangle$  are average  $\beta$  functions in the ring in horizontal and vertical plane respectively.

The beam lifetime due to elastic coulomb scattering for different scraper positions was calculated using partial pressure of residual gases [94] obtained from mass spectra of quadrupole mass analyzer as follows:

$$\frac{1}{\tau_{el}} = \frac{2r_0^2 c}{\gamma^2} \frac{1}{\theta_m^2} \frac{P}{kT} \sum_i Z_i^2 N_i f_i \quad 5.3$$

where  $P$  is the total pressure of all gases present,  $Z_i, N_i$  and  $f_i$  are the atomic number, number of atoms per molecules and partial fraction of gas  $i$  respectively,  $k$  is the Boltzmann constant and  $T$  is the ambient temperature. The total pressure of residual gases at stored beam current 100 mA was  $6.47 \times 10^{-9}$  Torr and percentage of residual gas contents are given in Table 5.1. The vacuum pressure in the ring was also measured using BAGs and the ring average vacuum pressure at 100 mA stored current was  $1.8 \times 10^{-9}$  Torr nitrogen equivalent gas pressure.

Table 5.1. Partial pressure of residual gases at stored beam current 100 mA

Mass number and gas species	Pressure (Torr)	% contents
2 ( $H_2$ )	$4.76 \times 10^{-9}$	73.60
28 ( $CO$ )	$1.53 \times 10^{-9}$	23.72
32 ( $O_2$ )	$1.28 \times 10^{-10}$	1.98
44 ( $CO_2$ )	$4.53 \times 10^{-11}$	0.70

The measured  $\beta$  functions in Indus-2 [82] are near to its theoretical estimated values, so for the analysis we have taken theoretical value of  $\beta_x$  and  $\beta_z$  at the scraper location. As vertical and horizontal beam scrapers are close to each other in the ring, we have taken the same values of  $\beta$  function at their locations. The  $\beta$  function at their location are  $\beta_{xs}=10.2 m$ ,  $\beta_{zs}=4.2 m$  and average value of  $\beta$  function in ring are  $\langle \beta_x \rangle = 6.97 m$ ,  $\langle \beta_z \rangle = 5.56 m$ .

#### 5.4.1.1 $\tau_{el}$ with movement of vertical scraper

During this scraper movement, as vertical aperture  $b$  decreases, the scattering angle is reduced resulting in a reduction in beam lifetime.

Using the  $\beta$  functions as mentioned above and measured value of aperture  $a=12.45 mm$  and  $b=4.1 mm$  to  $0.58 mm$ , minimum scattering angle  $\theta_m$  using relation 5.2 was calculated.

With substitution of vacuum pressure and minimum scattering angle in relation 5.3, beam lifetime  $\tau_{el}$  is calculated. The variation in scattering angle and beam lifetime  $\tau_{el}$  at different vertical scraper position is shown in Figure 5.4.

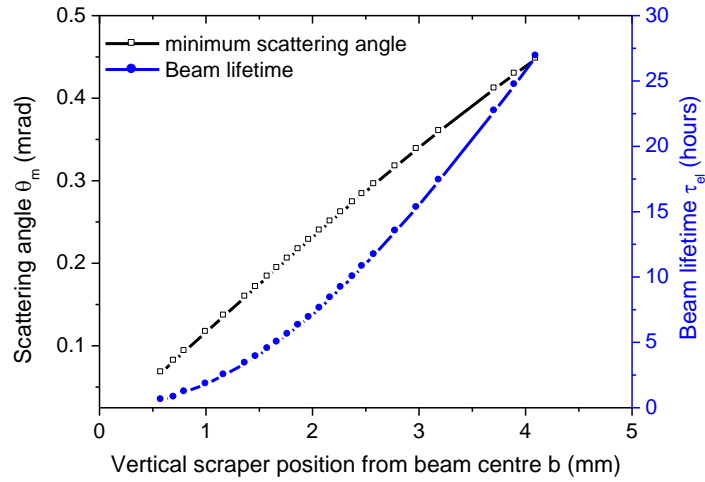


**Fig.5.4. Scattering angle and beam lifetime at different position of vertical scraper**

#### 5.4.1.2 $\tau_{el}$ with movement of horizontal scraper

Using the  $\beta$  functions as mentioned above and  $b=4.1\text{mm}$ ,  $a=12.45\text{mm to }7.0\text{mm}$ , minimum scattering angle  $\theta_m$  and beam lifetime  $\tau_{el}$  is calculated using relation 5.2 and 5.3 respectively. The variation of  $\theta_m$  and beam lifetime  $\tau_{el}$  with horizontal scraper position is shown in Figure 5.5.

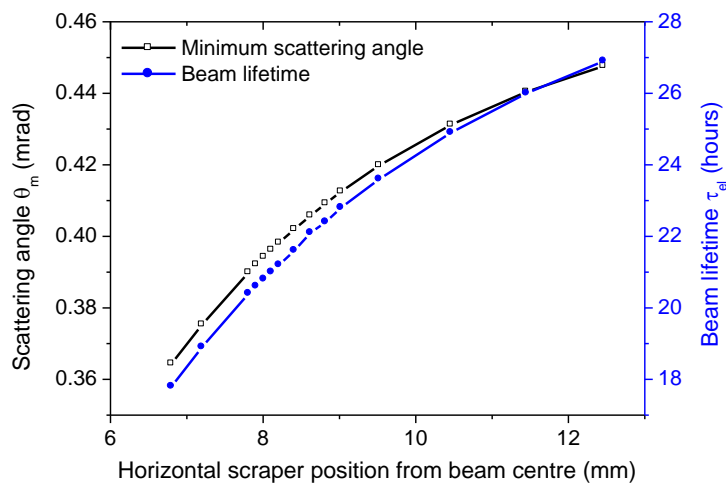


**Fig.5.5.Scattering angle and beam lifetime at different position of horizontal scraper**

## 5.4.2 Beam lifetime due to inelastic scattering $\tau_{br}$

The vacuum lifetime due to inelastic scattering between the electrons and nuclei of residual gas atoms is given by equation 1.55 of chapter 1. It depends on the average vacuum pressure  $P$  and weakly depends on the momentum acceptance  $\varepsilon$  [95, 96] in the ring. The value of momentum acceptance  $\varepsilon$  is the minimum value either in transverse or in longitudinal directions.

### 5.4.2.1 $\tau_{br}$ with movement of vertical scraper

The vertical dispersion in the ring is negligible small, so the momentum acceptance is the same in the ring during vertical scraper movement. The momentum acceptance corresponds to applied RF cavity peak voltage 1200 kV,  $\varepsilon = 0.7\%$  is the minimum value.

With substitution of  $\varepsilon = 0.7\%$  and measured vacuum pressure in relation 1.55, we obtained bremsstrahlung lifetime. As there is no change in vacuum pressure and momentum acceptance during vertical scraper movement, so the bremsstrahlung lifetime remains same.

### 5.4.2.2 $\tau_{br}$ with movement of horizontal scraper

During the movement of horizontal scraper towards the beam centre, the horizontal aperture as well as the momentum aperture reduces. The momentum aperture for different position of scraper from beam centre is estimated using particle tracking code ELEGANT and is shown in Figure 5.6. In Indus-2 operating lattice, dispersion is finite in the long straight section. At scraper location, magnitude of dispersion is 0.3 m, so during scraper movement, there will also be reduction in aperture due to dispersion. Using the value of minimum momentum acceptance in the ring at different scraper positions and vacuum pressure in relation 1.55, beam lifetime due to bremsstrahlung is calculated.

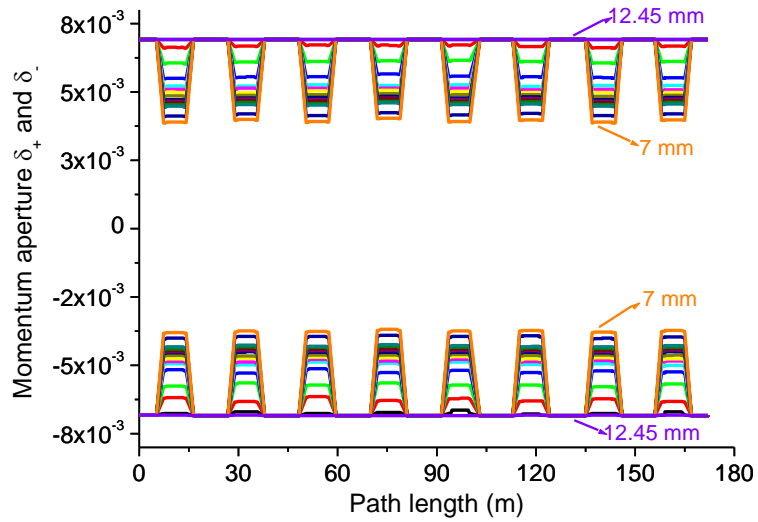


*Fig.5.6. Momentum aperture with the horizontal scraper at  $a=12.45-7.0$  mm*

### 5.4.3 Beam lifetime due to Touschek scattering $\tau_{tous}$

The Touschek lifetime  $\tau_{tous}$  is given by relation 1.59 in chapter 1.

#### 5.4.3.1 $\tau_{tous}$ with the movement of vertical scraper

As there is no change in momentum aperture during vertical scraper movement, the Touschek lifetime remains the same.

#### 5.4.3.2 $\tau_{tous}$ with the movement of horizontal scraper

From the momentum acceptance in the ring at different horizontal scraper position as shown in Figure 5.6 and using measured betatron coupling 0.5%, Touschek lifetime is calculated using particle tracking code ELEGANT.

### 5.4.4 Quantum lifetime $\tau_q$

The quantum contribution to beam lifetime  $\tau_q$  is given by 1.51 in chapter 1.

#### 5.4.4.1 $\tau_q$ with movement of vertical scraper

Using  $\tau_d = 4.62 \text{ ms}$  and  $\sigma_z = 100 \mu\text{m}$ , quantum lifetime for different vertical scraper position is calculated.

#### 5.4.4.2 $\tau_q$ with movement of horizontal scraper

Using  $\tau_d = 4.74 \text{ ms}$  and  $\sigma_x = 1.3 \text{ mm}$ , quantum lifetime for different horizontal scraper position is calculated.

The values of beam lifetime due to elastic coulomb scattering  $\tau_{el}$ , bremsstrahlung  $\tau_{br}$ , Touschek  $\tau_{tous}$  and quantum excitation  $\tau_q$  are calculated for both vertical and horizontal scraper movement by using analytical relation. The beam lifetimes due to  $\tau_{el}$ ,  $\tau_{br}$ ,  $\tau_{tous}$ ,  $\tau_q$  with total theoretical and measured lifetime at different positions of the vertical and horizontal scraper are shown in Figure 5.7 and 5.8 respectively.

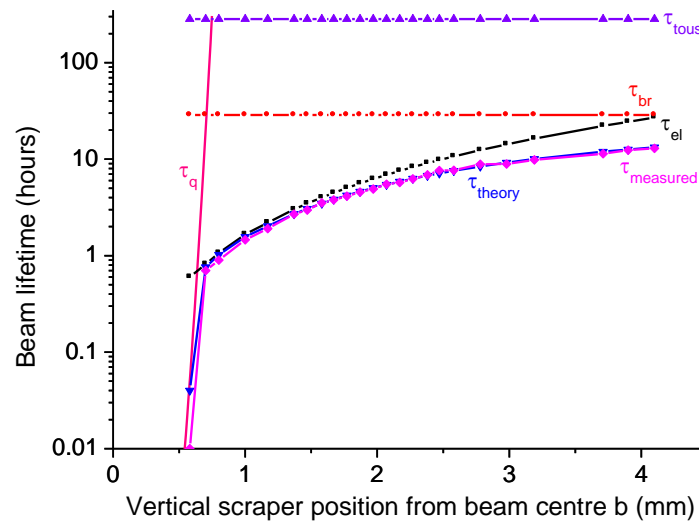


**Fig.5.7. Calculated and measured beam lifetime with vertical scraper position**

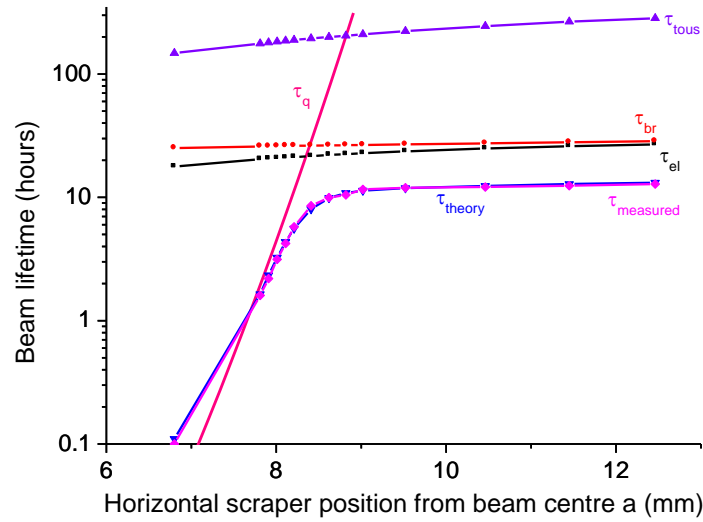


**Fig.5.8. Calculated and measured beam lifetime with horizontal scraper position**

From Figure 5.7, we see that when the vertical scraper position from the beam centre was 0.58 mm, a sudden beam loss occurred. The vertical beam size  $\sigma_z$  at scraper location is  $\sim 100 \mu\text{m}$  (normalized to  $\beta_z$  from the vertical beam size measured at X-ray diagnostic beamline), so the beam loss occurred at  $\sim 6$  times of the beam size which is theoretical quantum lifetime limit for vertical plane. From Figure 5.8, we see that when the horizontal scraper position from beam centre was 7.6 mm, a fast beam loss occurred and at 6.8 mm beam was lost completely. The horizontal beam size  $\sigma_x$  at scraper location is  $\sim 1.3\text{mm}$  (normalized to  $\beta_x$  from the horizontal beam size measured at X-ray diagnostic beamline), so the loss of beam occurred at  $\sim 6$  times of the beam size which is theoretical quantum lifetime limit for horizontal plane.

### 5.5 Verification of theoretical calculated results

The theoretical calculated value of  $\tau_{el}$ ,  $\tau_{br}$  and  $\tau_{tous}$  at 100 mA stored beam current for measured aperture and using analytical expressions are 26.9 hours, 28.7 hours and 285 hours respectively as discussed in section 5.4.

To verify the results obtained as above, an equation of curve of measured data of beam lifetime  $\tau_t$  with vertical scraper position  $b$  from beam centre was generated using least square minimization method. The measured data with a fitted curve is shown in Figure 5.9.

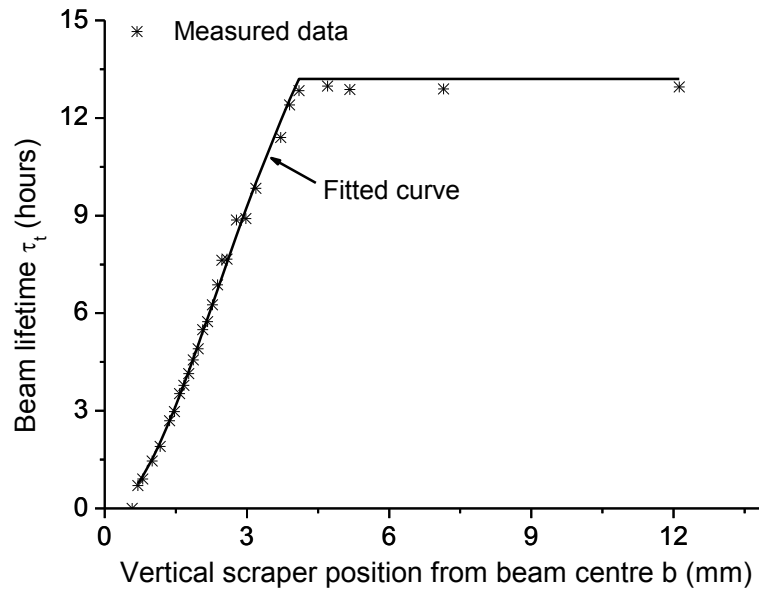


*Fig.5.9. Beam lifetime versus vertical scraper position with fitted curve*

The equation of curve relating beam lifetime  $\tau_t$  with vertical scraper position  $b$  is as follows

$$\frac{1}{\tau_t (\text{hours})} = \frac{1}{25.8} + \frac{0.6229}{b^2 (\text{mm}^2)} \quad \text{where } b \leq 4.1 \text{mm} \quad 5.5$$

The bremsstrahlung and Touschek lifetime contribution are constant during the vertical scraper movement, so the fitted data is described as

$$\frac{1}{\tau_t} = \frac{1}{\tau_{tb}} + \frac{1}{\tau_{el}} \quad 5.6$$

where  $\tau_{tb}$  is the combined lifetime due to bremsstrahlung  $\tau_{br}$  and Touschek lifetime  $\tau_{tous}$ ,  $\tau_{el}$  is elastic coulomb lifetime,  $b$  is the vertical scraper distance from the beam centre. The fitted

parameters results in  $\tau_{ib}=25.8\pm 1.4$  hours and  $\tau_{el}=27\pm 0.4$ . The fitted results of beam lifetime due to elastic coulomb scattering  $\tau_{el}$  closely agree with the value of the theoretical beam lifetime. The value of  $\tau_{ib}$  and  $\tau_{br}$  are close to each other. So the contribution of  $\tau_{br}$  in  $\tau_{ib}$  is more as compared to the contribution of  $\tau_{tous}$ .

The uncertainty in the value of measured vacuum pressure will cause the change in  $\tau_{el}$  and  $\tau_{br}$  but will not affect the Touschek lifetime. To approach or know the real value of  $\tau_{tous}$ , partial beam bunch fill experiments were conducted.

The partial beam fill experiments were conducted in continuation after the completion of beam scraper experiments. For the experiments, the ring was filled with 10% and 33% bunch gap and beam current decay was monitored. The beam current decay with 10% and 33% bunch gap is shown in Figure 5.10.

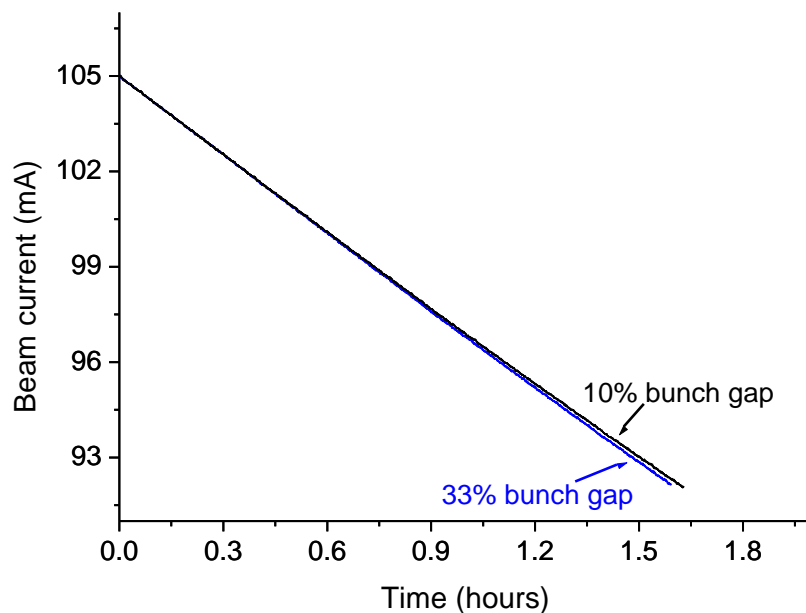


**Fig.5.10. Comparison of beam current decay with 10% and 33% bunch gap**

The horizontal and vertical beam sizes in these fill patterns were measured using X-ray diagnostic beamline and bunch length was also measured using visible diagnostic beamline. The beam sizes were found to be the same in both cases. As beam sizes in transverse and longitudinal planes in both cases are the same so the bunch volume is same. The Touschek lifetime is inversely proportional to the number of electrons in a bunch when bunch volume is same.  $\tau_{tous}$  is the Touschek lifetime when the beam current fill uniformly in all 291 RF buckets. Touschek lifetime with 10% and 33% bunch gap is  $9\tau_{tous}/10$  and  $2\tau_{tous}/3$  respectively. The vacuum pressure in both cases was also monitored and found to be the same at same stored beam current. Considering same vacuum lifetime in both cases of bunch fill pattern at stored beam current 100 mA, we obtained Touschek lifetime from measured lifetime as given in Table 5.2.

Table 5.2: Value of Touschek lifetime from measured beam lifetime

Filling pattern	Measured lifetime (hours)	Touschek lifetime (hours)
10% bunch gap	12.9	286
33% bunch gap	12.7	212

From the above results, we get Touschek lifetime  $\tau_{tous}=318$  hours for uniform fill of all RF buckets and vacuum lifetime 13.5 hours. Using  $\tau_{ib}=25.8$  hours as obtained from curve fit and  $\tau_{tous}=318$  hours, we get  $\tau_{br}=28.1$  hours.

The value of lifetime  $\tau_{el}$ ,  $\tau_{br}$  and  $\tau_{tous}$  at 100 mA stored beam current using equation 5.6 and  $\tau_q$  are given in Table 5.3.

Table 5.3: Contribution of different lifetime in total beam lifetime at 100 mA stored beam current

Contributors of total lifetime	Lifetime (hours)
$\tau_{el}$	27.0
$\tau_{br}$	28.1
$\tau_{tous}$	318.0
$\tau_q$	>1000

The theoretically calculated value of Touschek lifetime is 285 hours whereas measured value is 318 hours. The measured value of Touschek lifetime is near to the theoretical value which is theoretically calculated using particle tracking code ELEGANT.

The value of vacuum lifetime obtained from partial beam bunch fill experiments is found to be 13.5 hours whereas the theoretical calculated vacuum lifetime is 13.9 hours. The small difference between the experimental and theoretical calculated value of vacuum lifetime may be due to uncertainty in the measured vacuum pressure.

### 5.6 Further experiments for beam lifetime improvement

From the aperture measurement and beam lifetime analysis it was found that the measured aperture at scraper location  $\pm 4.1$  mm is significantly less as compared to value  $\sim 6$  mm as obtained using particle tracking. Beam experiments were conducted for the improvement in vertical aperture by applying vertical closed orbit correction whereas all other parameters were same. The vertical closed orbit before and after correction is shown in Figure 5.11. The beam lifetime at 100 mA stored current at beam energy 2.5 GeV which was  $\sim 13$  hours before correction was increased to  $\sim 18$  hours after correction was applied. The beam current decay at  $\sim 100$  mA stored current before and after vertical orbit correction is shown in Figure 5.12.

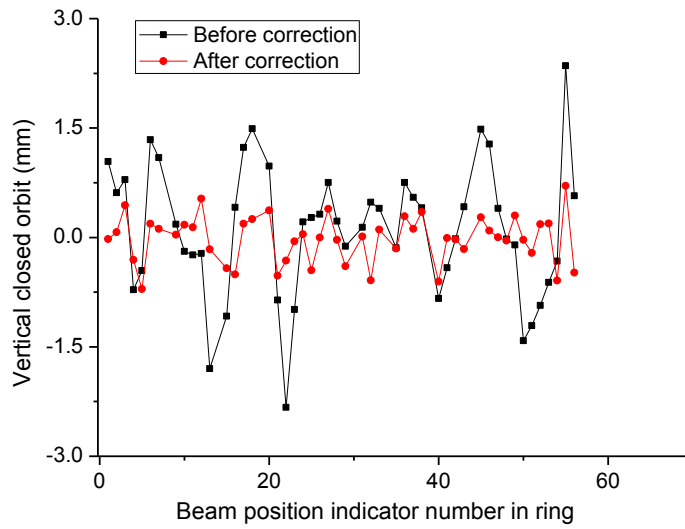


*Fig.5.11. Vertical closed orbit before and after correction*

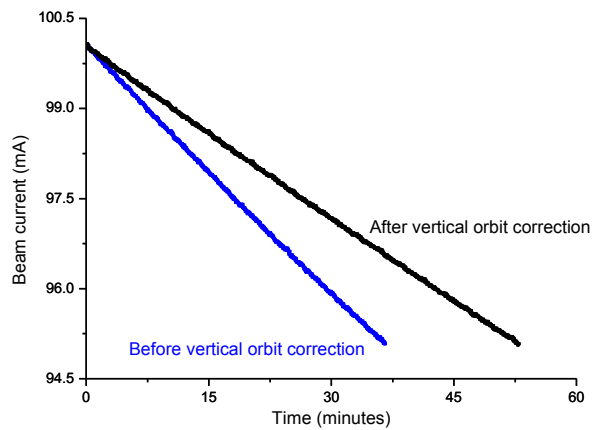


*Fig.5.12. Comparison in beam current decay before and after vertical orbit correction*

The vertical orbit correction was also applied at the higher stored beam current and ~40% increase in beam lifetime was observed. A comparison in beam current decay at higher stored beam current before and after vertical orbit correction is shown in Figure 5.13.

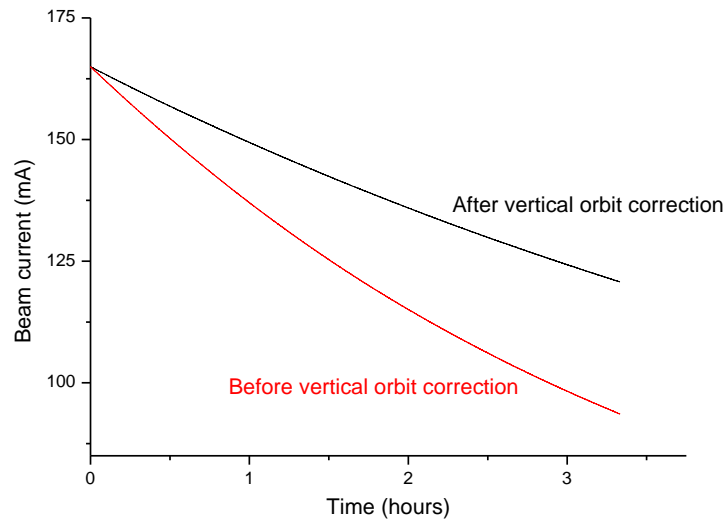


***Fig.5.13. Comparison in beam current decay before and after vertical orbit correction***

So by conducting experiments with beam scraper it was found that the lifetime of stored electron beam in Indus-2 depends on vertical aperture and with increase in vertical aperture there is significant increase in beam lifetime.

### **5.7 Beam experiments using single bunch mode**

To study the effect of higher density of electrons in a bunch i.e. Touschek scattering, beam experiments were conducted to fill electrons in single bunch in single RF bucket out of 291 RF buckets. The single bunch fill [76] was observed on wall current monitor installed in the ring for the observation of bunch fill pattern. The wall current monitor signal showing the storage of one bunch after repetition of revolution time i.e. 575 ns is shown in Figure 5.14(a) and (b). The photograph of single bunch taken using the streak camera installed in visible diagnostic beamline (BL-23) [97] is shown on Figure 5.15.

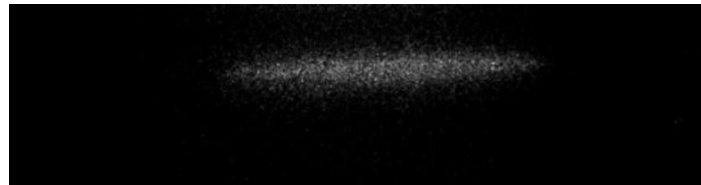
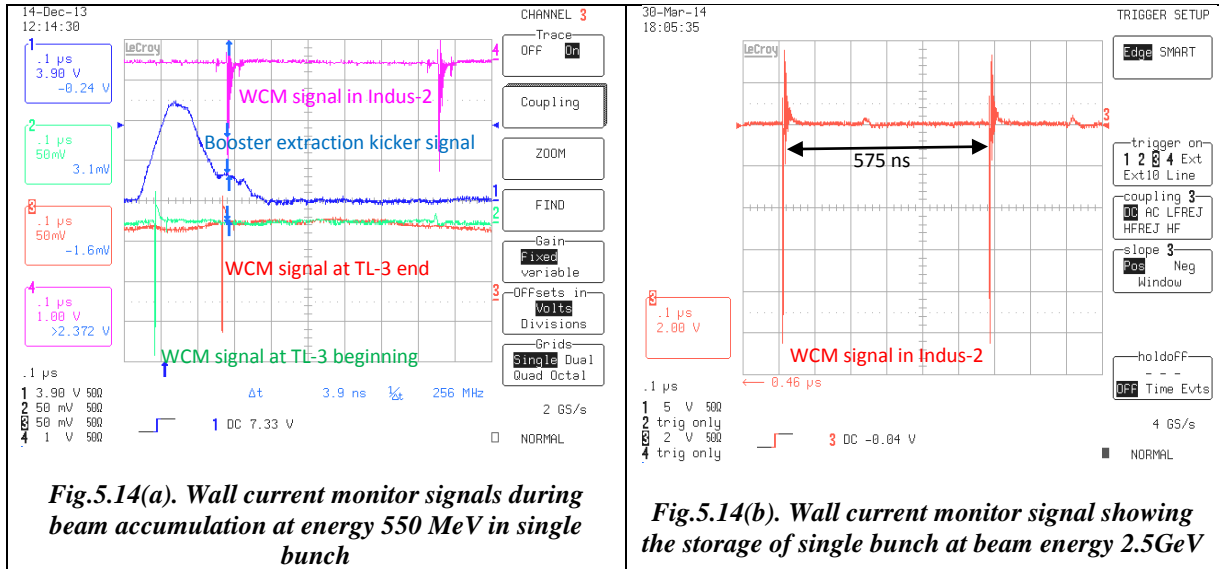


**Fig.5.15. Single bunch photograph taken using streak camera in visible diagnostic beamline**

In one experiment a beam current of 7 mA ( $2.5 \times 10^{10}$  electrons in a bunch) was stored in single bunch at beam energy 550 MeV and beam current decay was observed. In the second experiment, a beam current of 7 mA was stored in single bunch at beam energy 2.5 GeV and beam current decay was observed. A comparison in beam current decay of same amount of current in single bunch i.e. 7 mA at beam energy 550 MeV and 2.5 GeV is shown in Figure 5.16.

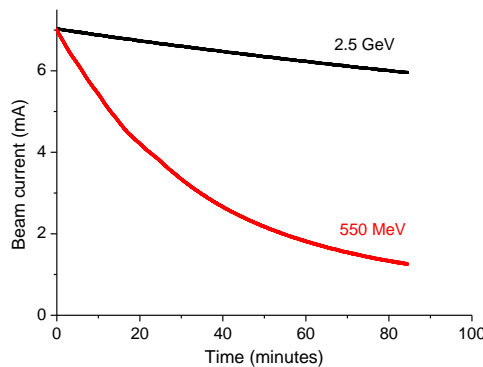
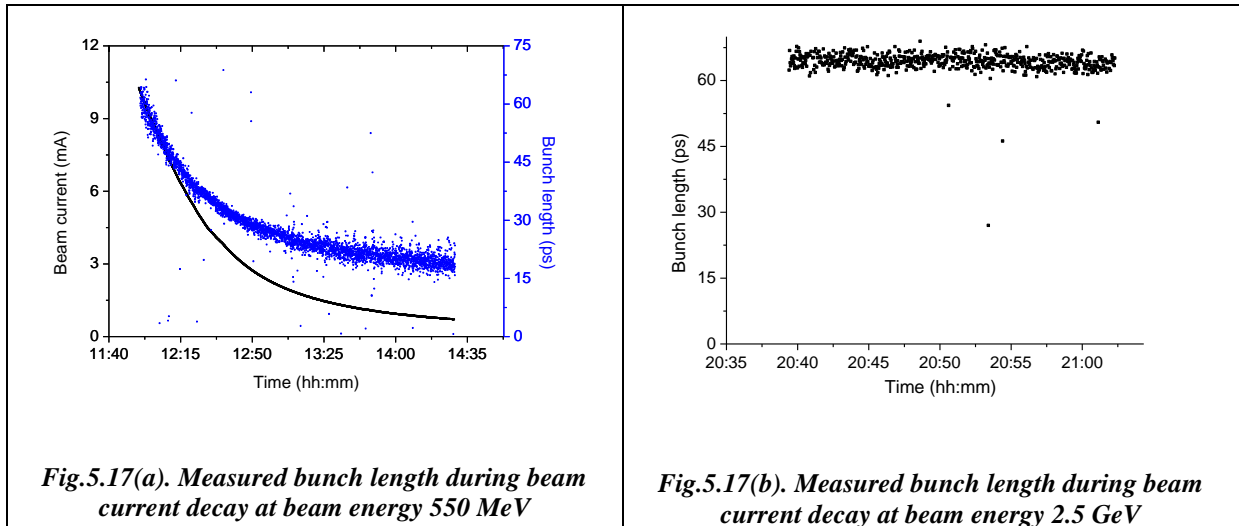


**Fig.5.16. Beam current decay in single bunch mode at different beam energy**

During the above experiments of beam current decay at beam energy 550 MeV and 2.5 GeV, bunch length was measured using visible diagnostic beamline in which streak camera are installed. The variation in bunch length during current decay is shown in Figure 5.17(a) and (b) respectively.



From the beam current decay, it was found that the beam lifetime at 7 mA @ 550 MeV is ~38 minutes whereas beam lifetime at 7 mA @ 2.5 GeV is ~9 hours. The results show that the Intra-beam scattering (IBS) effect (small angle Touschek scattering) is more significant at low energy 550 MeV as compared to high energy i.e. 2.5 GeV. From the measured bunch length, it was found that change in bunch length during beam decay takes place at 550 MeV but this effect was not observed at beam energy 2.5 GeV. The results indicate that the Touschek scattering effect is significant at low energy.

### 5.7.1 Effect of RF voltage on beam lifetime

A beam current ~14 mA at beam energy 2.5 GeV was filled in two bunches in two RF buckets (7 mA in one bunch as in first experiment) and rest RF buckets were kept empty. All parameters were the same as above except that two bunches of same amount of current were filled. The beam current decay is shown in Figure 5.18.

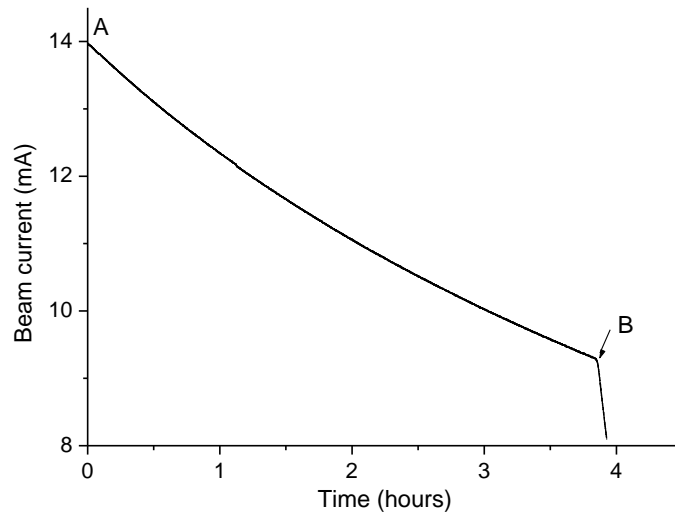


*Fig.5.18.Effect of RF voltage on beam lifetime at beam energy 2.5GeV*

The beam lifetime at 14mA@2.5 GeV was found to ~9 hours. Using ELEGANT code Touschek lifetime for 7 mA in single bunch with 0.5% coupling is ~16 hours, vacuum lifetime ~30 hours, so the theoretical lifetime at 7 mA in single bunch is ~10.4 hours. Experimental observed value of the beam lifetime is thus in agreement with the theoretical estimate.

A total RF cavity voltage ~1250 kV was applied. As seen in the Figure 5.18, up to the point B, it was normal beam decay. The effect of RF cavity voltage on beam lifetime was studied by reducing the cavity voltage. It was found that by reducing RF voltage to ~1100 kV, fast beam decay was observed. So the RF voltage ~1100 kV is the quantum lifetime limit of Indus-2 at beam energy 2.5 GeV. The result of quantum lifetime limit in longitudinal plane is close to the theoretical estimation (relation 1.52 in chapter 1).

## SUMMARY AND CONCLUSIONS

The acceptances of beam in Indus-2 electron storage ring has been studied by using analytical formulation and particle tracking codes MAD-8, ELEGANT, RACETRACK and TRACY-3 (Chapter 1). The loss of electrons due to elastic scattering between electrons and the nuclei of the residual gas atoms for rectangular and elliptical shape of the vacuum chamber was studied using linear beam dynamics. Analytical expressions for the shape factors for rectangular and elliptical shape of vacuum chamber as a function of position along the circumference of storage ring have been derived (Chapter 2). These expressions are very useful to estimate the beam lifetime due to elastic scattering of electrons with the nuclei of residual gas atoms in realistic conditions like non uniform vacuum pressure in storage ring. The expression for shape factor for the rectangular shape of vacuum chamber is similar to the expression for the average shape factor available in the literature. It indicates that the approach followed for deriving the expression is appropriate. The expression of shape factor for elliptical shape of vacuum chamber was derived using the same approach as used for rectangular chamber. The expression of shape factor for elliptical shape was found to be different from the existing expression because in existing expression the loss of electrons was considered at one location only which does not happen in a modern electron storage ring.

The electron-electron interaction within a bunch known as Touschek scattering was studied. Parameters affecting the Touschek scattering such as betatron coupling and RF phase modulation were also studied. The betatron coupling in Indus-2 was measured and found to be  $\sim 0.5\%$ , this value of coupling was used for the estimation of Touschek lifetime. Effect of RF phase modulation on beam lifetime in Indus-2 was studied (Chapter 3). The effect of aperture on beam lifetime was studied by conducting beam experiments without and with application of closed orbit correction. The results show that with closed orbit correction, there is an increase in beam lifetime. The contribution of vacuum lifetime and Touschek lifetime in

measured beam lifetime was separated by storing electrons uniformly in all 291 RF buckets and also storing electrons in two-third RF buckets keeping rest of the RF buckets empty (Chapter 4). These studies are very useful to know the limiting factor of beam lifetime i.e. either vacuum lifetime or Touschek lifetime. The effect of RF cavity voltage on beam lifetime was studied to find the limiting momentum acceptance either in transverse or in longitudinal plane.

The vertical and horizontal aperture available for stable beam motion at scraper location in Indus-2 at beam energy 2.5 GeV with 100 mA stored beam current was measured by using movable beam scrapers (Chapter 5). The objective of the measurement was to find an appropriate vertical aperture for undulators which are planned to be installed and also to understand the beam loss mechanism. The measured vertical and horizontal aperture at scraper location was found to be  $\pm 4.1$  mm and  $\pm 12.45$  mm respectively. The beam lifetime variation with the movement of vertical and horizontal scraper was measured and analyzed using analytical formulations and particle tracking code ELEGANT. Vacuum lifetime was calculated using partial pressure of the residual gases present in the vacuum chamber. From the measured beam lifetime with scraper position from the beam centre, the contribution of beam lifetime due to elastic scattering of electrons with the nuclei of residual gas atoms, bremsstrahlung, Touschek scattering and quantum excitation was estimated separately. The contribution to beam lifetime due to elastic coulomb scattering, bremsstrahlung and Touschek scattering are separated from the measured total beam lifetime. The theoretical value of vacuum lifetime due to elastic coulomb scattering in vertical plane closely follows the values obtained from fitted curve of measured data. The quantum lifetime is studied by inserting the vertical and horizontal scraper to the vicinity of the beam core (Chapter 5). The beam sizes obtained from quantum lifetime limitation are close to the beam sizes measured using X-ray diagnostic beamline. The quantum lifetime limit in longitudinal plane was studied by

reducing the RF cavity voltage. The vacuum and Touschek lifetimes obtained using scrapers were closely same as obtained using partial bunch fill experiments. The vertical and horizontal apertures studies using movable beam scrapers show that the beam lifetime is limited due to elastic coulomb scattering and inelastic scattering between electrons and nuclei of residual gas atoms. The measured vertical aperture at scraper location was found to be less than its theoretical estimated value. The vertical aperture was improved by minimizing the closed orbit distortion in vertical plane and it resulted into ~40% increase in beam lifetime (Chapter 5). It shows that the lifetime of stored electron beam in Indus-2 depends on the vertical aperture. These studies indicate that the beam lifetime in Indus-2 will further improve with reduction in vacuum pressure. The vertical aperture measurement carried out also indicate that the beam lifetime will not be reduced after installation of insertion devices as the vertical aperture available in undulators will be  $\pm 8$  mm. The beam lifetime due to a high density of electrons in a bunch was studied by storing the electrons in a single bunch in one RF bucket out of 291 RF buckets in Indus-2 ring. It was observed experimentally that the Touschek scattering effects are dominant at lower energy.

## APPENDIX A

Assuming that the loss of electrons takes place at one location. This implies that both  $\beta_x$  and  $\beta_z$  have maxima at this point, which is rarely the case for example, it can occur in weak focusing storage rings. Then we may substitute the following  $x$  and  $z$  in equation 2.9

$$\begin{aligned} x &= \sqrt{\beta_{x_0} \beta_{xm}} \theta_m \cos \phi \\ z &= \sqrt{\beta_{z_0} \beta_{zm}} \theta_m \sin \phi \end{aligned} \quad \text{A.1}$$

we get

$$F_j = \int_0^{2\pi} \frac{d\phi}{\theta_m^2(\phi)} = \int_0^{2\pi} \frac{\beta_x(s_0) \beta_{xm} \cos^2 \phi + \beta_z(s_0) \beta_{zm} \sin^2 \phi}{x^2 + z^2} d\phi \quad \text{A.2}$$

At the location of electron loss,  $x^2 + z^2 = \rho^2$  and  $(\rho \cos \phi, \rho \sin \phi)$  are arbitrary coordinates of  $P$ . The coordinate  $P(\rho \cos \phi, \rho \sin \phi)$  lies on ellipse  $\frac{x^2}{a^2} + \frac{z^2}{b^2} = 1$ , so using

$\frac{1}{\rho^2} = \frac{\cos^2 \phi}{a^2} + \frac{\sin^2 \phi}{b^2}$  in equation 2.3 we get

$$F_j = \int_0^{2\pi} [\beta_x(s_0) \beta_{xm} \cos^2 \phi + \beta_z(s_0) \beta_{zm} \sin^2 \phi] \left[ \frac{\cos^2 \phi}{a^2} + \frac{\sin^2 \phi}{b^2} \right] d\phi \quad \text{A.3}$$

After integration, we get similar relation 2.24

$$F_j = \pi \left[ \frac{\beta_x(s_0) \beta_{xm}}{a^2} + \frac{\beta_z(s_0) \beta_{zm}}{b^2} \right] \quad \text{A.4}$$

Taking average  $\beta$  in ring, we get average shape factor  $F$  as

$$F = \pi \left[ \frac{\langle \beta_x \rangle \beta_{xm}}{a^2} + \frac{\langle \beta_z \rangle \beta_{zm}}{b^2} \right]$$

In deriving this equation, we have assumed that the loss takes place at one location where both  $\beta_x$  and  $\beta_z$  are maximum. This relation is not applicable to the modern storage rings in which the maxima of  $\beta_x$  and  $\beta_z$  occurs at different places.

## REFERENCES

- [1] “Synchrotron light sources of the world” [www.lightsource.org](http://www.lightsource.org).
- [2] D. Angal-Kalinin, A. Banerji, P.R. Hannurkar, M.G. Karmarkar, S. Kotaiah, S.P. Mashkar, P.K. Nema, S.S. Prabhu, M. Pravin Kumar, S.S. Ramamurthi, S.K. Shukla, G. Singh, H.C. Soni and B.J. Vaidya, “Synchrotron radiation source Indus-1”, *Current Science* 82(3) (2002).
- [3] G. Singh, G.K. Sahoo, D. Angal, B. Singh, A.D. Ghodke and P. Kant, “Synchrotron radiation source Indus-2” *Indian Journal of Pure and Applied Physics* 35(3),183 (1997).
- [4] D.D. Bhawalkar, G. Singh and R.V. Nandedkar, “Synchrotron radiation sources Indus-1 and Indus-2” *PRAMANA, Journal of physics*, 50(6),467 (1998).
- [5] “Technical Report of Synchrotron radiation source Indus-2” Centre for Advanced Technology, Indore, India (1998).
- [6] R.V. Nandedkar and G. Singh, “Indus-1 and Indus-2: Indian synchrotron radiation sources” *Synchrotron radiation news*, 16(5), 43 (2003).
- [7] A.D. Ghodke, Riyasat Hussain, Gurnam Singh and Indus-2 commissioning team, “Progress in commissioning of Indus-2” *ICFA, Beam dynamics newsletter*, 41, 77 (2006).
- [8] S.K. Deb, G. Singh and P.D. Gupta, “Indus-2 Synchrotron radiation source: current status and utilization” 11<sup>th</sup> international conference on synchrotron radiation instrumentation, *Journal of Physics: conference series* 425, 072009 (2013).
- [9] P.R. Hannurkar, S.K. Deb, A.C. Thakurta, T.A. Puntambekar, S.R. Tiwari, M.R. Lad, P. Fatnani, R.S. Shinde, A.D. Ghodke, R. Sridhar, P. Shrivastava, R.K. Sahu, R.M. Pandey, J. Dwivedi, G.S. Lodha, S.S. Kulkarni, G. Singh and P.D. Gupta, “Indus

- Synchrotron Radiation Sources: A National Facility” Indian Nuclear Society News, 10, no. 3&4 (2013).
- [10] E. D. Courant and H. S. Snyder, "Theory of alternating gradient synchrotron", *Annals of Physics*, 3, 1(1958).
- [11] M. Sands, "The Physics of Electron Storage Ring", SLAC-121, (1970).
- [12] E.J.N. Wilson, "An introduction to particle accelerators", Oxford university press (2001).
- [13] K. Wille, "The physics of particle accelerators", Oxford university press (2001).
- [14] S. Turner, editor, *Proceedings of the 1992 CERN Accelerator School, Finland*, CERN-94-01 (1994).
- [15] Karl L. Brown, Roger V. Servranckx, "Optics modules for circular accelerator design", *Nuclear Instruments and Methods in Physics Research A*258 (1987).
- [16] R.H. Helm, M.J. Lee, P.L. Morton and M. Sands, "Evaluation of synchrotron radiation integrals", *IEEE Trans. Nucl. Sci.* NS-20, (1973).
- [17] K.Ohmi, K.Hirata and K.Oide, " from the beam envelope matrix to synchrotron radiation integrals", *Physical Review E*, 49(1), (1994).
- [18] T. Raubenheimer, "The generation and acceleration of low emittance flat beams for future linear colliders", SLAC-R-387, (1991).
- [19] S.A. Armitage, "Some aspects of ion production in the SRS", Technical memorandum, Daresbury laboratory DL/SRF/TM 3, (1976).
- [20] Shyogo Sankanaka, "The stability of ions in partially filled mode operation in the electron storage ring", KEK preprint 86-17, (1986).
- [21] R.L. Gluckstern and A.G. Ruggiero, "Ion production and Trapping in electron ring", BNL-26585, (1979).

- [22] C.J. Bocchetta, A. Wrulich, “The Trapping and clearing of ions in ELETTRA storage ring”, Nuclear Instruments and Methods in Physics Research A278, (1989).
- [23] A.W. Chao, Martin J. Lee, “Particle distribution parameters in an electron storage ring”, Journal of Applied Physics 47(10), (1976).
- [24] A.W. Chao, “Evaluation of beam distribution parameters in an electron storage ring”, Journal of Applied Physics 50(2), (1979).
- [25] H. Wiedemann, “Particle Accelerator Physics”, Third edition, Springer-Verlag, Berlin, (2007).
- [26] S.Y. Lee, “Accelerator Physics”, Third edition, World Scientific, New York, (2011).
- [27] M. Furman, J. Byrd and S. Chattopadhyay, “Beam instabilities”, Synchrotron Radiation Sources-A premier edited by H. Winick (1995).
- [28] M. Lonza, “Multi-bunch feedback systems”, CERN Accelerator School 2007.
- [29] A. Streun, “Lattices for light sources”, In proceedings of 2003 CERN Accelerator School, Brunnen, Switzerland, p. 55-82, CERN-2005-012 (2005).
- [30] L. Nadolski and J. Laskar, “Review of single particle dynamics for third generation light sources through frequency map analysis”, Physical Review Special Topics-Accelerator and Beam, 6, 114801, (2003).
- [31] F. Christoph Iselin, "The MAD Program: Physical Methods Manual", CERN/SL/92 (AP), (1994).
- [32] M. Borland, "ELEGANT: A Flexible SDDS-Compliant Code for Accelerator Simulation", Advanced Photon Source LS-287, September 2000, Version 25.1.0 (2012)
- [33] F. Iazzourene, C.J. Bocchetta, R. Nagaoka, L. Tosi and A. Wrulich, “RACETRACK USER’S GUIDE Version 4.01” ST/M-92/7 (1992).

- [34] Jianfeng Zhang, Laurent Nadolski, "User manual for Tracy-3, SOLEIL Version" (April 2011).
- [35] J. Le Duff, "Current and Current density limitations in existing electron storage ring" Nuclear Instruments and Methods in Physics Research A239, p.83 (1985).
- [36] A.W. Chao, "Quantum lifetime in electrons storage rings", IEEE Trans. on Nuclear Science, vol. NS-24, no. 3 (1977).
- [37] A. Wrulich, "Single beam lifetime", in proceedings of CERN Accelerator School CERN 94-01 (1994).
- [38] H.J. Halama, "Electron storage ring beam lifetime dependence on pressure and pumping speed", J. Vac. Sci. Technology A3(3) (1985).
- [39] H.J. Halama, "Vacuum and lifetime in electron storage ring", BNL-34177 (1984).
- [40] Alessandro Rindi, "Gas bremsstrahlung from electron storage ring", Health physics, 42(2), (1982).
- [41] C. Bernardini, G.F. Corazza, G. Di Guigno, Ghigo, J. Haissinski, P. Marin, R. Querzoli and B. Touschek, "Lifetime and beam size in a storage ring", Physical Review letters, vol. 10, number 9 (1963).
- [42] J. Le. Duff, "Single and multiple Touschek effects", LAL-RT-88-08 (1988).
- [43] Y. Miyahara, "Touschek lifetime of an elliptical electron beam with horizontal and vertical betatron oscillations", Japanese Journal of Applied Physics, 39 (2000).
- [44] M.S. Zisman, S. Chattopadhyay and J.J. Bisognano, "ZAP User's manual", LBL-21270 (1986).

- [45] Erik Wallen, "Aperture and lifetime measurements with movable scrapers at MAX II", Nuclear Instruments and Methods in Physics Research A508 (2003).
- [46] Xiaobiao Huang, Jeff Corbett, "Measurement of beam lifetime and applications for SPEAR3", Nuclear Instruments and Methods in Physics Research A629 (2011).
- [47] Pradeep Kumar, A.D. Ghodke, A. K. Karnewar, A.C. Holikatti, S. Yadav, T.A. Puntambekar, G. Singh and P. Singh, "Measurements of aperture and beam lifetime using movable beam scrapers in Indus-2 electron storage ring", Review of Scientific Instruments, 84,123301 (2013).
- [48] Jim Murphy, "Synchrotron light source data book", Brookhaven National Laboratory, BNL-42333 (1996).
- [49] T. Kaneyasu, Y. Takabayashi, Y. Iwasaki, S. Koda, "Beam lifetime study based on momentum acceptance restriction by movable beam scraper", Nuclear Instruments and Methods in Physics Research A694 (2012).
- [50] N. Mocheshnikov, A. Zelinsky, "The beam lifetime from elastic scattering on nuclei of residual gas in electron storage ring with the various shape of the vacuum chamber", in proceedings of particle accelerator conference PAC-1999.
- [51] C. Bocchetta, "Lifetime and beam quality", in proceedings of CERN Accelerator School, CERN 98-04 (1998).
- [52] Alan Jackson, "The challenges of third generation synchrotron light source", Particle Accelerators, vol. 33 (1990).
- [53] Annick Ropert, "Lifetime issues for third generation light sources", in Proceedings of EPAC-98 (1998).
- [54] S. Khan, "The lifetime of a stored electron beam", Collective Phenomena in Synchrotron Radiation Sources, Springer (2006).

- [55] A.A. Kolomensky and A.N. Lebedev, “Theory of cyclic accelerators”, Translated from the Russian by M. Barbier (CERN), North Holland Publishing Company Amsterdam (1966).
- [56] P.J. Bryant, “A simple theory for betatron coupling”, CERN ISR-MA 175-28 (1975).
- [57] D.A. Edwards and L.C. Teng, “Parameterization of linear coupled motion in periodic systems”, in proceedings of PAC-73 (1973).
- [58] S. Peggs, “Coupling and Decoupling in storage rings”, IEEE Trans. on Nuclear Science, Vol. NS-30, No. 4, (1983).
- [59] F. Willeke, G. Ripken, “Methods of beam optics”, DESY 88-114 (1988).
- [60] Marc Munoz, “Assessment of the achievable emittance ratio in Diamond”, in proceedings of EPAC-96 (1996).
- [61] R. Bartolini, N.G. Wyles, “Linear coupling and Touschek lifetime issues at Diamond storage ring”, in proceedings of EPAC-2004.
- [62] C.C. Kuo, J.R. Chen, P.J. Chou, H.P. Chang, K.T. Hsu, G.H. Luo, H.J. Tsai, D.J. Wang, M.H. Wang, “Vertical beam size control in TLS and TPS”, in proceedings of EPAC-2006.
- [63] R. Dowd, M. Boland, G. LeBlanc and Y.R. E. Tan, “Achievement of ultralow emittance coupling in the Australian Synchrotron Storage ring”, Physical Review Special Topics- Accelerator and Beams 14, 012804 (2011).
- [64] A.G. Valentinov, V.N. Korchuganov, Yu. V. Krylov, Yu. L. Yupinov, “Vertical size of an electron beam at SIBERIA-2”, in proceedings of RUPAC-2012.
- [65] G. Guignard, “Betatron coupling and related impact of radiation”, Physical Review E 51, 6 (1995).

- [66] H.S. kang, J.Y. Huang and S.H. Nam, “Measurement of Touschek lifetime in PLS storage ring”, in proceedings of Asian Particle Accelerator Conference (APAC) (2001).
- [67] M.K. Tiwari, S.R.Kane, A.K. Sinha, C.K. Garg, A.K. Singh, P. Gupta, S.R. Garg, G.S. Lodha and S.K. Deb, “A microprobe-XRF beamline on Indus-2 Synchrotron light source”, *Journal of Physics: Conference Series* 425, 072020 (2013).
- [68] S. Sakanaka, M. Izawa, T. Mitsuhashi and T. Takahashi, “Improvement in the beam lifetime by means of an RF phase modulation at the KEK photon factory storage ring”, *Physical Review Special Topics- Accelerator and Beams* 3, 050701 (2000).
- [69] S. Sakanaka and T. Obina, “Observation of longitudinal quadrupole mode oscillations of a bunch which were induced by RF phase modulation in the electron storage ring”, *Japanese Journal of Applied Physics*, Vol. 40 (2001).
- [70] Yu Senichev, N. Hertel, S. Lunt, S.P. Moeller and J.S. Neilsen, “Increasing the lifetime of SR surces by RF phase modulation”, in proceedings of EPAC-1998.
- [71] N.P. Abreu, R.H.A. Farias and P.F. Tavares, “Longitudinal dynamics with RF phase modulation in the Brazilian electron storage ring”, *Physical Review Special Topics- Accelerator and Beams* 9, 124401 (2006).
- [72] I.M. Hwang, S. Shin, M. Yoon, E.S. Kim, J. Yang and T. Naito, “The effects of low RF modulation frequencies on the longitudinal beam motion at the Pohang Light Source”, *Journal of the Korean physical society*, vol. 44(5), (2004).
- [73] M. H. Wang, L.H. Chang, P. Chang, K.T. Hsu, C.C. Kuo, W.K. Lou and C.S. Hsue, “Effect of RF phase modulation on the longitudinal beam dynamics” in proceedings of Particle Accelerator Conference-1997.
- [74] F. Orsini and A. Mosnier, “Effectiveness of RF phase modulation for increasing bunch length in electron storage ring”, *Physical Review E* 61, 4 (2000).

- [75] Riyasat Husain, A.D. Ghodke, S. Yadav, A.C. Holikatti, R.P. Yadav, P. Fatnani, T.A. Puntambekar and P.R. Hannurkar, “Measurement, analysis and correction of the closed orbit distortion in Indus-2 Synchrotron Radiation Source”, PRAMANA, Journal of Physics 80(2), (2013).
- [76] D. Angal Kalinin and G. Singh, “Beam lifetimes and filling schemes for synchrotron radiation source Indus-2”, in proceedings of EPAC-2002.
- [77] S.K. Shukla, R. Shridhar, D.P. Yadav, R.J. Patel, A.S. Raja Rao, “Design aspects of UHV systems for Indus-2”, in proceedings of Asian Particle Accelerator Conference-98 (1998).
- [78] S.K. Shukla, “Vacuum systems of accelerators at Indus complex”, in proceedings of International symposium on vacuum science and Technology and its application for accelerator, 15-17 February, 2012 at VECC Kolkata.
- [79] J. Corbett, X. Huang, M. Lee and P. Lui, “Electron beam lifetime in SPEAR3: Measurement and simulation” in proceedings of PAC-2007.
- [80] Philip R. Bevington and D. Keith Robinson, “Data Reduction and Error Analysis for the Physical Sciences”, second edition, McGraw-Hill, New-York, 1992.
- [81] Pradeep Kumar, A.D. Ghodke and Gurnam Singh, “Beam lifetime measurement and analysis in Indus-2 electron storage ring”, PRAMANA: Journal of physics, 80(5), 855 (2013).
- [82] A.D. Ghodke, Riyasat Husain, Pradeep Kumar, Surendra Yadav and T.A. Puntambekar, “Measurement of parameters in Indus-2 synchrotron radiation source”, Review of Scientific Instruments 83, 103303 (2012).
- [83] Tae-Yeon Lee, “Simple formula for the beam lifetime analysis in an electron storage ring”, Physical review E69, 046501 (2004).

- [84] Tae-Yeon Lee, Jinhyuk Choi, H.S. Kang, “Simple determination of Touschek and beam-gas scattering lifetime from measured beam lifetime”, Nuclear Instruments and Methods in Physics Research A554 (2005).
- [85] H. Wiedemann, “Coulomb scattering and vacuum chamber aperture”, SSRL ACD-NOTE 8 (1983).
- [86] S.Khan, “Study of Bessy II beam lifetime”, in proceedings of PAC-1999.
- [87] C.D. Park, T.Y. Lee, I.H. Bae and S.M. Chung, “Measurement of beam gas scattering lifetime in Pohang light source”, J. Vac. Sci. Technology A18(6), (2000).
- [88] E. Huttel, I. Birkel, A.S. Muller, F. Perez, M.Pont, “Studies of beam lifetime at ANKA”, in proceedings of PAC-2003.
- [89] N.P. Abreu, P.F. Tavares, “Lifetime studies in the LNLS electron storage ring”, in proceedings of EPAC-2004.
- [90] A. Hansson, “Electron beam sizes and lifetimes at MAXII and MAXIII”, Doctoral Thesis (2012).
- [91] A. Hansson, A. Andersson, J. Breunlin, G. Skripka, E. Wallen, “Studies of the electron beam lifetime at MAXIII”, In proceedings of IPAC-2013.
- [92] A.K. Karnewar, A. Banerji, S. Kotaiah, “Mechanical design of Indus-2 beam scraper”, in proceedings of Indian Particle Accelerator Conference (2005).
- [93] T.A. Puntambekar, A.C. Holikatti, A. Banerji, S. Kotaiah, “Microcontroller based interface unit for Indus-2 beam scraper”, in proceedings of Indian Particle Accelerator Conference (2005).
- [94] Yulin Li, Xianghong Liu, “Vacuum Science and Technology for Accelerator vacuum systems”, US Particle Accelerator School, January 2013.

- [95] C. Steier, D. Robin, L. Nadolski, W. Decking, Y. Wu and J. Laskar, “Measuring and optimizing the momentum aperture in a particle accelerator”, Phys. Rev. E65, 056506 (2002).
- [96] M. Borland, “Momentum aperture determination with ELEGANT”, OAG-TN-2006.
- [97] T.A. Puntambekar, “Design and development of visible diagnostic beamline at Indus-2 and initial measurement results” RRCAT Newsletter vol. 26, 1 (2013).